UNIVERSITY OF SOUTHAMPTON

FACULTY OF ENGINEERING AND APPLIED SCIENCE
INSTITUTE OF SOUND AND VIBRATION RESEARCH

SOUND MINIMISATION FOR LOCAL ACTIVE CONTROL

by

Wen-Kung Tseng

A thesis submitted for the award of
Doctor of Philosophy

March 2001

UNIVERSITY OF SOUTHAMPTON

ABSTRACT

FACULTY OF ENGINEERING AND APPLIED SCIENCE
INSTITUTE OF SOUND AND VIBRATION RESEARCH

Doctor of Philosophy

SOUND MINIMISATION FOR LOCAL ACTIVE CONTROL

by Wen-Kung Tseng

This thesis is concerned with sound minimisation in space and frequency for local active control. Theoretical studies have been performed to develop methods of designing larger zones of quiet than are obtained with conventional systems, while a comprehensive study of a practical active headrest system was performed with the aim of improving its performance. A general formulation for 2-norm and ∞-norm sound minimisation over a space is described, which in contrast to conventional approaches, which use pressure or pressure and particle velocity cancellation at one point, has no cancellation points within the minimisation region. This method therefore provides the best overall attenuation of sound within the space due to the optimal design. The performance of the sound minimisation method for local active control has been evaluated in this work using computer simulations. Larger zones of quiet were achieved compared with conventional methods for two or three secondary sources. These new design methods could be applied to a practical application, such as a headrest system.

The methods described above are then extended to active control of broadband noise. This involves the acoustic pressure minimisation over both space and frequency. The performance was investigated through computer simulations, and the results showed that good attenuation could be achieved at desired regions over both space and frequency. These methods could be realised in practice by using virtual microphones to estimate the pressure fields away from the position of the microphones.

H_2 and H_2/H_∞ methods for designing feedback controllers have also been presented, and implemented in an active headrest system which used single channel feedback controllers to attenuate the noise at a virtual microphone. This is the first time that real-time virtual microphone feedback controllers have been implemented in an active headrest system. The theoretical and practical stability and performance issues of the active headrest system have also been investigated in this work. The results showed that good performance could only be achieved with unstable open-loop controllers due to the reduced magnitude of the virtual plant response. This novel analysis could provide guidelines to designing better performing active headrest systems. The performance of an active headrest system has also been evaluated in a realistic environment to predict performance in a passenger aircraft.

Acknowledgements

The author would like to thank his supervisors, Dr. Boaz Rafaely and Professor Steve Elliott, for their help and guidance throughout this work, especially Boaz Rafaely for his great support and patience.

The author would also like to thank the Lectret Precision Ltd. and Ultra Electronic Ltd. for their support throughout the studies.

Special thanks to Dr. Phillip Joseph for the useful comments during reviews.

Thanks also go to all the members of the SPCG group for providing the pleasant atmosphere.

Finally, the authors would like to thank his parents Tien-Wang and Chan-Shi, and my entire family, for their tremendous support.

CONTENT

Part IV. Application in a headrest system

Part I: Introduction and review

Chapter 1 Introduction

1.1 Thesis objectives

The objective of this thesis is to study and develop the theory of sound minimisation, and to apply this technique to improve the performance of local active sound control systems, such as an active headrest. The theory involves sound minimisation over space for pure tone diffuse fields and sound minimisation over space and frequency for broadband plane wave fields. Both the average pressure (2-norm) and the maximum pressure (∞-norm) are used as criteria in the optimisation process. A secondary objective is the study and enhancement of practical active headrest systems.

1.2 Thesis contributions and structure

The contributions of the thesis are described in this section. The structure of the thesis is also presented. The thesis is divided into five parts. The first part includes introductory and literature review chapters, which provide a background for the work presented in the thesis. The second part is concerned with local active control of sound in pure tone sound fields, which involves pressure minimisation over space. In the third part local active control of sound is extended to broadband sound fields. This involves the pressure minimisation over both space and frequency. In the fourth part results from the study of a headrest system are presented. The fifth part includes conclusions and suggestions for future work.

This thesis has six main contributions which can be described as follows.

1. Design methods of quiet zones by using 2-norm and ∞-norm pressure minimisation strategies over space for pure tone sound fields have been developed, and the zones of quiet created by using these methods were shown to be larger than those created by using conventional methods. The novelty of this method is the minimisation of sound in an entire region rather than at specific points in space. These methods could be applied to local active sound control systems to increase the extent of the quiet zones.

2. Performance limits for an active headrest system have been studied. A novel analysis showed that the performance of a virtual microphone headrest system is limited due to the difference in gain between the virtual and physical plants. This new results can facilitate the design of improved active headrest system.
3. A new method for guaranteeing open-loop stability in the design of internal model controllers has been developed and applied. This is an important advance that forces the controller to be stable and more easily implementable.
4. Virtual microphone feedback controllers have been implemented in an active headrest system and the performance has been evaluated. This is the first time that a virtual microphone controller for active headrest is implemented in real-time. Also, a unique implementation of an open-loop unstable real-time controller is performed.
5. The expected performance of an active headrest system in a realistic environment has been investigated. This can help in predicting the performance of commercial headrest systems, when used in passenger aircraft.
6. Broadband sound minimisation over both frequency and space has been further studied. This can facilitate the design of local active control system with specified performance over space and frequency.

A detailed description of each chapter is presented below.

Chapter 2 describes a review of active sound control. Local active sound control is discussed first, which provides an introduction to recent work in this area. Then the control theory used for the controller design in this thesis is described, which involves a general feedback system description, plant uncertainty and robust stability. Finally optimisation theory used in the formulation and solution of the control problems in this thesis is presented.

Chapter 3 presents the general formulation for 2-norm and ∞-norm minimisation strategies over space, which involves pressure minimisation over a given region. The approach used in calculating the secondary field can be divided into two stages. First the desired spatial extend of the quiet zones is defined. Then, the secondary field is computed to minimise the pressure at the desired region. Both space average pressure

(2-norm) and maximum pressure (∞-norm) are used as criteria for pressure minimisation. This approach will not necessarily produce a cancellation point, i.e. a point where the total pressure is zero. However due to the optimal design, the best overall attenuation of sound is achieved in the desired region. The formulations of other minimisation methods are also proposed which include a constraint for limiting sound amplification, maximisation of the quiet zone extent, and pressure minimisation over a line.

Chapter 4 presents simulations and experiments of pressure minimisation over space. The performance of sound minimisation for local active control by using 2-norm and ∞-norm pressure minimisation strategies is evaluated through computer simulations and experiments. Pure tone sound fields are used as the primary fields. Pressure minimisation over a specified region at various locations and sizes using 2-norm and ∞-norm strategies is investigated in this chapter. Local control experiments and some initial results are also presented in the chapter.

Chapter 5 is an extension of chapters 3 and 4 to broadband primary fields. This chapter presents the theory and simulations of local active sound control for broadband disturbance using single-channel and two-channel systems. This is achieved by minimising the acoustic pressure over both space and frequency. Constrained minimisation of the pressure is also introduced, to achieve control over pressure amplification outside the attenuation zone.

Chapter 6 describes the design of a SISO (single-input single-output) virtual microphone feedback controller. The design methods are formulated as H_2 and H_2/H_∞ optimisations, where an H_2 objective is used to achieve reduction in the overall noise level, and H_∞ constraints are used to guarantee robust stability in the face of plant uncertainties, and to prevent the noise enhancement at any frequency. The H_2 and H_2/H_∞ methods are formulated as convex optimisation problems using FIR filters, and solved numerically. An H_2 method is used to initially estimate the performance, since an H_2 formulation is easy to solve and take less computational effort. Once the performance has been estimated an H_2/H_∞ method could be used to obtain a more accurate solution and better performance.

Chapter 7 investigates performance and stability of a SISO virtual microphone feedback controller in an active headrest. The limitation on performance of an active headrest system by using virtual microphone feedback controllers is discussed in this chapter. The stability issue when using virtual microphone feedback controller is also analysed. The attenuation using open-loop stable and open-loop unstable controllers is evaluated. The feedback controller in this work is designed to minimise the noise at the virtual microphone, with the virtual plant used in the performance objective. However the physical plant which uses the physical microphone is used in the stability constraint. It is shown that the magnitude of the frequency response of the virtual plant is lower than that of the physical plant. This then results in a conflicting requirement from the control filter and good performance is only achieved with a feedback controller which is open-loop unstable.

Chapter 8 presents real-time implementation of an unstable virtual microphone feedback controller for an active headrest system. The headrest system is designed to attenuate the noise at a point near the listener's ear, rather than at the control microphone. In chapter 7 we concluded that good performance could only be achieved with unstable controllers. Therefore unstable controllers are implemented in real-time to attenuate a broadband random disturbance by using the DSP processor TMS320C54x.

Chapter 9 presents the potential performance of an active noise control system in the headrest of an aircraft passenger seat. Attenuation as a function of source position in an enclosure and head position was also investigated.

Finally, chapter 10 presents some conclusions and suggestions for future research.

1.3 Connections between the separate chapters

In chapters 3 and 4 2-norm and ∞-norm minimisation strategies are used as criteria in the optimisation process. The acoustic pressure is minimised at an area over space for pure tone noise. 2-norm and ∞-norm represent the average or maximum values of a vector, matrix, signal or a system. In this work it is the acoustic pressure. However in

chapters 6, 7, 8 and 9 H_2 and H_2/H_∞ are used in the controller design for an active headrest system. The acoustic pressure is minimised at a microphone over frequency for broadband noise. H_2 and H_∞ represent some transfer function to be minimised over frequency.

In parts II and III a theoretical study is presented. Pressure minimisation over space for pure tone noise and pressure minimisation over space and frequency for broadband noise are described in these parts. However in the application part only pressure minimisation at a virtual microphone for broadband noise in a single channel active headrest system is investigated. This is because there are a lot of issues in single channel systems to be investigated. Once those issues have been studied pressure minimisation over space and frequency for broadband noise can be applied to multi-channel active headrest systems. This is left as future research.

Chapter 2 Literature review

2.1 Introduction

In this chapter we present a review of some topics relating to active control of sound which is relevant to the research areas of this thesis. First a review of local active control of sound is presented, which describes recent work on the study of quiet zones. Then the theory of feedback control systems is introduced, which is used for controller design in this thesis. Finally we present a review of optimisation theory, which is concerned with finding optimal values of coefficients of control filters or optimal values of secondary sources in the design process.

2.2 Local active control of sound

Active noise control (ANC) has been widely studied to better understand how to cancel noise by introducing an anti-noise wave. The ANC method works very well especially against low-frequency noise which is hard to attenuate by passive methods. Previous work on active noise control in free space has shown that the performance of the control system is largely dependent on the distance between primary sources and secondary sources (Nelson and Elliott, 1992). The most desirable noise control result would be the attenuation of sound pressure in all directions in space. Unfortunately, such global control can only be achieved when primary sources and control sources are closely located (Nelson and Elliott, 1986, Elliott *et al*, 1991, and Nelson and Elliott, 1992). Nelson and Elliott have examined an active control system with a pair of point sources on the basis of sound energy analysis (Nelson and Elliott, 1986). They developed a set of matrix equations for a number of noise sources and control point sources located in a free space and presented in great detail on the principles of global control of sound fields. Their work indicated that for a global control of noise, substantial reductions in total power output can be achieved only if the secondary sources are less than one half-wavelength away from the primary sources at the interest frequency. However in practical applications, this condition for maximal separation between primary and secondary sources may not always be satisfied. Under these circumstance, to cancel the sound pressure in restricted regions and to achieve quiet zones seem to be the only choice for active noise control in free space. This control strategy is called local control.

The conventional method of achieving local active noise control is to cancel the pressure at a point using a single monopole secondary source. Ross performed analysis of such a system with a monopole secondary source, with a plane wave primary sound field (Ross, 1980). He found that the shape of the quiet zone was a shell-like volume surrounding the secondary source at low frequencies, and degraded rapidly as frequency increased, being dependent on the relative orientation of the error microphone and the incident wave. Joseph (1990) and Joseph *et al* (1994) also investigated the zone of quiet created when a total pressure was driven to zero at a field point on the axis of a piston source by assuming a pure tone diffuse sound field, and a feedforward control strategy. They found that the resulting on-axis pressure distribution is determined by the near field characteristics of the secondary source. They also derived an analytical expression for the size of the on-axis quiet zone as a function of the near field properties of the secondary source. For a monopole secondary source a simple expression was obtained as follows.

$$\varepsilon(\Delta r) = (1 + kr_0)^2 (\frac{\Delta r}{r_0})^2 \qquad (2.1)$$

where $10 \log_{10}(\varepsilon(\Delta r))$ is the active attenuation in dB at a point Δr away from the cancellation point which is located a distance r_0 away from the secondary source, and k is the wavenumber.

David and Elliott (1994) explored the zone of quiet using one monopole secondary source to minimise the pressure at one and two points. They investigated the on-axis and off-axis spatial extent of the zone of quiet created around the point of cancellation, using computer simulations, for both a uniform and diffuse primary sound field. They found that as the cancellation microphone is moved away from the secondary source, the extent of the zone of quiet, within which the sound pressure has been reduced by at least 10 dB, is increased up to the limiting value of about one tenth of a wavelength of the excitation frequency. They also investigated the on-axis extent of the zone of quiet using an optimally adjusted secondary source strength to minimise the sum of the squared pressures at two control microphone positions. The results showed that the zone of quiet is moved away from the secondary source as the

second control microphone is moved further from the secondary source, but the extent of quiet zone within which the pressure is reduced by more than 10 dB never becomes larger than in the case of a single control microphone.

Cancelling the pressure at one point or two points using a single monopole secondary source can produce a zone of quiet with an extent limited to one tenth of a wavelength of the excitation frequency. Therefore, Ise (1994) used multi-pole secondary sources to cancel the pressure and velocity at several points. He investigated the possibility of ''active impedance control'' to create the zone of quiet. He found that controlling both the pressure and the velocity can produce any shape of the discontinuous layer of acoustic impedance, and this kind of control strategy is more effective than the conventional active noise control techniques that control the pressure alone.

Garcia-Bonito and Elliott (1994) and Elliott and Garcia-Bonito (1995) also investigated the effect of simultaneously cancelling the acoustic pressure and the total particle velocity components in the near field of a secondary source in a diffuse sound field. The secondary source has been modelled as an array of two independent monopoles whose source strengths are adjusted so that the acoustic pressure and the total particle velocity on the axis of the secondary source and the error sensor, at the error sensor location, are cancelled. Results showed that the cancellation of pressure and total particle velocity considerably increases the extension of the zone of quiet with respect to the strategy of simply cancelling the pressure.

The work described above did not consider the optimal arrangement of cancellation points. There might exist some optimal arrangement of cancellation points, which can produce larger quiet zone. Miyoshi *et al* (1994) performed computer simulations to investigate the effects of error microphone arrangements on the size of quiet zones produced by a multi-channel active control system. They showed that the extent of the zones of quiet is dependent upon the separation of the cancellation points. They also showed that the spaces between the cancellation points which produced larger zones of quiet were dependent upon the wavelength and therefore varied with frequency.

Guo and Pan (1995) and Guo *et al* (1997) have also examined the optimal arrangement for secondary sources and the cancellation points. They investigated the

zone of quiet produced by a control system with multiple secondary sources and error microphones in a pure tone sound field, in which both secondary sources and error microphones are equally placed in two parallel lines. A feedforward control mechanism has been assumed, with a reference signal correlated to the output of the primary source. They performed computer simulation and experiments in an anechoic chamber and found that there exists a range of optimal spacing for the secondary sources and error microphones. The control system generated the larger quiet zone and suffered the least increase in total power output in the optimal configuration, i.e. $r_{ss}=r_{ee}=\lambda/2$, where r_{ss} and r_{ee} are the spacing of the secondary sources and the error microphones respectively, and λ is the acoustic wavelength.

The work described above showed how larger zones of quiet can be achieved by cancelling both pressure and particle velocity, or by using multiple cancellation points. All the above approaches used ''cancellation points'' in the process of calculating the best secondary field, i.e. the pressure (or particle velocity) at discrete points near the quiet zones were driven to zero, thus producing lower total pressure at the quiet zone.

In this work a different approach is used in calculating the secondary field. First, the desired spatial extent of the zone of quiet is defined. Then, the secondary field is calculated to minimise the pressure at the desired zone. Both space averaged pressure (2-norm) and maximum pressure (∞-norm) are used as criteria for pressure minimisation. This approach will not necessarily produce a cancellation point, i.e., a point where the total pressure is zero. However, due to the optimal design, the best overall attenuation of sound is achieved in the desired region.

2.3 Control theory

In this section a review of selected fundamental topics in feedback control is presented. This provides a background for the control methods used in this work to actively control sound fields. The reader is referred to Morari and Zafiriou (1989), Doyle *et al* (1992), Franklin *et al* (1994), and Skogestad and Postlethwaite (1996), for further reading.

2.3.1 General feedback system description

A block diagram of a typical feedback control system is shown in Figure 2.1, where C denotes the controller, P is the plant transfer function, d is the disturbance, r is the reference, e is the error, u is the control output and y is the output. The controller determines its output on the basis of the error e. In order to be physically realizable, the transfer functions have to be proper and causal. In a well designed control system the output signal y should track the reference signal r, and the frequency response from r to y, as in equation (2.2), should be close to unity:

$$T = \frac{y}{r} = \frac{PC}{1+PC} \tag{2.2}$$

The function T is called the complementary sensitivity function and is the transfer function between the reference input r and the output y; that is, it is a closed-loop system transfer function. A well designed control system will also keep the output y small for a disturbance input d, and the frequency response from d to y, as in equation (2.3), should be close to zero:

$$S = \frac{y}{d} = \frac{1}{1+PC} \tag{2.3}$$

The function S is called sensitivity function. From equations (2.2) and (2.3) the two functions should obey the relation (Franklin *et al*, 1994)

$$S + T = 1 \tag{2.4}$$

In active control of sound $r = 0$, and the main objective is to reject the disturbances, so the sensitivity function S should be minimised to be as small as possible. In MIMO (multi-input multi-output) systems the frequency response functions and signals are matrices and vectors, respectively, and the following relation can be written (Morari and Zafiriou, 1994):

$$\boldsymbol{S} + \boldsymbol{T} = \boldsymbol{I} \tag{2.5}$$

where $\boldsymbol{S}=[\boldsymbol{I}+\boldsymbol{PC}]^{-1}$, $\boldsymbol{T}=[\boldsymbol{I}+\boldsymbol{PC}]^{-1}\boldsymbol{PC}$ and $\boldsymbol{I}$ is the identity matrix.

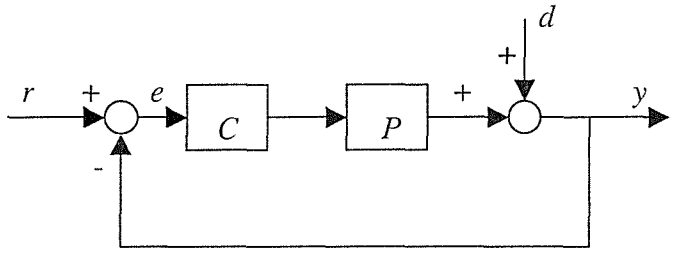

FIGURE 2.1 General block diagram of a feedback control system.

2.3.2 Plant uncertainty and robust stability

Most control system designs are based on a model of the plant; however, it is inevitable that the model we use is only an approximation of the true plant. The difference between the model on which the design is based and the actual plant is referred to generally as plant model uncertainty (Franklin *et al*, 1994). If the design performs well for substantial variation in the dynamics of the plant from the design values, we say the design is robust. Uncertainty can be represented in the form of an additive or multiplicative perturbations. In this work the multiplicative uncertainty model as shown in Figure 2.2 is used as the plant uncertainty description. For the multiplicative case in SISO (single-input single-output) system, the true plant response is (Skogestad and Postlethwaite, 1996)

$$P(j\omega) = P_0(j\omega)\,(1 + B(\omega)\,\Delta(j\omega)) \tag{2.6}$$

where $P_0(j\omega)$ is the frequency response of the plant model, also called the nominal plant, $B(\omega)$ is the uncertainty bound and $\Delta(j\omega)$ is a complex value which satisfies $|\Delta(j\omega)| < 1$. The plant uncertainty at any frequency ω in the Nyquist plane can be described as disc with centre $C(j\omega)P_0(j\omega)$, and a radius $|C(j\omega)P_o(j\omega)|B(\omega)$ as shown in Figure 2.3. The uncertainty bound $B(\omega)$ can be calculated from the measurements as follows.

$$B(\omega) = \max_{P \in \tilde{P}} \left| \frac{P(j\omega)}{P_0(j\omega)} - 1 \right| \tag{2.7}$$

where $\tilde{P}$ is the set of plant measurements. The plant uncertainty in a MIMO system for multiplicative input uncertainty can be written as:

$$\boldsymbol{P}(j\omega) = \boldsymbol{P}_0(j\omega)(\boldsymbol{I} + \boldsymbol{B}(\omega)\,\boldsymbol{\Delta}(j\omega)) \tag{2.8}$$

where $\boldsymbol{P}(j\omega)$ is a plant response matrix, $\boldsymbol{P}_0(j\omega)$ is a nominal model matrix, and $\boldsymbol{\Delta}(j\omega)$ is the perturbation matrix satisfying $\bar{\sigma}(\Delta(j\omega)) < 1$, where $\bar{\sigma}(.)$ represents the largest singular value.

In a feedback control system the plant response may change and the system may become unstable. Therefore a robustly stable system will maintain stability even when the plant response is different from the model used in the design. Consider the Nyquist plot of the perturbed open-loop system in Figure 2.3. The system will remain stable as long as the circle does not enclose the (-1,0) point for all ω (Franklin *et al*, 1994), i.e. the distance between the centre of the circle and the (-1,0) point must be greater than the radius of the circle. This condition can be written as:

$$|1 + P_0(j\omega)C(j\omega)| > |P_0(j\omega)C(j\omega)|B(\omega) \qquad \text{for all } \omega \tag{2.9}$$

$$\Rightarrow |P_0(j\omega)C(j\omega)| / |1 + P_0(j\omega)C(j\omega)| < 1 / B(\omega) \qquad \text{for all } \omega \tag{2.10}$$

The term on the left hand side of equation (2.10) is the nominal complementary sensitivity function, so equation (2.10) can be written as:

$$\left|B(\omega)T_0(j\omega)\right| < 1 \qquad \text{for all } \omega \qquad (2.11)$$

Equation (2.11) can be written in terms of the ∞-norm as (Doyle *et al*, 1992):

$$\left\|B(\omega)T_0(j\omega)\right\|_\infty < 1 \qquad (2.12)$$

This means that the modelling error defines an upper bound on the complementary sensitivity function T_0. This demonstrates the design trade-off, i.e.

when $S \rightarrow 0$, a good disturbance rejection is achieved, and

when $T \rightarrow 0$, robust stability is maintained for large plant uncertainty.

But since $S + T = 1$, both disturbance rejection and robust stability for large plant uncertainties cannot be achieved simultaneously.

For MIMO systems with unstructured multiplicative input uncertainty described in equation (2.8), the robust stability condition can be written as (Skogestad and Postlethwaite, 1996):

$$\bar{\sigma}(\boldsymbol{B}\boldsymbol{T}_0) \leq 1 \qquad (2.13)$$

where $\bar{\sigma}(.)$ represents the largest singular value, $\boldsymbol{T}_0 = (\boldsymbol{I}+\boldsymbol{P}_0\boldsymbol{C})^{-1}\boldsymbol{C}\boldsymbol{P}_0$.

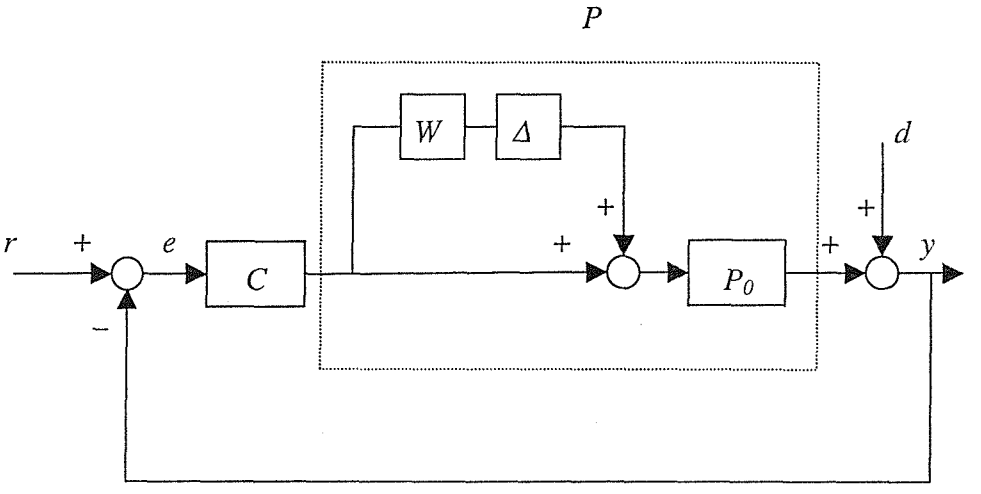

FIGURE 2.2 A general feedback system with multiplicative input plant uncertainty.

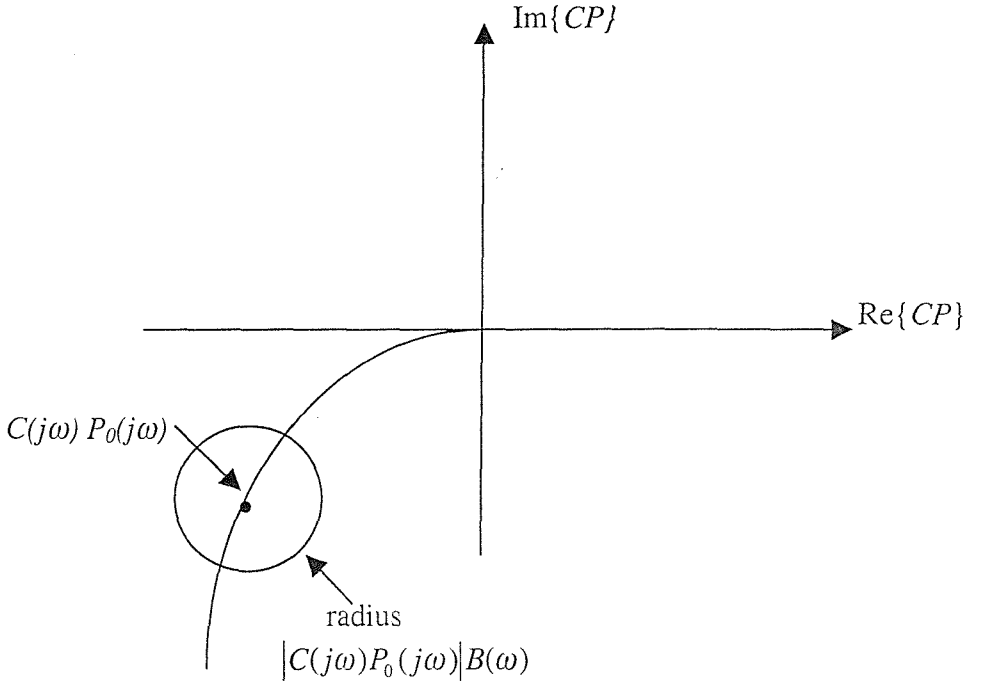

FIGURE 2.3 Nyquist plot of the circle of uncertainty around the nominal point.

2.4 Optimisation theory

Optimisation plays an important role in the design of many active control of sound and vibration. In this section a brief review of selected optimisation methods used in this thesis is presented. These methods will be used in calculating the coefficients of control filters and the optimal values of the secondary source strength. The reader is referred to Fletcher (1987), Grace (1995), and Greig (1980), for further reading.

A general problem description of constrained parametric optimisation can be stated as (Grace, 1995)

$$\begin{aligned} &\underset{x\in R^n}{\text{minimise}}\, f(\boldsymbol{x}) \\ &\text{subject to: } g_i(\boldsymbol{x}) = 0, \quad i = 1,\ldots, m_e \\ &\qquad\qquad g_i(\boldsymbol{x}) \leq 0, \quad i = m_e + 1,\ldots, m \end{aligned} \tag{2.14}$$

Where $\boldsymbol{x}$ is the vector of design parameters, ($x \in R^n$), R^n is the n-dimensional real space, f is the objective function ($f: R^n \Rightarrow R$), and $\boldsymbol{g}$ is the vector of equality and inequality constraints ($g: R^{n\times m} \Rightarrow R^m$). The aim of solving this problem is to find a set of design parameters, $\boldsymbol{x} = \{x_1, x_2, \ldots x_n\}$, which are defined as optimal. In a simple case this may be the minimisation of some system characteristic which is dependent on $\boldsymbol{x}$. In a more advanced formulation the objective function, $f(\boldsymbol{x})$, to be minimized may be subject to constraints which may be in the form of equality constraints, $g_i(\boldsymbol{x}) = 0$ ($i = 1 \ldots m_e$), inequality constraints, $g_i(x) \leq 0$ ($i = m_e + 1 \ldots m$).

An efficient and accurate solution to this problem is not only dependent on the size of the problem in terms of the number of constraints and design variables but also on the characteristics of the objective function and constraints. When both the objective function and the constraints are linear functions of the design variable the problem is known as a Linear Programming problem (LP). Quadratic Programming (QP) concerns the minimisation of a quadratic objective function which is linearly constrained. For both the LP and QP problems reliable solution procedures are readily available. More difficult to solve is the Nonlinear Programming (NP) problem in which the objective function and constraints may be non-linear functions of the design variables. A solution of the NP problem generally requires an iterative procedure to

establish a direction of search at each major iteration. This is usually achieved by the solution of an LP, a QP, or an unconstrained sub-problem.

2.4.1 Unconstrained optimisation

Although a large number of methods exist for unconstrained optimisation, methods can be broadly categorized in terms of the derivative information that is, or is not, used. Search methods which used only function evaluations are most suitable for problems which have a number of discontinuities (Grace, 1995). Gradient methods are generally more efficient when the function to be minimized is continuous in its first derivative. Higher order methods, such as Newton's method, are only really suitable when the second order information is readily and easily calculated since calculation of second order information, using numerical differentiation, is computationally expensive (Grace, 1995).

Gradient methods use information about the slope of the function to dictate a direction of search where the minimum is thought to lie. The simplest of these is the method of steepest descent, in which a search is performed in a direction, $-\nabla f(x)$, where $\nabla f(x)$ is the gradient of the objective function. This method is very inefficient when the function to be minimised has long narrow valleys.

Quasi-Newton Methods: A favoured family of methods which use gradient information, are the quasi-Newton methods. These methods build up curvature information at each iteration to formulate a quadratic model problem of form

$$\underset{x\in R^n}{\text{minimise}} \{f(\boldsymbol{x}) = \frac{1}{2}\boldsymbol{x}^T\boldsymbol{H}\boldsymbol{x}+\boldsymbol{b}^T\boldsymbol{x}+c\} \qquad (2.15)$$

Where the Hessian matrix, $\boldsymbol{H}$, is a positive definite symmetric matrix, $\boldsymbol{b}$ is a constant vector, and c is a constant. The optimal solution for this problem occurs when the partial derivatives of x go to zero, i.e.,

$$\nabla f(\boldsymbol{x}^*) = \boldsymbol{H}\boldsymbol{x}^* + \boldsymbol{b} = 0 \qquad (2.16)$$

The optimal solution point, x^*, can be written as

$$x^* = -H^{-1}b \tag{2.17}$$

The Hessian matrix H can be updated by using BFGS formulation (Broyden, 1970, Fletcher, 1970, Golfarb, 1970, and Shanno, 1970), which is thought to be the most effective for use in a general purpose method of updating the Hessian matrix. The formula is given by

$$H_{k+1} = H_k + \frac{q_k q_k^T}{q_k^T s_k} - \frac{H_k^T H_k}{s_k^T H_k s_k}$$

where $s_k = x_{k+1} - x_k$

$$q_k = \nabla f(x_{k+1}) - \nabla f(x_k) \tag{2.18}$$

As a starting point H_0 can be set to any symmetric, positive definite matrix, for example, the identity matrix, I. To avoid the inversion of the Hessian H you can derive an updating method in which the direct inversion of H is avoided by using a formula which makes an approximation of the inverse Hessian, H^{-1} , at each update (Grace, 1995).

Line Search: Most unconstrained and constrained methods use the solution of a sub-problem to yield a search direction in which the solution is estimated to lie. The minimum along the line formed from this search direction is generally approximated using a search procedure. The problem is to find a new iterate x_{k+1} of the form

$$x_{k+1} = x_k + \alpha^* d \tag{2.19}$$

where x_k denotes the current iterate, d the search direction obtained by an appropriate method and α^* is a scalar step length parameter indicating the distance to the minimum.

2.4.2 Constrained optimisation

In constrained optimisation, the general aim is to transform the problem into an easier sub-problem which can then be solved and used as the basis for an iterative process. A characteristic of a large class of early methods is the translation of the constrained problem to a basic unconstrained problem by using a penalty function for constraints, which are near or beyond the constraint boundary. In this way the constrained problem is solved using a sequence of parameterised unconstrained optimisations, which in the limit converge to the constrained problem. These methods are now considered relatively inefficient and have been replaced by methods which have focused on the solution of the Kuhn-Tucker (KT) equations (Fletcher, 1987). The KT equations are necessary conditions for optimality for a constrained optimisation problem. If the problem is a so-called convex programming problem, that is, $f(x)$ and $g_i(x)$, $i = 1,...m$, are convex functions (Grace, 1995), then the KT equations are both necessary and sufficient for a global solution point. The Kuhn-Tucker equations for equation (2.15) can be stated as

$$\begin{aligned} &\nabla f(x^*) + \sum_{i=1}^{m} \lambda_i^* \nabla g_i(x^*) = 0 \\ &\lambda_i^* g_i(x^*) = 0 \qquad i = 1,..., m_e \\ &\lambda_i^* \geq 0 \qquad\qquad i = m_e + 1,..., m \end{aligned} \tag{2.20}$$

The first equation describes a cancelling of the gradients between the objective function and the active constraints (i.e. g_i=0) at the solution point. In order for the gradients to be cancelled, Lagrangian Multipliers (λ_i, $i = 1,...,m$) are necessary to balance the deviations in magnitude of the objective function and constraint gradients. Since only active constraints are included in this cancelling operation, constraints which are not active must not be included in this operation and so are given Lagrangian multipliers equal to zero. This is stated implicitly in the last two equations of equation (2.20). The solution of the KT equations forms the basis to many nonlinear programming algorithms. These algorithms attempt to compute directly the Lagrangian multipliers. Constrained quasi-Newton methods guarantee fast convergence by accumulating second order information regarding the KT equations using a quasi-Newton updating procedure. These methods are commonly referred to

as Sequential Quadratic Programming (SQP) methods since a QP sub-problem is solved at each major iteration.

Sequential Quadratic Programming (SQP): SQP methods are common in solving nonlinear programming problems (Grace, 1995). The general method can be stated as (Grace, 1995):

"Given the problem description in equation (2.14) the principal idea is the formulation of a QP sub-problem based on a quadratic approximation of the lagrangian function." The lagrangian function is defined as:

$$L(x,\lambda) = f(x) + \sum_{i=1}^{m} \lambda_i g_i(x) \tag{2.21}$$

Here the problem is simplified by assuming that constraints have been expressed as equality constraints. The QP sub-problem is obtained by linearizing the nonlinear constraints, as follows:

$$\begin{aligned} &\underset{d \in R^n}{\text{minimise}} \frac{1}{2} d^T H_k d + \nabla f(x_k)^T d \\ &\nabla g_i(x)^T d + g_i(x) = 0 \qquad i = 1,\ldots, m_e \\ &\nabla g_i(x)^T d + g_i(x) \leq 0 \qquad i = m_{e+1},\ldots, m \end{aligned} \tag{2.22}$$

This sub-problem can be solved using any QP algorithm. The solution is used to form a new iterate.

$$x_{k+1} = x_k + \alpha_k d_k \tag{2.23}$$

The step length parameter, α_k is determined by an appropriate line search procedure. The matrix H_k is a positive definite approximation of the Hessian matrix of the lagrangian function. H_k can be updated by any of the quasi-Newton methods. A nonlinearly constrained problem can often be solved in fewer iterations using SQP than an unconstrained problem. One of the reasons for this is that, due to limits on the

feasible area, the optimiser can make well informed decisions regarding directions of search and step length. The SQP method available in Matlab (Grace, 1995) was used in this work to solve constrained optimisation problems for active sound control.

2.5 Conclusions

A review of selected topics in local active control of sound, control theory and optimisation theory, which serves as a background for the rest of the thesis has been presented. In the local active control section recent work relating to the study of quiet zones has been described. In the control theory section a description of a general feedback system, plant uncertainties and robust stability has been presented which is relevant to the controller design methods introduce in this thesis. The condition for robust stability in the face of multiplicative plant uncertainty was derived. Unconstrained and constrained optimisation have also been described in this chapter which will be used in calculating the optimal values of the secondary sources and optimal values of coefficients of control filters used in the controller design process.

Part II: Local active control of pure tone sound fields

Chapter 3. Theory of pressure minimisation over space

3.1 Introduction

The conventional method of generating a zone of quiet in local active noise control is to cancel the pressure at a point by using a single secondary source. The shape of the quiet zone created by using a single cancellation point and a secondary monopole source is a shell-like volume surrounding the secondary source at low frequencies, and a small volume surrounding the cancellation point at higher frequencies (Ross, 1980). The resulting on-axis pressure around the cancellation point is determined by the near field characteristics of the secondary source, which limits the diameter of the zone of quiet so that they are less than one tenth of a wavelength at the excitation frequency (Joseph, 1990, Joseph et al, 1994, and David et al, 1994). An alternative method in local active noise control is to cancel the pressure or the pressure and particle velocity at some points using multi-pole secondary sources. Cancelling the pressure at several cancellation points could produce larger zones of quiet (Miyoshi et al, 1994, and Guo et al, 1997), however the optimal spacing between the cancellation points is dependent on the wavelength and therefore varies with frequency. Cancelling the pressure and particle velocity could considerably increase the extension of the zone of quiet compared to simply cancelling the pressure (Ise, 1994, Garcia and Elliott, 1994, and Elliott and Garcia, 1995).

All the approaches described above used "cancellation points" in the process of calculating the best secondary field, i.e. the pressure (or particle velocity) at discrete points in the quiet zones was driven to zero, thus producing lower total pressure in quiet zones, but with no control over the shape of quiet zones. In this work a different approach is used in calculating the secondary field. First the desired spatial extend of quiet zones is defined. Then, the secondary field is chosen which minimise the pressure at the quiet zones. Both space averaged pressure (2-norm) and maximum pressure (∞-norm) are used as criteria for pressure minimisation. This approach will not necessarily produce cancellation points, i.e. point where the total pressure is zero. However due to the optimal design, the best overall attenuation of sound is achieved in the desired region.

3.2 General formulation

In this section the formulation of the 2-norm and the ∞-norm pressure minimisation is presented, which is then used for local sound control in a diffuse primary field. In general, the 2-norm of a scalar function g(x) is defined as (Skogestad and Postlethwaite, 1996)

$$\|g(x)\|_2 = \left(\int_{-\infty}^{\infty} |g(x)|^2 dx\right)^{1/2} \tag{3.1}$$

In this work the pressure is minimised over an area, and it is a function of two spatial variables, x and y, so a double integral over x and y would be used. Also, the continuous function of pressure is approximated at finite number of discrete points with spacing much smaller than a wavelength, forming a matrix $\boldsymbol{P}$ of pressure values. The 2-norm of the pressure matrix is now defined as

$$\|\boldsymbol{P}\|_2^2 = \sum_{x_i, y_j \in S} \left|p(x_i, y_j)\right|^2 \tag{3.2}$$

where $p(x_i, y_j)$ is the complex acoustic pressure at position (x_i, y_j) inside the area S at a single excitation frequency and corresponds to the element i, j in matrix $\boldsymbol{P}$. In active control of sound, the total pressure $\boldsymbol{P}$ is composed of primary and secondary components, $\boldsymbol{P}_P$ and $\boldsymbol{P}_S$ respectively, such that $\boldsymbol{P} = \boldsymbol{P}_P + \boldsymbol{P}_S$. The optimal secondary field $\boldsymbol{P}_S$, which minimises the 2-norm of the total pressure in a given area can then be calculated by minimising the sum of squared pressure as follows:

$$\min_{\boldsymbol{P}_S} \|\boldsymbol{P}\|_2^2 = \min_{\boldsymbol{P}_S} \|\boldsymbol{P}_p + \boldsymbol{P}_s\|_2^2 = \min_{\boldsymbol{P}_S} \sum_{x_i, y_j \in S} \left|p_p(x_i, y_j) + p_s(x_i, y_j)\right|^2 \tag{3.3}$$

The 2-norm quiet zone minimisation is performed by first defining the area of the quiet zone, and then for a given geometry computing the strengths of secondary sources which will minimise the sum of square total pressure in the quiet zone. This approach ensures maximum overall reduction in the sound level over the area of the quiet zone.

The ∞-norm of a scalar function g(x) is defined as (Skogestad and Postlethwaite, 1996)

$$\|g(x)\|_\infty = \sup_x |g(x)| \tag{3.4}$$

where sup is the lowest upper limit. The ∞-norm corresponds to the peak magnitude of the function. p(x,y) is evaluated at discrete points to again form the matrix $\boldsymbol{P}$ and the ∞-norm is approximated by the matrix max-norm:

$$\|\boldsymbol{P}\|_\infty = \max_{x_i, y_j \in S} |p(x_i, y_j)| \tag{3.5}$$

The optimal secondary field, $\boldsymbol{P}_S$, which minimises the maximum value of the total pressure, $\boldsymbol{P}$, can be found by:

$$\min_{P_s} \|\boldsymbol{P}\|_\infty = \min_{P_s} \|\boldsymbol{P}_p + \boldsymbol{P}_s\|_\infty = \min_{P_s} \max_{x_i, y_j \in S} |p_p(x_i, y_j) + p_s(x_i, y_j)| \tag{3.6}$$

The ∞-norm quiet zone minimisation will result in minimal peak of the pressure at the quiet zone. This approach ensures that the pressure in the quiet zone has the lowest possible maximum value.

3.3 Control of plane waves

In this section we present the formulations of active noise control in a plane wave primary field using 2-norm and ∞-norm pressure minimisation strategies by introducing one and two secondary monopoles.

We consider a propagating plane wave primary field arriving from any direction. Although the waves occupy a three-dimensional space, the quiet zone analysis is performed, for simplicity, over a two-dimensional area. In this study one and two secondary monopole sources which seek to minimise the primary field at a minimisation area are introduced. Figure 3.1(a) and (b) show the geometry of the problem.

The primary acoustic field pressure, P_p, on the x-y plane can be expressed as (see next section for full derivation)

$$P_p(x,y) = (a+jb)\, exp(-jk(x\, sin\theta\, cos\varphi + y\, sin\theta\, sin\varphi)) \qquad (3.7)$$

where $(a+jb)$ account for the amplitude and phase of this incident plane wave at $(x,y) = (0,0)$, θ is the angle between the direction of propagation and the positive z-axis and φ is the angle between the direction of propagation and the positive x-axis.

The secondary acoustic field pressure on the x-y plane for one secondary monopole can be expressed as

$$P_{s1}(x,y) = A\,\frac{e^{-jkr(x,y)}}{r(x,y)}, \qquad (3.8)$$

where $A = \dfrac{j\omega\rho_0 q}{4\pi}$, with $\omega = 2\pi f$ the angular frequency, ρ_0 is the density of the air, q is the source strength, $r(x,y) = \sqrt{(x^2 + y^2)}$ is the distance between the field point (x,y) and the secondary monopole, and k is the acoustic wavenumber.

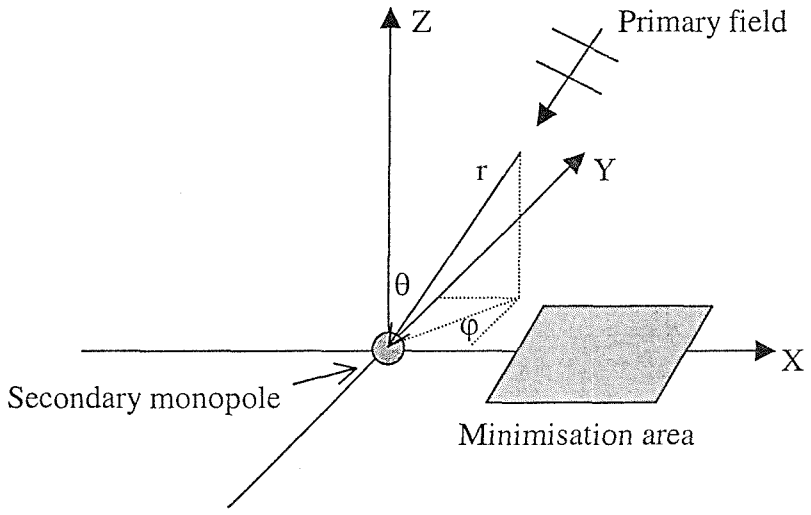

(a)

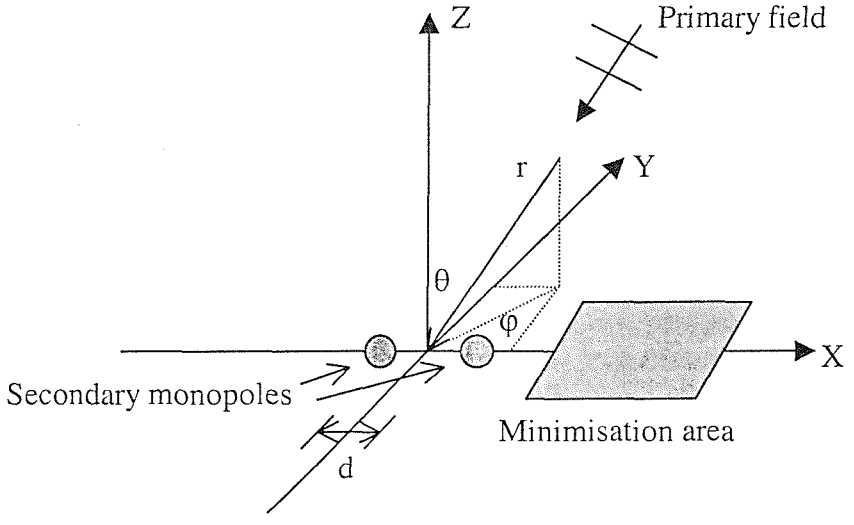

(b)

FIGURE 3.1 Geometry of active sound control in an incident plane wave travelling from any direction. (a) One secondary monopole. (b) Two secondary monopoles.

For two secondary monopoles which are a distance d apart in the x-direction as shown in Figure 3.1 (b). The secondary acoustic field pressure on the x-y plane for two secondary monopoles can be expressed as

$$P_{s2}(x,y) = A_1 \cdot \frac{e^{-jkr_1(x,y)}}{r_1(x,y)} + A_2 \cdot \frac{e^{-jkr_2(x,y)}}{r_2(x,y)} \cdot \qquad (3.9)$$

where in the term describing the first monopole, $A_1 = \frac{j\omega\rho_0 q_1}{4\pi}$, q_1 the source strength and $r1(x,y) = \sqrt{(x-d/2)^2 + y^2}$ is the distance between the field point *(x,y)* and the secondary monopole. For the second monopole $A_2 = \frac{j\omega\rho_0 q_2}{4\pi}$, and $r2(x,y) = \sqrt{(x+d/2)^2 + y^2}$ is the distance between the field point *(x,y)* and the second secondary monopole. The total acoustic pressures at a field point due to a primary plane wave and one secondary monopole can be expressed as

$$P_{T1}(x,y) = P_p(x,y) + A\frac{e^{-jkr(x,y)}}{r(x,y)}, \tag{3.10}$$

and for two secondary monopoles:

$$P_{T2}(x,y) = P_p(x,y) + A_1 \cdot \frac{e^{-jkr_1(x,y)}}{r_1(x,y)} + A_2 \cdot \frac{e^{-jkr_2(x,y)}}{r_2(x,y)}, \tag{3.11}$$

where $P_{T1}(x_i,y_j)$ and $P_{T2}(x_i,y_j)$ are the total acoustic pressures within the minimisation area.

For 2-norm pressure minimisation the cost function for one secondary monopole can be expressed as

$$J_{21} = \sum_{x_i,y_j \in S} \left|P_{T1}(x_i,y_j)\right|^2 = \sum_{x_i,y_j \in S} \left|P_p(x_i,y_j) + A \cdot \frac{e^{-jkr(x_i,y_j)}}{r(x_i,y_j)}\right|^2, \tag{3.12}$$

and with two secondary monopoles:

$$J_{22} = \sum_{x_i,y_j \in S} \left|P_{T2}(x_i,y_j)\right|^2 = \sum_{x_i,y_j \in S} \left|P_p(x_i,y_j) + A_1 \cdot \frac{e^{-jkr_1(x_i,y_j)}}{r_1(x_i,y_j)} + A_2 \cdot \frac{e^{-jkr_2(x_i,y_j)}}{r_2(x_i,y_j)}\right|^2 \tag{3.13}$$

We can find the optimal values of A, A_1 and A_2 which minimise the cost functions J_{21} and J_{22} by using the function fmins( ) in MATLAB (Grace, 1995), or analytically by converting equations (3.12) and (3.13) to an Hermitian quadratic form (Nelson and Elliott, 1992).

Substituting the optimal values A_0, A_{10} and A_{20} into equations (3.10) or (3.11), we can calculate the controlled field. The reduction $R(x,y)$ in the 2-norm of the sound pressure in the zone of quiet is then calculated as the ratio of the total (controlled) squared pressure, and the primary squared pressure, as follows:

$$R(x,y) = \frac{\left|P_T(x,y)\right|^2}{\left|P_p(x,y)\right|^2}. \tag{3.14}$$

For ∞-norm minimisation strategy, we want to minimise a cost function

$$J_{\infty 1} = \left\|P_{T1}(x_i,y_j)\right\|_\infty = \left\|P_p(x_i,y_j) + A\frac{e^{-jkr(x_i,y_j)}}{r(x_i,y_j)}\right\|_\infty$$

$$= \max_{x_i,y_j \in S}\left|P_p(x_i,y_j) + A\frac{e^{-jkr(x_i,y_j)}}{r(x_i,y_j)}\right| \tag{3.15}$$

for one monopole secondary source, and

$$J_{\infty 2} = \left\|P_{T2}(x_i,y_j)\right\|_\infty = \left\|P_p(x_i,y_j) + A_1\frac{e^{-jkr_1(x_i,y_j)}}{r_1(x_i,y_j)} + A_2\frac{e^{-jkr_2(x_i,y_j)}}{r_2(x_i,y_j)}\right\|_\infty$$

$$= \max_{x_i,y_j \in S}\left|P_p(x_i,y_j) + A_1\frac{e^{-jkr_1(x_i,y_j)}}{r_1(x_i,y_j)} + A_2\frac{e^{-jkr_2(x_i,y_j)}}{r_2(x_i,y_j)}\right| \tag{3.16}$$

for two monopole secondary sources.

This ∞-norm minimisation can be written as a linear minimisation problem with ∞-norm constraint, i.e.

for one monopole

$$\begin{aligned} &\textit{Minimise} \quad \sigma \\ &\textit{Subject to} \quad \left\| P_{T1}(x,y) \right\|_{\infty} < \sigma \end{aligned} \tag{3.17}$$

and for two monopoles

$$\begin{aligned} &\textit{Minimise} \quad \sigma \\ &\textit{Subject to} \quad \left\| P_{T2}(x,y) \right\|_{\infty} < \sigma \end{aligned} \tag{3.18}$$

where $P_{T1}(x,y)$ and $P_{T2}(x,y)$ are the total acoustic pressure within the minimisation area, and σ is a real scalar parameter used in the optimisation process. The optimal values of A, A_1 and A_2 can be calculated using the function constr( ) in MATLAB (Grace, 1995). The reduction for ∞-norm minimisation is the same as in equation (3.14).

3.4 Control of diffuse fields

In this section the wave model of a diffuse primary sound field is derived first, and then the formulation of 2-norm and ∞-norm minimisation strategies to control the diffuse primary field is presented.

3.4.1 The wave model of a diffuse primary sound field

Local control in enclosed sound fields is investigated in this work. We therefore assume that the primary sound field is diffuse. Garcia-Bonito (Garcia, 1996) used the wave model for a diffuse field, which is comprised of large number of propagating waves arriving from various directions. However, a complete mathematical derivation of this model, which was taken from Jacobson (Jacobsen, 1979), was not found. For completeness, this mathematical derivation is given below.

When a source produces sound in an enclosure, the sound field is composed of two fields. One is the sound field radiated directly from the source called the direct sound field. The other is reflection of sound waves from surfaces of the enclosure, which contributes to the overall sound field, this contribution being known as the reverberant field. Therefore at any point in the room, the sound field is a function of direct and reverberant sound fields. The sound field in a reverberant space can be divided into two frequency ranges. In the low frequency range, the room response is dominated by standing waves at certain frequencies. In the high frequency range, the resonances become so numerous that they are difficult to distinguish from one another. For excitation frequencies greater than the Schroeder frequency, for which $M(\omega) = 3$, where $M(\omega)$ is the modal overlap (Jacobsen, 1979), the resulting sound field is essentially diffuse and may be described in statistical terms or in terms of its average properties. The diffuse sound field model can be derived as follows.

In the model described below, the diffuse field is comprised of many propagating waves with random phases, arriving from uniformly distributed directions. Although the waves occupy a three-dimensional space, the quiet zone analysis is performed, for simplicity, over a two-dimensional area.

Consider a single incident plane wave travelling along line r with its wave front parallel to lines A and B as shown in Figure 3.2. We assume that the plane wave has some phase when approaching line A, and has some phase shift due to the time delay when approaching line B both on the x-y plane. We next find the phase of the plane wave at (x_0,y_0) on line B.

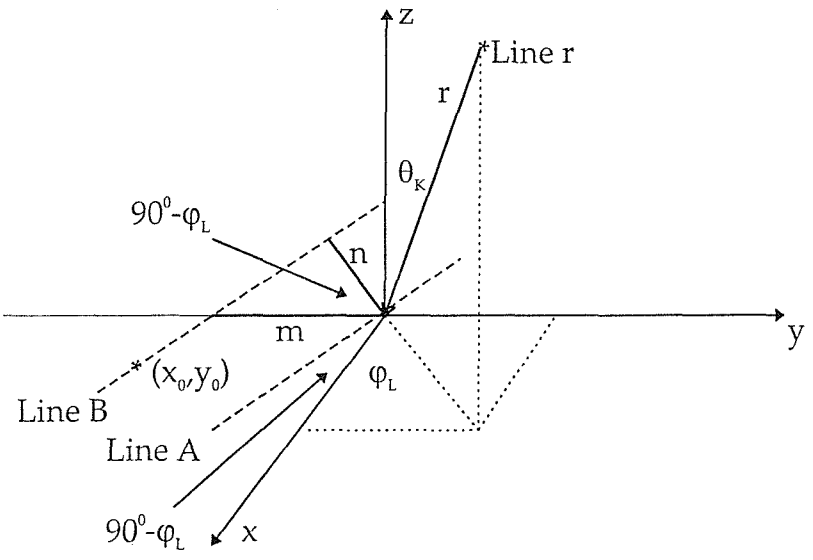

Figure 3.2 Definition of spherical co-ordinates r, θ, φ for an incident plane wave travelling alone line r direction.

We now consider the plane perpendicular to lines A and B and parallel to line r, as illustrated in figure 3.3.

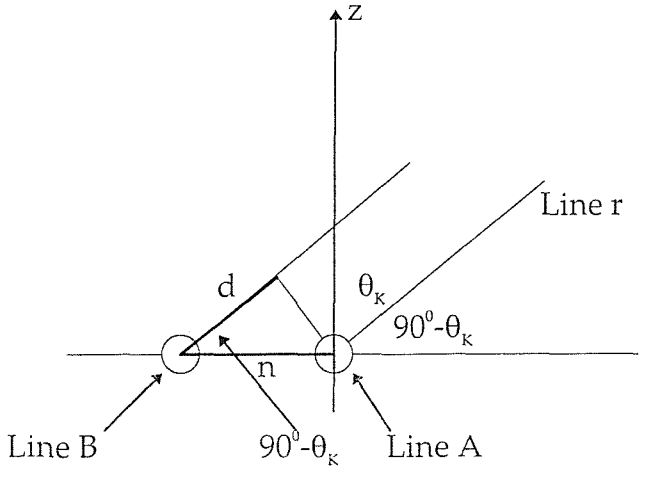

Figure 3.3 The plane perpendicular to lines A and B and parallel to line r.

This incident plane wave has phase shift when approaching point (x_0,y_0) on line B. The pressure at this point can therefore be expressed as (Jacobsen, 1979)

$$P(x_0,y_0) = (a+jb) \exp(-jkd) \tag{3.19}$$

where a+jb account for the amplitude and phase of this incident plane wave when approaching line A, and d is the additional distance travelled by the plane wave when approaching point (x_0,y_0) on line B as shown in figure 3.3.

The equation of line A on the x-y plane can be written as

$$y = - x \tan(90^0-\varphi_L) = -x \cot\varphi_L \tag{3.20}$$

The equation of line B on x-y plane can also be written using figure 3.2 as

$$y = - x \tan(90^0-\varphi_L) + m = - x \cot\varphi_L - m \tag{3.21}$$

where m is the distance between lines A and B on the y-axis.

Substituting (x_0,y_0) into equation (3.21) gives

$$m = - y_0 - x_0 \cot\varphi_L \tag{3.22}$$

The distance n between lines A and B as in figure 3.2 can now be calculated as

$$n = m \cos(90^0-\varphi_L)$$

$$= m \sin \varphi_L \tag{3.23}$$

Substituting equation (3.22) into equation (3.23), the distance n becomes

$$n = - y_0 \sin \varphi_L - x_0 \cos \varphi_L \tag{3.24}$$

The distance d in figure 3.3 can now be calculated as

$$d = n \cos (90^0 - \theta_K)$$

$$= n \sin \theta_K \qquad (3.25)$$

Equation (3.24) can be substituted into equation (3.25) and the distance d becomes

$$d = - y_0 \sin \theta_K \sin \varphi_L - x_0 \sin \theta_K \cos \varphi_L \qquad (3.26)$$

Therefore equation (3.19) can be written as

$$P(x_0,y_0) = (a+jb) \exp(jk(y_0 \sin \theta_K \sin \varphi_L + x_0 \sin \theta_K \cos \varphi_L)) \qquad (3.27)$$

In our study we chose 72 such incident plane waves together with random amplitudes and phases to generate an approximation of a diffuse sound field in order to coincide with that in previous work[3.12]. Thus the diffuse sound field was generated by adding together the contributions of 12 plane waves in the azimuthal directions (corresponding to azimuthal angles $\varphi_L = L \times 30^0$, L=1,2,3, . . . , 12) for each of six vertical incident directions (corresponding to vertical angles $\theta_K = K \times 30^0$ for K = 1, 2, 3, . . . , 6). The net pressure in the point (x_0,y_0) on the x-y plane due to the superposition of these 72 plane waves was then calculated from the expression

$$P_p(x_0,y_0) = \sum_{K=1}^{K\max} \sum_{L=1}^{L\max} (a_{KL} + jb_{KL}) \sin\theta_K \exp(jk(x_0 \sin\theta_K \cos\varphi_L + y_0 \sin\theta_K \sin\varphi_L)) \qquad (3.28)$$

in which both the real and imaginary parts of the complex pressure are randomly distributed. The values of a_{KL} and b_{KL} are chosen from a random population with Gaussian distribution N(0,1) and the multiplicative factor $\sin\theta_K$ is included to ensure that, on average, the energy associated with the incident waves was uniform from all directions. Each set of 12 azimuthal plane waves arriving from a different vertical direction θ_K , is distributed over a length of $2\pi r \sin\theta_K$, which is the circumference of the sphere defined by (r,φ,θ) for θ_K. This results in higher density of waves for

smaller θ_K , and thus more energy associated with small θ_K . To ensure uniform energy distribution, the amplitude of the waves is multiplied by $\sin\theta_K$, thus making the waves coming from the ''dense'' direction, lower in amplitude.

Equation (3.28) will be used for diffuse primary sound field in the simulations presented in the next chapter. Next we will describe the formulation of the 2-norm and ∞-norm optimisation techniques, and their use in design of diffuse field quiet zones.

3.4.2 Formulation of 2-norm and ∞-norm pressure minimisation to control the diffuse primary sound field

The design of quiet zones using 2-norm and ∞-norm minimisation is studied in this work by assuming that the secondary field is produced by monopole sources. Although this is not an accurate model of practical sources, it simplifies the design procedure and assists comparison with previous studies. Although the formulation is similar to that of plane wave field, we present it here for completeness. We start, for simplicity, by considering one secondary source located at the origin. The total acoustic pressure at a field point a distance r from the origin due to both the diffuse primary field and the single secondary monopole can be expressed as

$$p_T(x,y) = p_p(x,y) + A\,\frac{e^{-jkr(x,y)}}{r(x,y)}\,, \qquad (3.29)$$

where $p_p(x,y)$ is the complex pressure due to the diffuse primary field at the point (x,y), $A = \dfrac{j\omega\rho_0 q}{4\pi}$, with $\omega = 2\pi f$ the angular frequency, ρ_0 is the density of the air, q is the source strength, $r(x,y) = \sqrt{(x^2 + y^2)}$ is the distance between the field point (x,y) and the secondary monopole, and k is the acoustic wavenumber.

For two secondary monopoles which are a distance d apart in the x-direction as shown in Figure 3.4, the total acoustic pressure at a field point a distance r from the origin

due to both the diffuse primary field and the two secondary monopoles can be expressed as

$$p_T(x,y) = p_p(x,y) + A_1 \frac{e^{-jkr_1(x,y)}}{r_1(x,y)} + A_2 \frac{e^{-jkr_2(x,y)}}{r_2(x,y)}, \tag{3.30}$$

where in the term describing the first monopole, $A_1 = \frac{j\omega\rho_0 q_1}{4\pi}$, q_1 the source strength and $r_1(x,y) = \sqrt{(x-d/2)^2 + y^2}$ is the distance between the field point *(x,y)* and the secondary monopole. For the second monopole $A_2 = \frac{j\omega\rho_0 q_2}{4\pi}$, and $r_2(x,y) = \sqrt{(x+d/2)^2 + y^2}$ is the distance between the field point *(x,y)* and the secondary monopole. The results can then easily be extended for a larger number of secondary sources.

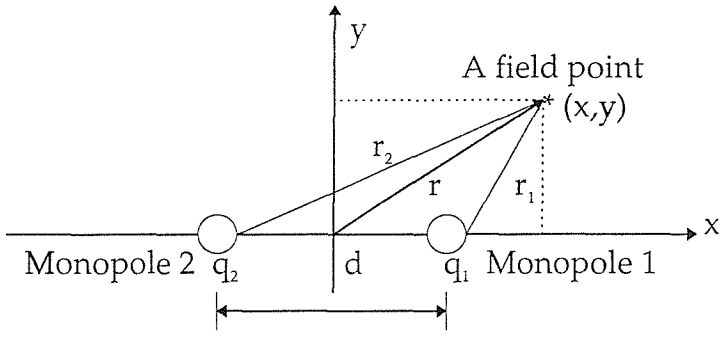

Figure 3.4 Configuration of active noise control using two secondary monopole sources.

The minimisation cost function for the 2-norm pressure minimisation using two secondary monopoles is therefore written by substituting equation (3.30) into equation (3.3) as

$$J_2 = \sum_{x_i, y_j \in S} \left| p_T(x_i, y_j) \right|^2 = \sum_{x_i, y_j \in S} \left| p_p(x_i, y_j) + A_1 \frac{e^{-jkr_1(x_i, y_j)}}{r_1(x_i, y_j)} + A_2 \frac{e^{-jkr_2(x_i, y_j)}}{r_2(x_i, y_j)} \right|^2 \quad (3.31)$$

where $p_T(x_i,y_j)$ is the total acoustic pressure within the minimisation area as described in equation (3.30). We can find the optimal values of the complex variables A_1 and A_2 which minimise the cost function J_2 by using the function fmins( ) in MATLAB (Grace, 1995), or analytically by converting equation (3.31) to an Hermitian quadratic form (Nelson and Elliott, 1992).

Substituting the optimal values of A_1 and A_2 into equation (3.30), we can calculate the controlled field, $P_T(x,y)$, for each diffuse field sample (as described at the beginning of this section) generated using equation (3.28) at each position (x,y) in the quiet zone. The average reduction $R(x,y)$ in the 2-norm of the sound pressure in the zone of quiet for many samples of the diffuse field is then calculated as the ratio of the mean total (controlled) squared pressure, and the mean primary squared pressure, as follows:

$$R(x,y) = \frac{\overline{\left| p_T(x,y) \right|^2}}{\overline{\left| p_p(x,y) \right|^2}} \quad (3.32)$$

For ∞-norm pressure minimisation, the following cost function is minimised:

$$J_\infty = \max_{x_i, y_j \in S} \left| p_T(x_i, y_j) \right| = \max_{x_i, y_j \in S} \left| p_p(x_i, y_j) + A_1 \frac{e^{-jkr_1(x_i, y_j)}}{r_1(x_i, y_j)} + A_2 \frac{e^{-jkr_2(x_i, y_j)}}{r_2(x_i, y_j)} \right| \quad (3.33)$$

This ∞-norm minimisation which is a convex optimisation problem, i.e. it has a unique solution (Gonzalez et al, 1998), can be rewritten as linear minimisation problem with ∞-norm constraint (Vandenberghe and Boyd, 1996), i.e.

$$\begin{aligned} &\textit{Minimise} \quad \sigma \\ &\textit{Subject to} \quad J_\infty < \sigma \end{aligned} \quad (3.34)$$

where σ is a real scalar parameter used in the optimisation process.

The optimal values of A_1 and A_2 can be calculated using the function *constr( )* in MATLAB (Grace, 1995). The method used here to calculate the average zones of quiet is similar to that described in the 2-norm minimisation procedure. In this work only 2-dimensional zones of quiet were considered. The algorithm to calculate the quiet zones could be easily extended to 3-dimensional zones of quiet, although the computation will be more time-consuming. For the 3-dimensional zones of quiet considered in this chapter, the quiet zones on the x-z plane should be the same as those on the x-y plane due to the rotational symmetry of the secondary field around the x-axis.

3.5 Other minimisation formulations

This section presents some minimisation formulations which include constraints for limiting sound amplification and an area maximisation.

3.5.1 Constraint for limiting sound amplification

The 2-norm and ∞-norm methods described above did not constrain the amplification of sound pressure level. They might cause some amplification outside the zone of quiet. Therefore an amplification constraint could be added into the minimisation process. In this work a amplification constraint was added into the minimisation process to avoid the 10 dB amplification at some points outside the zone of quiet. The 10 dB amplification constraint is as follows.

$$10 \log_{10} \frac{\overline{\left|p_T(x,y)\right|^2}}{\left|p_p(x,y)\right|^2} < 10 \text{ dB}$$ at some points close to secondary monopoles outside the zone of quiet. (3.35)

All the approaches described above used minimisation of sound pressure level. The sound pressure level is minimised as low as possible at some predefined areas. However the size of the 10 dB quiet zone was not taken into the consideration in the

optimisation process. In the next section we will describe area maximisation theory equivalent to maximising the size of the 10 dB quiet zone.

3.5.2 Maximisation of 10 dB quiet zone area

In this section we present a proposal for an area maximisation method which maximises the size of the 10 dB quiet zone. The principle of area maximisation is to maximise the area of the 10 dB zone of quiet. The formulation of area maximisation is as follows.

Maximising A

$$\textbf{Subject to} \quad 10\log_{10}\frac{\overline{\left|p_T(x,y)\right|^2}}{\overline{\left|p_p(x,y)\right|^2}} < -10 \text{ dB} \text{ inside the area } A \qquad (3.36)$$

where A is the area of the quiet zone. This approach ensures that the area of the 10 dB quiet zone is maximised. In this work we investigated quiet zones by using the area maximisation procedure as follows.

a. Set the initial and final values of x and y for the area of the quiet zone.
b. Maximise the area of the quiet zone by increasing the initial and final values of x and y.
c. Repeat (b) until the equation (3.36) is satisfied with the maximum area of the quiet zone.

The results show that poor performance is achieved. This is probably since the optimisation problem is not convex. Therefore the optimal solution to the problem has not been found. Development of such method using convex optimisation is proposed for future work.

3.5.3 Pressure minimisation over a line in space

In sections 3.3 and 3.4 we presented the pressure minimisation over an area in space for plane wave and diffuse primary fields respectively. However some useful zones of quiet could be achieved by minimising the acoustic pressure over a line. The formulation for pressure minimisation over a line is the same as that in pressure minimisation over an area, but the minimisation area should change to the minimisation line.

3.5 Conclusions

In this chapter we presented the general formulation for 2-norm and ∞-norm minimisation strategies over space, which included pressure minimisation over a given area. This is in contrast to the conventional method, which used pressure or pressure and particle velocity cancellation at a point. There are no cancellation points within the minimisation area in this method and the best overall attenuation of sound could be achieved due to the optimal design. The formulations for other minimisation methods were proposed which included the constraint for limiting sound amplification, area maximisation and pressure minimisation over a line. In the next chapter a series of local control simulations will be presented using 2-norm and ∞-norm pressure minimisation over various areas and lines by introducing one, two and three secondary sources.

Chapter 4. Simulations and experiments of pressure minimisation over space and point cancellation

4.1 Introduction

In this chapter we evaluate the performance of sound minimisation for local active control by using 2-norm and ∞-norm pressure minimisation strategies through computer simulations and experiments. Plane waves and diffuse fields are used as the primary fields. The results are compared with those created by using the pressure or the pressure and particle velocity cancellation. Previous work showed that the zones of quiet created by cancelling the pressure and particle velocity at one point were larger than those created by cancelling the pressure only at one point in the primary diffuse field (Elliott and Garcia, 1995). However in this work minimising the pressure over an area using 2-norm pressure minimisation strategy by introducing two secondary monopoles creates larger zones of quiet than those created by using the pressure and particle velocity cancellation at one point. This chapter is presented as follows. In section 4.2 we first show the quiet zones created by using 2-norm and ∞-norm pressure minimisation strategies to minimise the pressure over an area by introducing one and two secondary monopoles in the primary plane wave field and comparing to those created by cancelling the pressure or the pressure and particle velocity at one point. Then in section III zones of quiet created by using 2-norm and ∞-norm strategies minimising the pressure over various areas in the primary diffuse field are shown and compared with those created by cancelling the pressure and particle velocity at one point. The local control experiment and some initial results are presented in section IV. Finally the chapter is then concluded in section V.

4.2 Quiet zone simulations in a primary plane wave field

In this section quiet zones created by using 2-norm and ∞-norm minimisation strategies to minimise the pressure over an area in a primary plane wave field by introducing one and two secondary monopoles are presented. The primary field is a plane wave propagating along the positive x-axis. The excitation frequency of 108 Hz is used for the primary plane wave. The results are also compared to those created by cancelling the pressure or the pressure and particle velocity at one point. The model of the plane wave and minimisation formulations described in chapter 3 are used in the simulations. The model of the primary field used in the simulations can be expressed (see chapter 3).

$$P_p(x,y) = (a+jb)\, exp(-jk(x\, sin\theta\, cos\varphi + y\, sin\theta\, sin\varphi)) \qquad (4.1)$$

where $(a+jb)$ account for the amplitude and phase of this incident plane wave at $(x,y) = (0,0)$, θ, the angle between the direction of propagation and the positive z-axis, is 90 degrees, and φ, the angle between the direction of propagation and the positive x-axis, is 180 degrees.

The formulation used in the simulations for the cost function of 2-norm pressure minimisation for one secondary monopole can be expressed (see chapter 3)

$$J_{21} = \sum_{x_i,y_j \in S} \left|P_{T1}(x_i,y_j)\right|^2 = \sum_{x_i,y_j \in S} \left|P_p(x_i,y_j) + A \cdot \frac{e^{-jkr(x_i,y_j)}}{r(x_i,y_j)}\right|^2, \qquad (4.2)$$

and with two secondary monopoles:

$$J_{22} = \sum_{x_i,y_j \in S} \left|P_{T2}(x_i,y_j)\right|^2 = \sum_{x_i,y_j \in S} \left|P_p(x_i,y_j) + A_1 \cdot \frac{e^{-jkr_1(x_i,y_j)}}{r_1(x_i,y_j)} + A_2 \cdot \frac{e^{-jkr_2(x_i,y_j)}}{r_2(x_i,y_j)}\right|^2 \qquad (4.3)$$

where $P_{T1}(x_i,y_j)$ and $P_{T2}(x_i,y_j)$ are the total acoustic pressures within the minimisation area.

We can find the optimal values of A, A_1 and A_2 which minimise the cost function J_{21} and J_{22} by using the function fmins( ) in MATLAB (Grace, 1995). In the simulations the spatial resolution at the x-axis and y-axis is 120 points.

In the first simulation zones of quiet for one secondary monopoles case are presented. Figure 4.1 shows the 10 dB reduction contour line for 2-norm minimisation (solid line) of the pressure in an area represented by the rectangular frame. The 10 dB reduction contour line for cancelling the acoustic pressure (dash-dot line) at location (0.25,0) marked by '+' is also shown in this figure. The secondary monopole source is marked as a '*'. The 10 dB amplification in the acoustic pressure for 2-norm minimisation (dashed line) and cancelling the pressure at a point (dotted line) are also shown in Figure 4.1. It can be seen that the zone of quiet created by using 2-norm strategy minimising the pressure over an area is similar to that created by cancelling the pressure at one point. This is since only two parameters, magnitude and phase, could be controlled in one secondary monopole. Therefore the zones of quiet are very similar for both cases.

In this simulation the magnitude of the primary, secondary and controlled fields along the x-axis is also investigated through computer simulations. Figures 4.2 (a) and (b) show the spatial variation of the primary, secondary and controlled fields along the x-axis for cancelling the pressure at the point (0.25,0) and for minimising the pressure at an area as shown in Figure 4.1 respectively. We notice that the secondary and primary fields are equal at the cancellation point for both cases. Therefore the zone of quiet is the same in both cases.

In the second simulation zones of quiet for the two monopoles case are presented. Figure 4.3 shows the 10 dB reduction contour line (solid curve) for the 2-norm strategy minimising the pressure over an area represented by a rectangular frame. The 10 dB reduction contour line for the acoustic pressure and particle velocity cancellation (dash-dot line) at location (0.25,0) is also shown in this figure. The two secondary monopoles located at (0.05,0) and (-0.05,0) are marked by '*'. The 10 dB amplification is also shown for the 2-norm minimisation strategy (dashed line) and for cancelling the pressure and particle velocity at one point (dotted line). Figure 4.3

shows that 2-norm strategy minimising the pressure over an area produces a larger zone enclosed by the 10 dB reduction contour compared with that created by cancelling the pressure and particle velocity at one point. The reason for this is because the 2-norm strategy is to minimise the sum of the squared pressure over the whole minimisation area resulting in the optimal secondary field over the area. However the secondary field at the cancellation point only is controlled for cancelling the pressure and particle velocity at one point. Therefore the 2-norm strategy creates a larger zone of quiet than that created by cancelling the pressure and particle velocity at one point.

The magnitude of the pressure fields along the x-axis only is also investigated through the simulations. Figures 4.4 (a) and (b) show the spatial variation of the primary, secondary and controlled fields generated in the simulations above for cancelling the pressure and particle velocity at one point and minimising the pressure over an area by using 2-norm strategy. We can see that there is a dip location on the controlled field at the cancellation point for cancelling the pressure and particle velocity at one point. This is because the controlled field is zero at that point. However 2-norm strategy is to minimise the sum of the squared pressure difference between the primary and secondary fields over the whole area. Therefore the controlled field in 2-norm computation is flatter than that in cancelling the pressure and particle velocity at one point.

In the next simulation zones of quiet created by using ∞-norm minimisation to minimise the acoustic pressure at an area are investigated. The optimisation process used in the simulation is as follows (see chapter 3).

Minimise σ

$$\textit{Subject to } \left\|P_{T2}(x,y)\right\|_{\infty} = \max_{x_i,y_j \in S}\left|P_p(x_i,y_j) + A_1\frac{e^{-jkr_1(x_i,y_j)}}{r_1(x_i,y_j)} + A_2\frac{e^{-jkr_2(x_i,y_j)}}{r_2(x_i,y_j)}\right| < \sigma \quad (4.4)$$

where $P_{T2}(x,y)$ are the total acoustic pressure within the minimisation area, and σ is a real scalar parameter used in the optimisation process. The optimal values of A_1 and A_2 can be calculated using the function constr( ) in MATLAB (Grace, 1995).

Figure 4.5 shows the same configuration as in Figure 4.3 for minimising the acoustic pressure over an area by using 2-norm and ∞-norm strategies. As can be seen the zone of quiet created by using ∞-norm strategy is smaller and closer to secondary monopoles than that created by using 2-norm computation. This is due to the fact that ∞-norm is to minimise the maximum pressure within the minimisation area. The pressure at some area within the minimisation area is difficult to control. The secondary monopoles need to focus on this area resulting in reducing the performance at other locations.

Figure 4.6 shows the magnitude of the primary, secondary and controlled fields for ∞-norm pressure minimisation. It can be seen that the secondary and primary fields overlap around the point (0.2,0). Therefore the zone of quiet is closer to secondary monopole and smaller in this case, since the closer the location where the secondary and primary fields overlap the smaller the quiet zone.

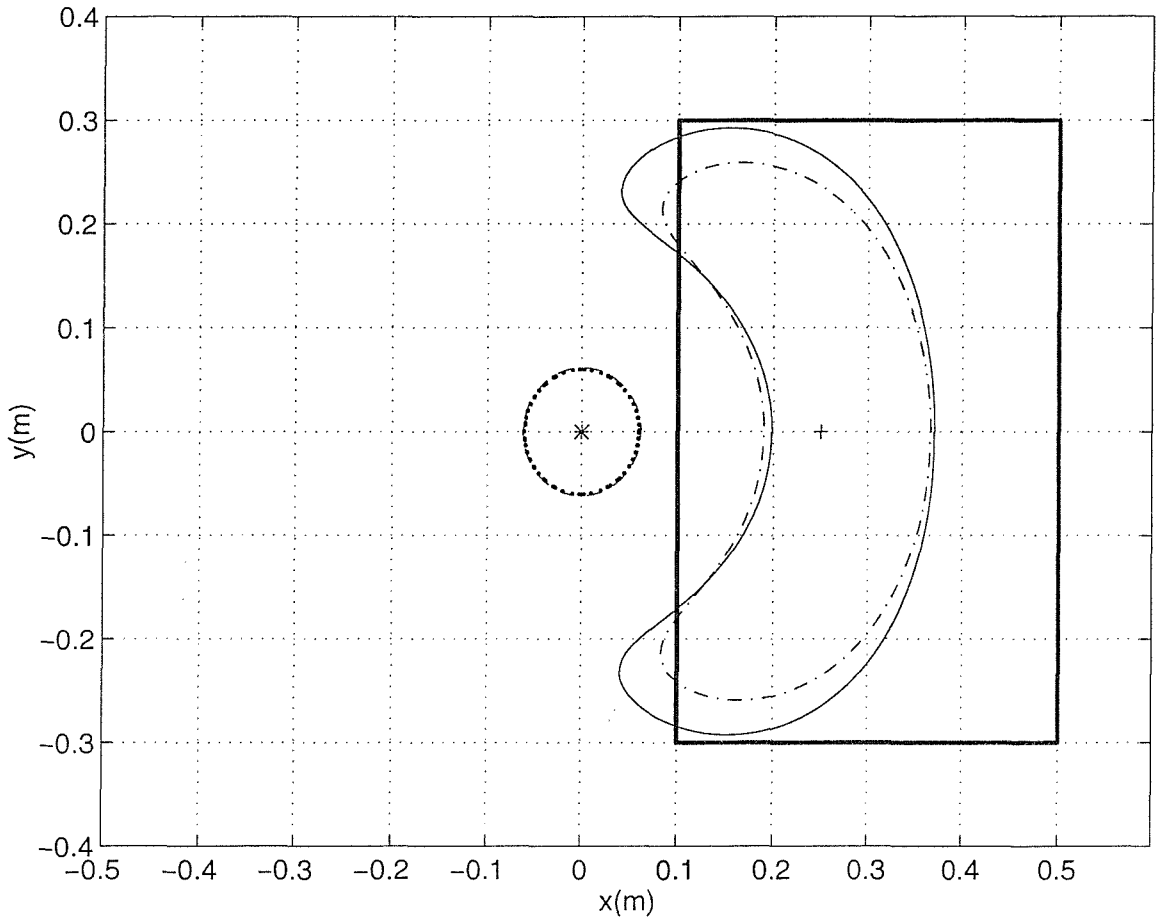

FIGURE 4.1. The 10 dB reduction contour of the zone of quiet created by a secondary monopole source located at position (0,0), cancelling the acoustic pressure at (0.25,0) point (-.-.-.) and minimising the acoustic pressure at an area represented by a bold rectangular frame using 2-norm minimisation strategy (____), and the 10 dB amplification in the acoustic pressure of the plane primary field for cancelling the pressure at one point (. . . . .) and for minimising the pressure at a large area (- - - - -). The primary field is a plane wave propagating along the positive x-axis.

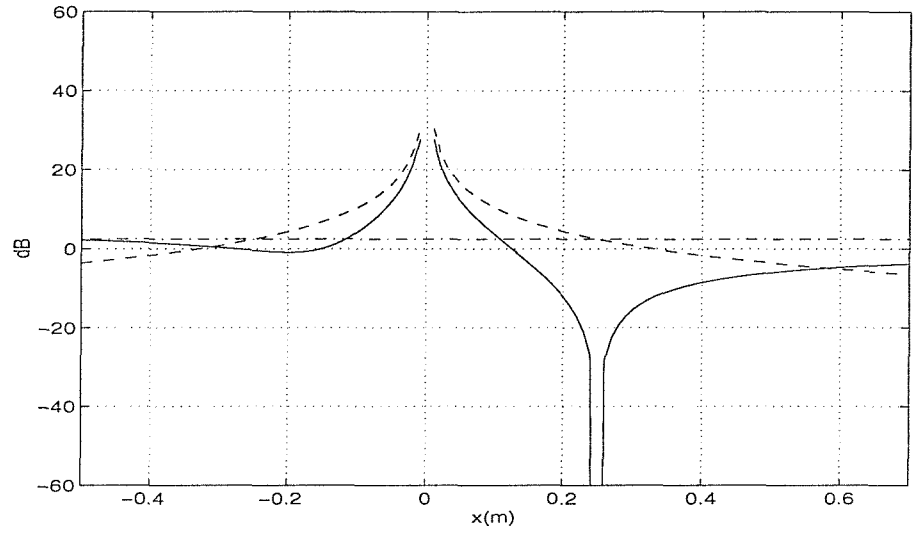

(a)

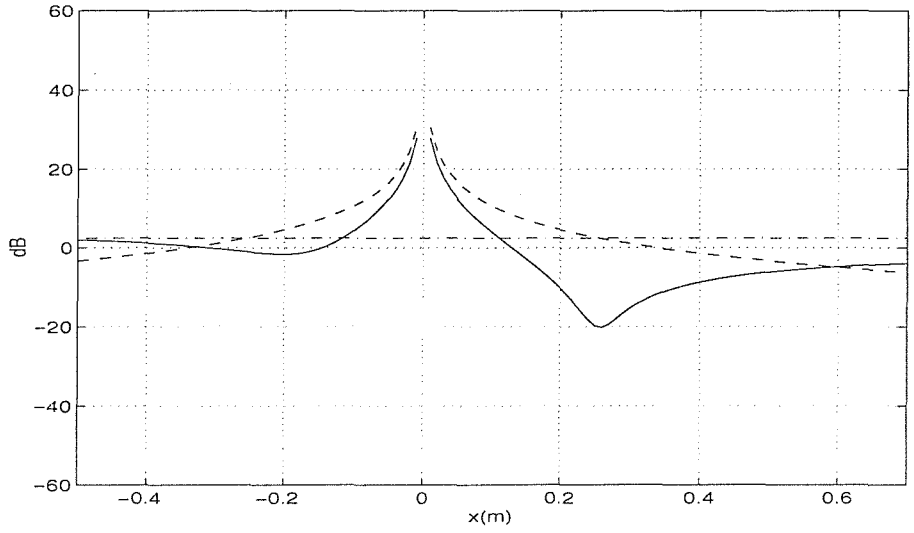

(b)

FIGURE 4.2 The squared pressure for primary field (-.-.-.), secondary field (- - - - -) and controlled field (———). (a) Cancelling the acoustic pressure at point (0.25,0). (b) Minimising the acoustic pressure at a rectangular area using the 2-norm minimisation strategy.

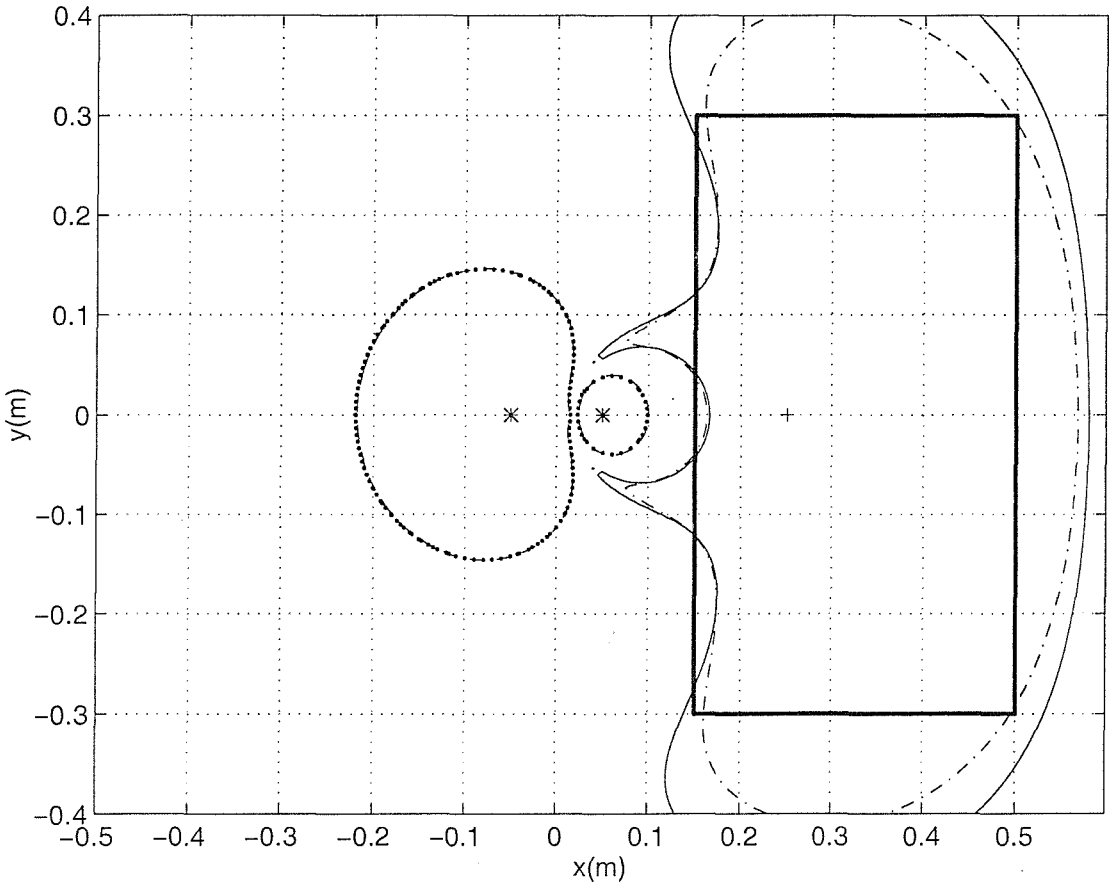

FIGURE 4.3. The 10 dB reduction contour of the zones of quiet created by two secondary monopole sources located at positions (0.05,0) and (-0.05,0) minimising the acoustic pressure at an area represented by a bold rectangular frame using 2-norm minimisation strategy (——) and cancelling the acoustic pressure and particle velocity at (0.25,0) point (-.-.-.), and the 10 dB increase in the primary field for 2-norm minimisation strategy (- - - - -) and cancelling the acoustic pressure and particle velocity at one point (. . . . .). The primary field is a plane wave propagating along the positive x-axis.

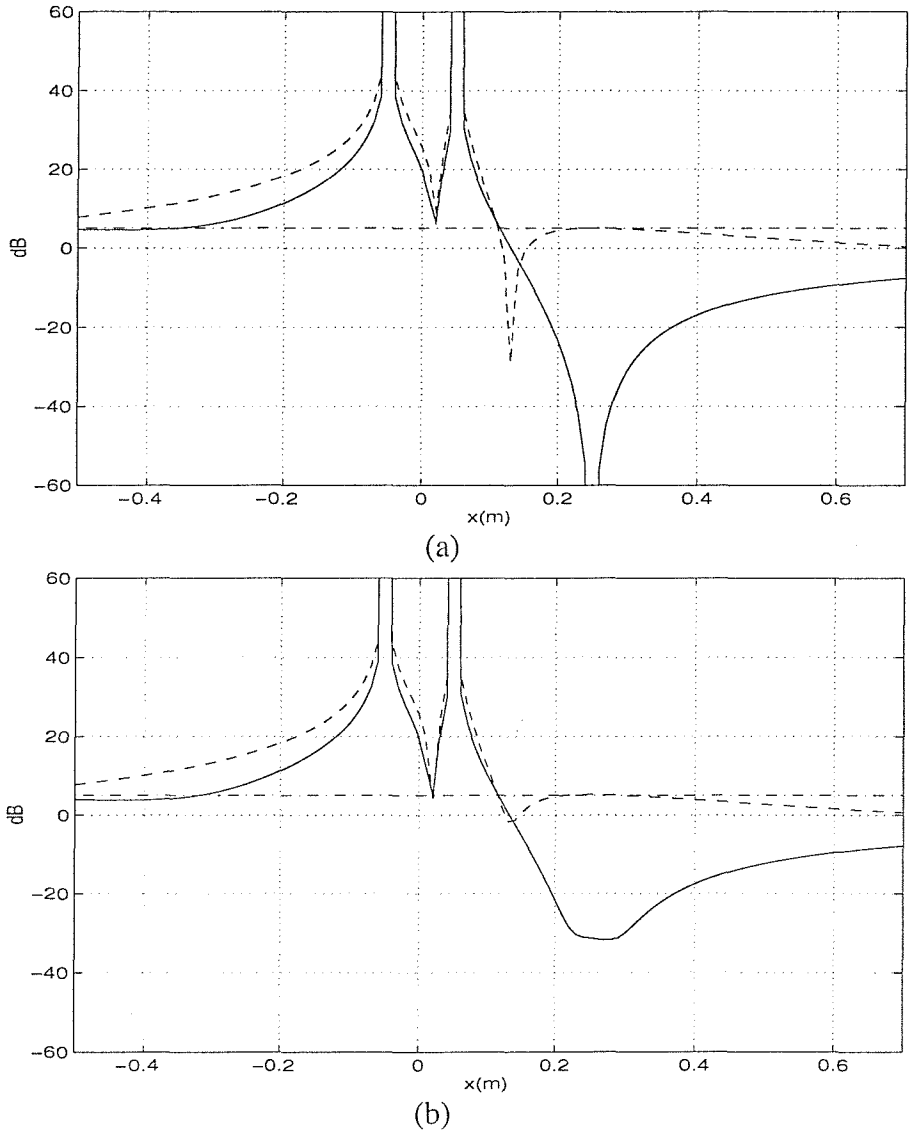

FIGURE 4.4. The squared pressure for primary field (-.-.-.), secondary field (- - - - -) and controlled field (_____). (a) Cancelling the acoustic pressure and particle velocity at point (0.25,0). (b) Minimising the acoustic pressure at a rectangular area using the 2-norm minimisation strategy.

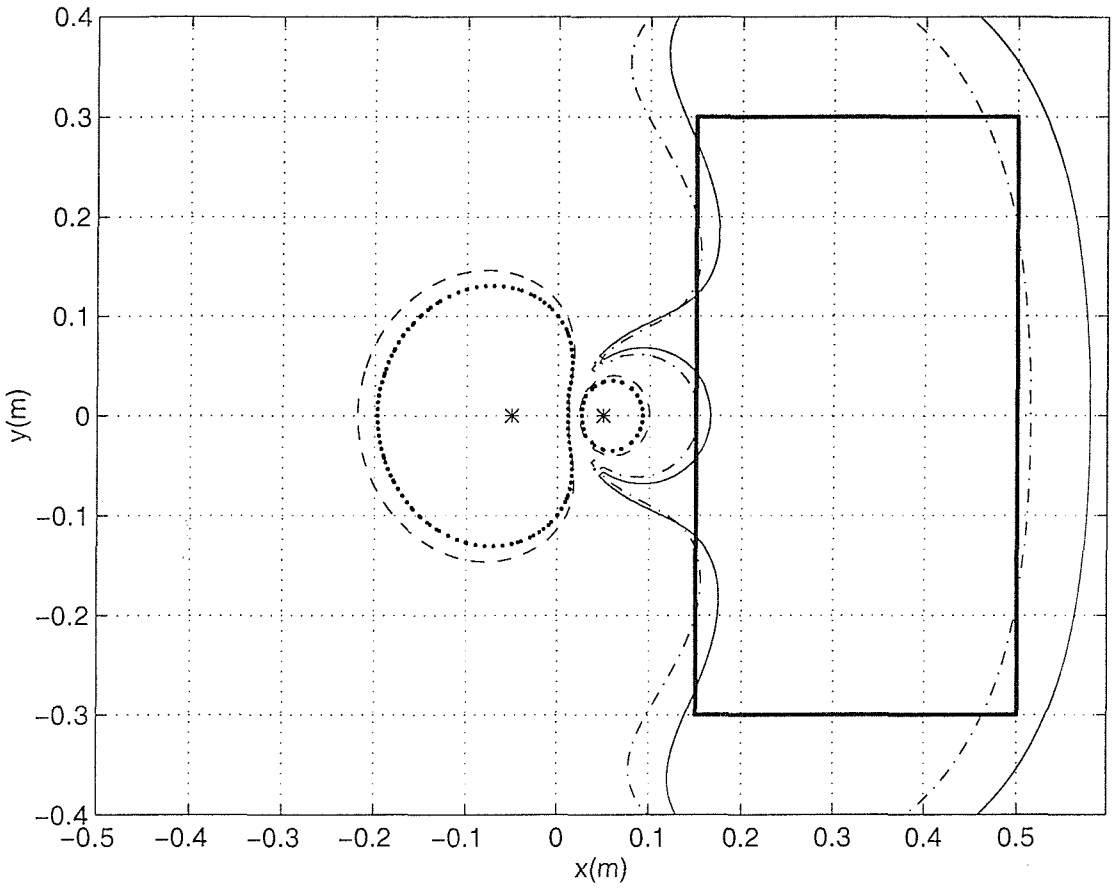

FIGURE 4.5. The 10 dB reduction contour of the zones of quiet created by two secondary monopole sources located at positions (0.05,0) and (-0.05,0) minimising the acoustic pressure at an area represented by a bold rectangular frame, using 2-norm minimisation strategy (——) and using ∞-norm minimisation strategy (-.-.-.).The primary field is a plane wave propagating along the positive x-axis.

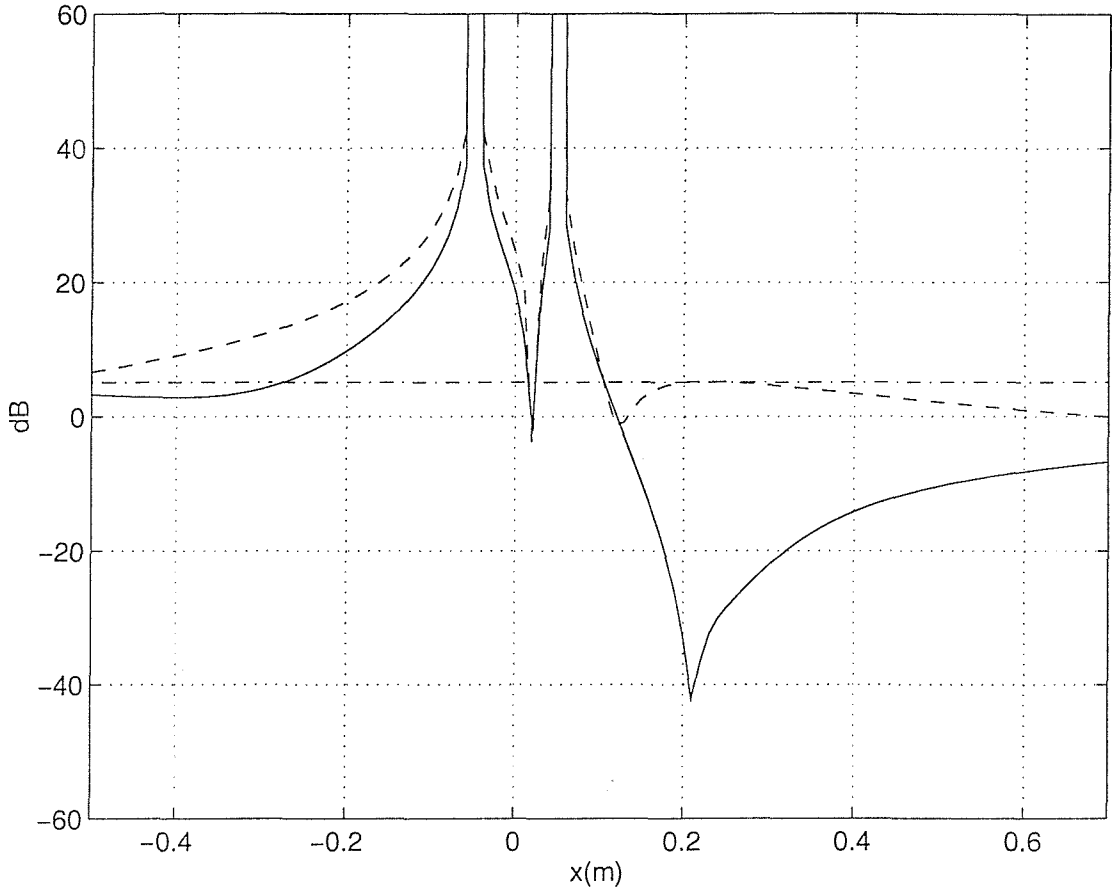

FIGURE 4.6 The squared pressure for primary field (-.-.-.), secondary field (- - - - -) and controlled field (_____) for minimising the acoustic pressure at a rectangular area using the ∞-norm minimisation strategy.

4.3 Quiet zone simulations in a primary diffuse field

In this section the simulated average zones of quiet created by one, two or three monopole secondary sources seeking to minimise the 2-norm and ∞-norm of the total acoustic pressure at various areas in a pure tone diffuse primary field are presented, and then compared to those obtained by cancelling the acoustic pressure or the acoustic pressure and particle velocity at one point. The average quiet zones are obtained from 50 samples of the primary diffuse fields. The spatial resolution is the same as the previous section. The model of the primary diffuse field used in the simulations was generated by adding together the contributions of 12 plane waves in the azimuthal directions (corresponding to azimuthal angles $\varphi_L = L \times 30^0$, L=1,2,3, . . . , 12) for each of six vertical incident directions (corresponding to vertical angles $\theta_K = K \times 30^0$ for K = 1, 2, 3, . . . , 6). Therefore the net pressure in the point (x_0,y_0) on the x-y plane due to the superposition of these 72 plane waves was then calculated from the expression (see chapter 3)

$$P_p(x_0,y_0) = \sum_{K=1}^{K\max} \sum_{L=1}^{L\max} (a_{KL} + jb_{KL}) \sin\theta_K \exp(-jk(x_0\sin\theta_K \cos\varphi_L + y_0\sin\theta_K\sin\varphi_L)) \quad (4.5)$$

The way to calculate the optimal values of the strength of the secondary monopoles is similar to that in previous section.

In the first simulation, the zone of quiet created using a single monopole source is computed using 2-norm pressure minimisation and compared to that created by cancelling the acoustic pressure at a single point. A pure tone diffuse primary field for kL=0.6 is generated in this case, where L is the distance from the secondary monopole to the cancellation point, k the acoustic wavenumber, and for L=0.3m, as shown in figures, this will correspond to an excitation frequency of 108 Hz. Figure 4.7 shows the 10 dB reduction contour line for 2-norm minimisation (solid line) of the pressure in an area represented by the rectangular frame. Also shown is the 10 dB reduction contour line for cancelling the acoustic pressure (dash-dot line) at location (0.3,0) marked by '+'. The secondary monopole source is marked as a '*'. The 10 dB

amplification in the acoustic pressure for 2-norm minimisation (dashed line) and cancelling the pressure at a point (dotted line) are also shown in Figure 4.7. Figure 4.7 shows that the zone of quiet created by using 2-norm pressure minimisation over this carefully selected area is similar to that created by cancelling the acoustic pressure at a point. This is due to the fact that the secondary field produced by a single monopole is in both cases a symmetrically decaying field, which is controlled by only two parameters, the source strength and the phase, resulting in the design method having little effect on the optimal secondary field shape in this case. The shape of the quiet zone changes with kx when cancelling the acoustic pressure at a single point, as has been discussed in previous papers (Joseph et al, 1994, and Garcia, 1996).

A single secondary monopole can only produce a symmetrically decaying field. If two secondary monopoles are used, four parameters can be adjusted and more complicated secondary fields can be produced. Therefore larger zones of quiet could be obtained. In the next simulations two secondary monopoles are introduced, minimising the acoustic pressure at various areas using the 2-norm computation. The zones of quiet are then compared to those designed by cancelling the acoustic pressure and particle velocity at a point (Garcia and Elliott, 1994, and Elliott and Garcia, 1995), and those created by minimising the acoustic pressure using the ∞-norm.

Figure 4.8 shows the 10 dB reduction contour line (solid curve) for the 2-norm minimisation with the minimisation area represented by the bold rectangular frame. Also shown is the 10 dB reduction contour line for the case in which the acoustic pressure and particle velocity are cancelled (dash-dot line) at location (0.3,0). The two secondary monopoles located at (0.05,0) and (-0.05,0) are marked by '*'. The 10 dB amplification is also shown for the 2-norm minimisation strategy (dashed line) and for cancelling the acoustic pressure and particle velocity at one point (dotted line). Previous work showed that cancelling the acoustic pressure and particle velocity at one point by introducing two secondary monopoles created larger zones of quiet than those created by cancelling the acoustic pressure at one point only using a single secondary monopole (Garcia and Elliott, 1994, and Elliott and Garcia, 1995). This finding is confirmed from the comparison between Figures 4.7 and 4.8. However Figure 4.8 shows that minimising the acoustic pressure over an area by using 2-norm

minimisation produces a larger zone enclosed by the 10dB reduction contour compared to that created when cancelling the acoustic pressure and particle velocity at one point. This is because the two secondary monopoles in the 2-norm computation attempt to minimise the sum of squared pressure over an area, so the amplitude of the secondary field is as close as possible to the amplitude of the primary field with the opposite phase over the complete minimisation area. This is in contrast to cancelling the acoustic pressure and the particle velocity at one point, where the secondary field parameters at that point only are controlled. The size of the 10 dB amplification of the diffuse primary field is slightly smaller for 2-norm computation and the magnitude of the strength of the secondary sources, A_1 and A_2 as in equation (3.31) in chapter 3, for 2-norm computation is about 3dB smaller than those when cancelling the acoustic pressure and particle velocity. This reflects the fact that the control effort of the secondary monopoles for the 2-norm computation is smaller in this case.

In order to observe the spatial variation of the primary, secondary and controlled fields generated in the simulations above, the magnitude of the pressure fields along the x-axis only is investigated. Figure 4.9 (a) shows the three fields for cancelling the pressure and particle velocity, and Figure 4.9 (b) for minimising the 2-norm of the pressure, both as presented in Figure 4.8. Comparing these results, we notice that the secondary and primary fields overlap around the cancellation point for the case of two secondary sources cancelling the acoustic pressure and particle velocity at this point. Therefore the controlled field is zero at location (0.3,0) for this case. This is since perfect cancellation is achieved at the cancellation point. However the 2-norm minimisation strategy is to minimise the sum of the squared pressure difference between the primary and secondary fields over the whole minimisation area, so the controlled field is flatter than that produced by cancelling the acoustic pressure and particle velocity at one point. The zone of quiet is therefore larger in this case. Notice that no cancellation point, or a point of zero controlled pressure is obtained in this case.

The result in Figure 4.10 shows the contour lines of 10dB reduction in the sound pressure level calculated using the 2-norm minimisation strategy (solid line, as in Figure 4.8), and ∞-norm minimisation strategy (dash-dot line). The pressure inside the

rectangular frame shown in Figure 4.8 was minimised using two secondary monopoles located at (0.05,0) and (-0.05,0) in a pure tone diffuse primary field of 108 Hz. We observe that the minimisation of the acoustic pressure by using 2-norm minimisation creates a larger 10dB reduction contour than that with ∞-norm minimisation. This is due to the fact that in the ∞-norm minimisation the highest acoustic pressure from all the points within the minimisation area is minimised. The acoustic pressure at some regions within the area is difficult to control. The extra effort required to minimise the pressure at these areas reduces the performance at other locations. This is in contrast to the 2-norm minimisation, where the sum of squared pressure at the minimisation area is minimised, and the effect of a small area on the average pressure is small. Table 1 shows that the 2-norm strategy produces 9.3dB reduction in 2-norm of the pressure within the minimisation area. However ∞-norm strategy produces 8.4dB reduction in 2-norm of the pressure within the minimisation area. The table also shows that the 2-norm strategy produces only 4.8dB reduction in ∞-norm of the pressure and ∞-norm strategy produces 5.9dB reduction in the ∞-norm of the pressure.

The effect of different minimisation regions and shapes on the size of the 10dB reduction contours created by the 2-norm minimisation strategy has also been investigated in this study. Figures 4.11 (a) and (b) show the contour lines of 10dB reduction in the sound pressure level calculated using 2-norm minimisation (solid line) for different minimisation regions, as represented by the bold rectangular frames. It can be seen that the locations of the 10dB reduction contour change with the minimisation regions as expected. Figures 4.12 (a) and (b) show the 10dB reduction contour created by 2-norm minimisation for different minimisation shapes. It can be seen that the shapes of the quiet zone change with the minimisation shapes. In Figure 4.12 (a) the quiet zone has a narrow shape in x-axis direction and longer in y-axis direction similar to the minimisation area. When the minimisation area changes to be narrower in y-axis direction and longer in x-axis direction, the quiet zone tends to extend its size in the x-axis direction as shown in Figure 4.12 (b). Therefore the locations and shapes of the quiet zones can be designed using 2-norm minimisation in a way which is not possible using pressure and pressure gradient cancellation.

The zone of quiet created by introducing three secondary monopoles using 2-norm minimisation has also been explored. Figure 4.13 shows the 10 dB reductions in the pressure level (solid line) for 2-norm minimisation of the pressure in an area represented by the bold rectangular frame. The three secondary monopoles are located at (0,0), (0.05,0) and (-0.05,0) represented by '*', and the 10 dB amplification in the acoustic pressure of the diffuse primary field is represented by a dashed line. Figure 4.13 shows that three secondary monopoles create a significantly larger zone of quiet than that in the two secondary monopoles case. However the size of the 10 dB amplification in the acoustic pressure away from the zone of quiet is also larger in this case. This shows that larger number of secondary sources provide better control over the secondary field, with the potential of producing larger zones of quiet at required locations.

All the simulations performed above are pressure minimisation in an area. In this chapter other pressure minimisations have also been investigated through computer simulations. First the pressure minimisation at a line using 2-norm strategy is presented. Figure 4.14 shows the 10 dB reduction contour line (solid curve) for the 2-norm minimisation with the minimisation line represented by the bold line. Also shown is the 10 dB reduction contour line for the case in which the acoustic pressure is minimised (dash-dot line) at an area represented by the bold rectangular frame. The 10 dB amplification is also shown for the line minimisation (dashed line) and for area minimisation (dotted line). It can be seen that the quiet zone created by line minimisation is longer along the x-axis and narrower along the y-axis around the location close to the secondary monopoles than that created by area minimisation. This suggests that area minimisation creates more round shape of quiet zones. Also the 10dB amplification obtained by using area minimisation is smaller than that obtained by using line minimisation.

In this work pressure minimisation over an area with the constraint on the 10dB amplification has also been performed. Figure 4.15 shows the 10dB reduction contour line (dash-dot curve) for the ∞-norm strategy minimising the pressure at an area represented by a bold rectangular frame with the constraint on the 10dB amplification at (-0.15,0), (-0.05,0.09) and (-0.05,-0.09) points and without the constraint (solid

curve). Also shown is the 10dB amplification with the constraint (doted curve) and without the constraint (dashed curve). As can be seen the size of the 10dB amplification with amplification constraint is smaller than that without the amplification constraint, and 10dB amplification constraint is met at the three points for the case with the amplification constraint. However the zone of quiet created by ∞-norm strategy with the constraint on 10dB amplification is smaller than that created without the constraint. This means that if the pressure amplification is constrained at some locations the zone of quiet would be smaller than that without the amplification constraint.

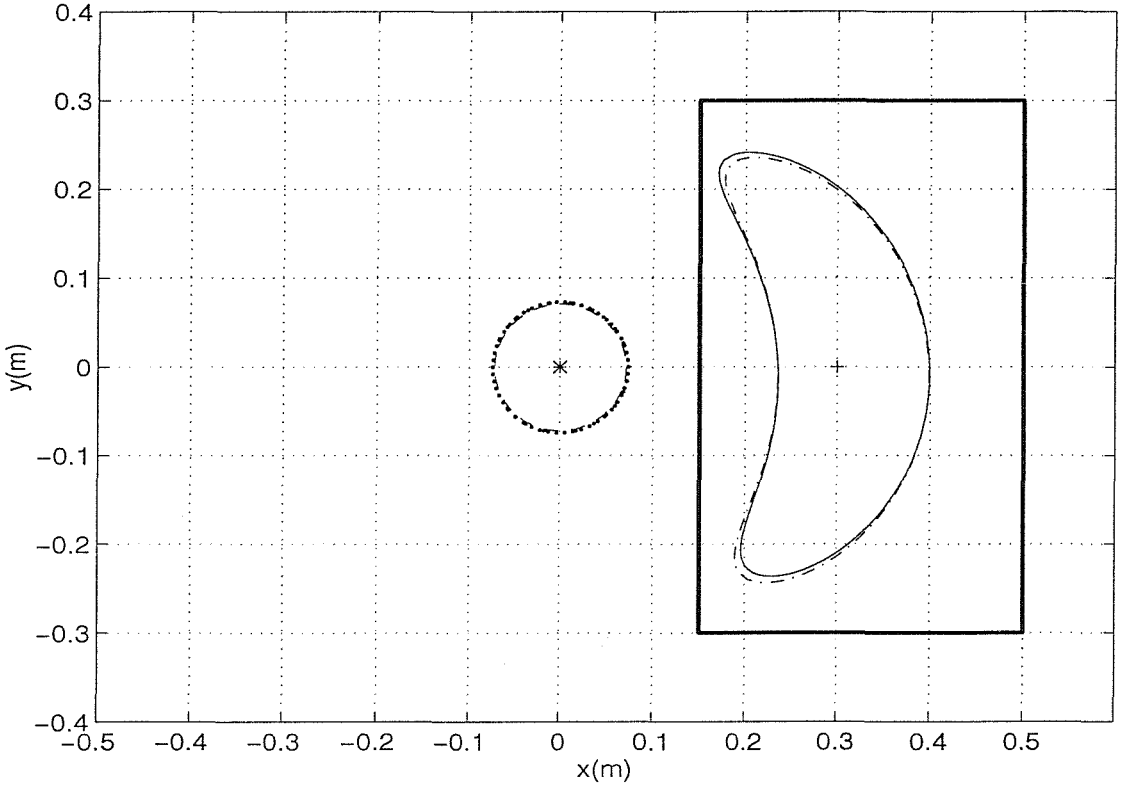

FIGURE 4.7. The 10 dB reduction contour of the average zone of quiet created by a secondary monopole source located at position (0,0), cancelling the acoustic pressure at (0.3,0) point (-.-.-.) and minimising the acoustic pressure at an area represented by a bold rectangular frame using 2-norm minimisation strategy (——), and the 10 dB amplification in the acoustic pressure of the diffuse primary field for cancelling the pressure at one point (. . . . .) and for minimising the pressure at a large area (- - - - -).

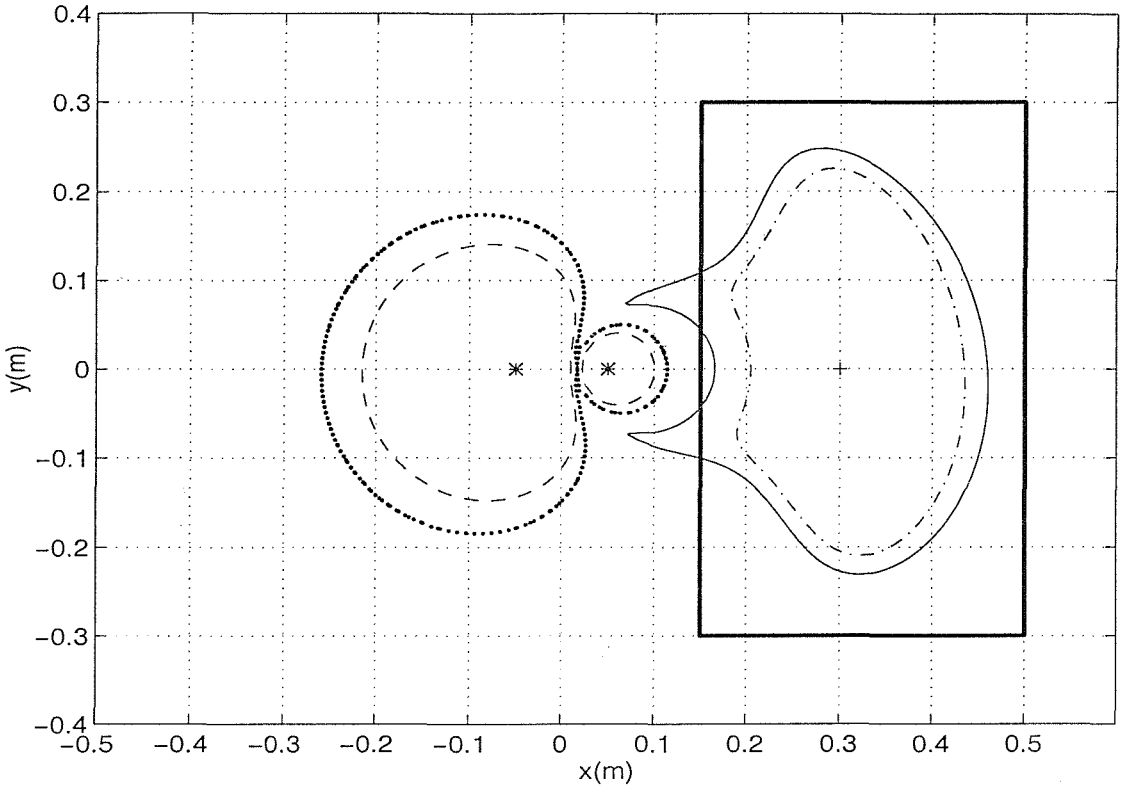

FIGURE 4.8. The 10 dB reduction contour of the average zones of quiet created by two secondary monopole sources located at positions (0.05,0) and (-0.05,0) minimising the acoustic pressure at an area represented by a bold rectangular frame using 2-norm minimisation strategy (———) and cancelling the acoustic pressure and particle velocity at (0.3,0) point (-.-.-.), and the 10 dB increase in the primary field for 2-norm minimisation strategy (- - - - -) and cancelling the acoustic pressure and particle velocity at one point (. . . . .).

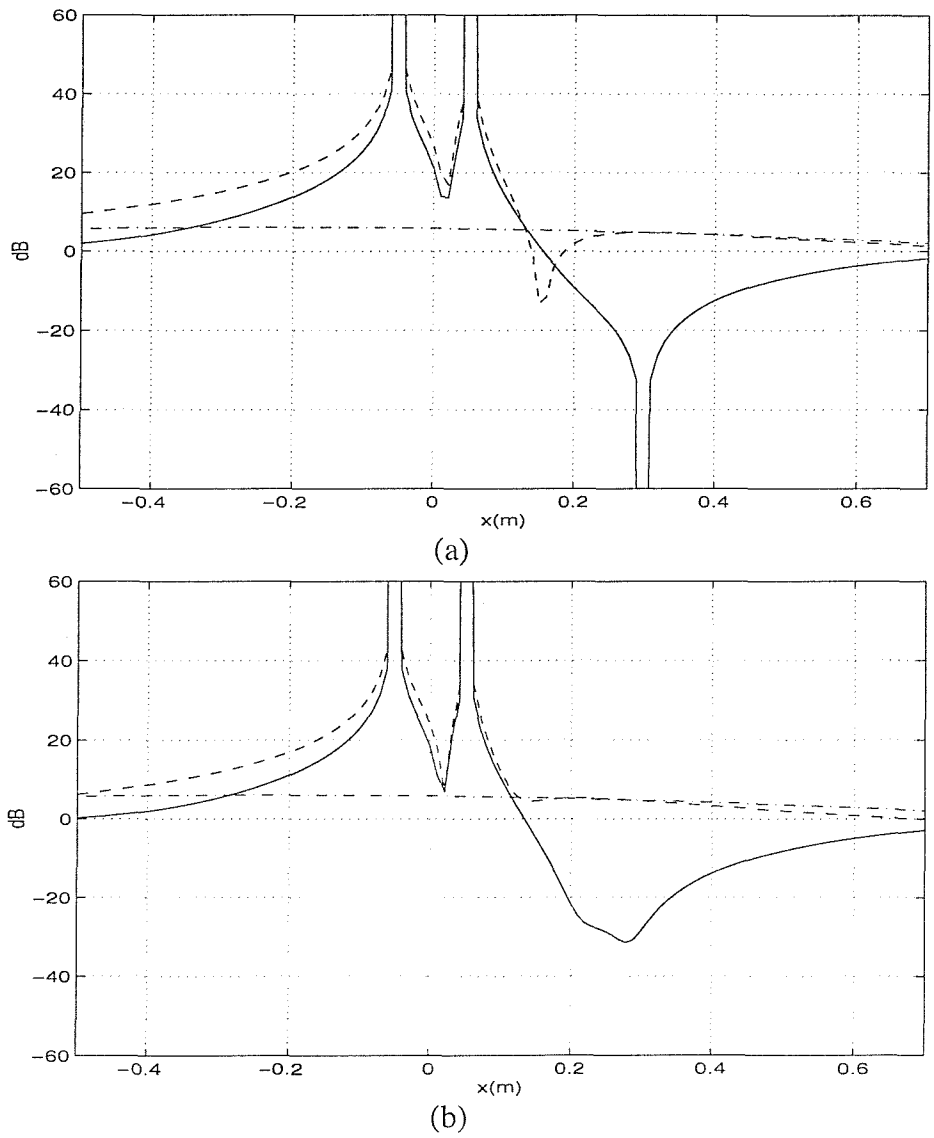

FIGURE 4.9. The mean squared pressure for primary field (-.-.-.), secondary field (- - - - -) and controlled field (_____). (a) Cancelling the acoustic pressure and particle velocity at point (0.3,0). (b) Minimising the acoustic pressure at a rectangular area using the 2-norm minimisation strategy.

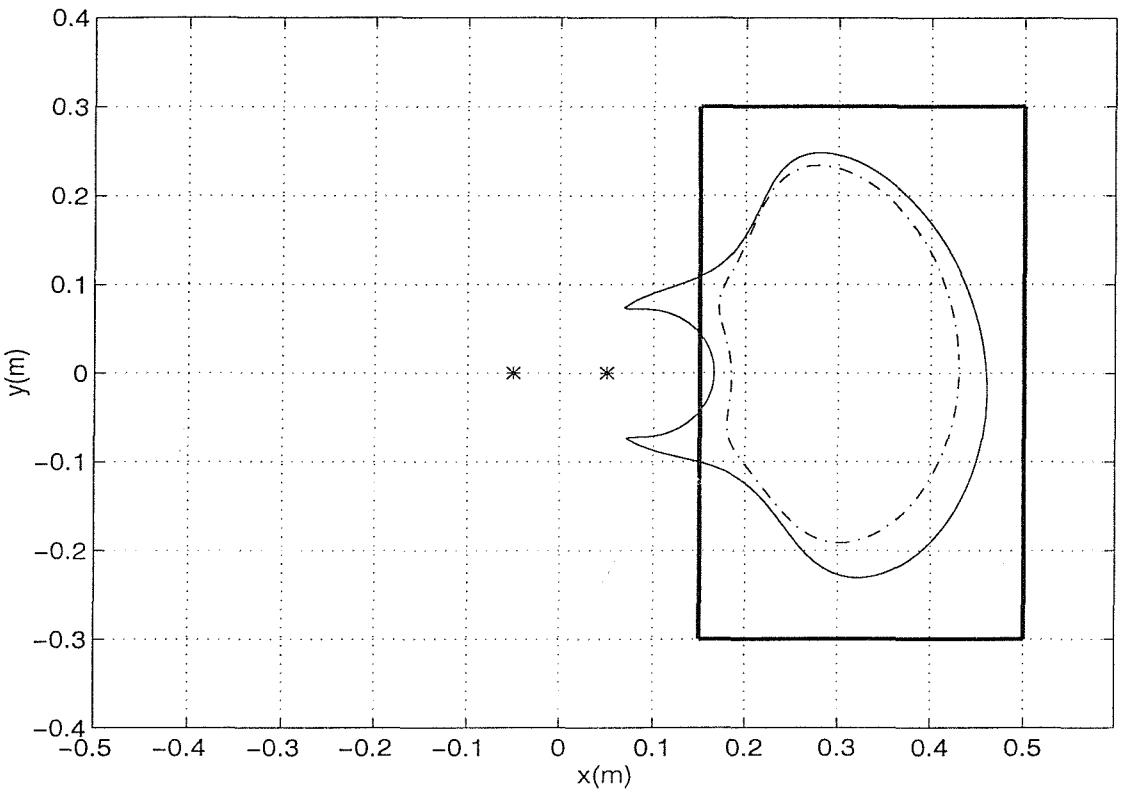

FIGURE 4.10. The 10 dB reduction contour of the average zones of quiet created by two secondary monopole sources located at positions (0.05,0) and (-0.05,0) minimising the acoustic pressure at an area represented by a bold rectangular frame, using 2-norm minimisation strategy (———) and using ∞-norm minimisation strategy (-.-.-.).

		ATTENUATION (dB)	
		$\|P\|_2$	$\|P\|_\infty$
MINIMISATION STRATEGY	2-NORM	9.3	4.8
	∞-NORM	8.4	5.9

TABLE 1. Attenuation after control for the 2-norm and the ∞-norm minimisation strategies.

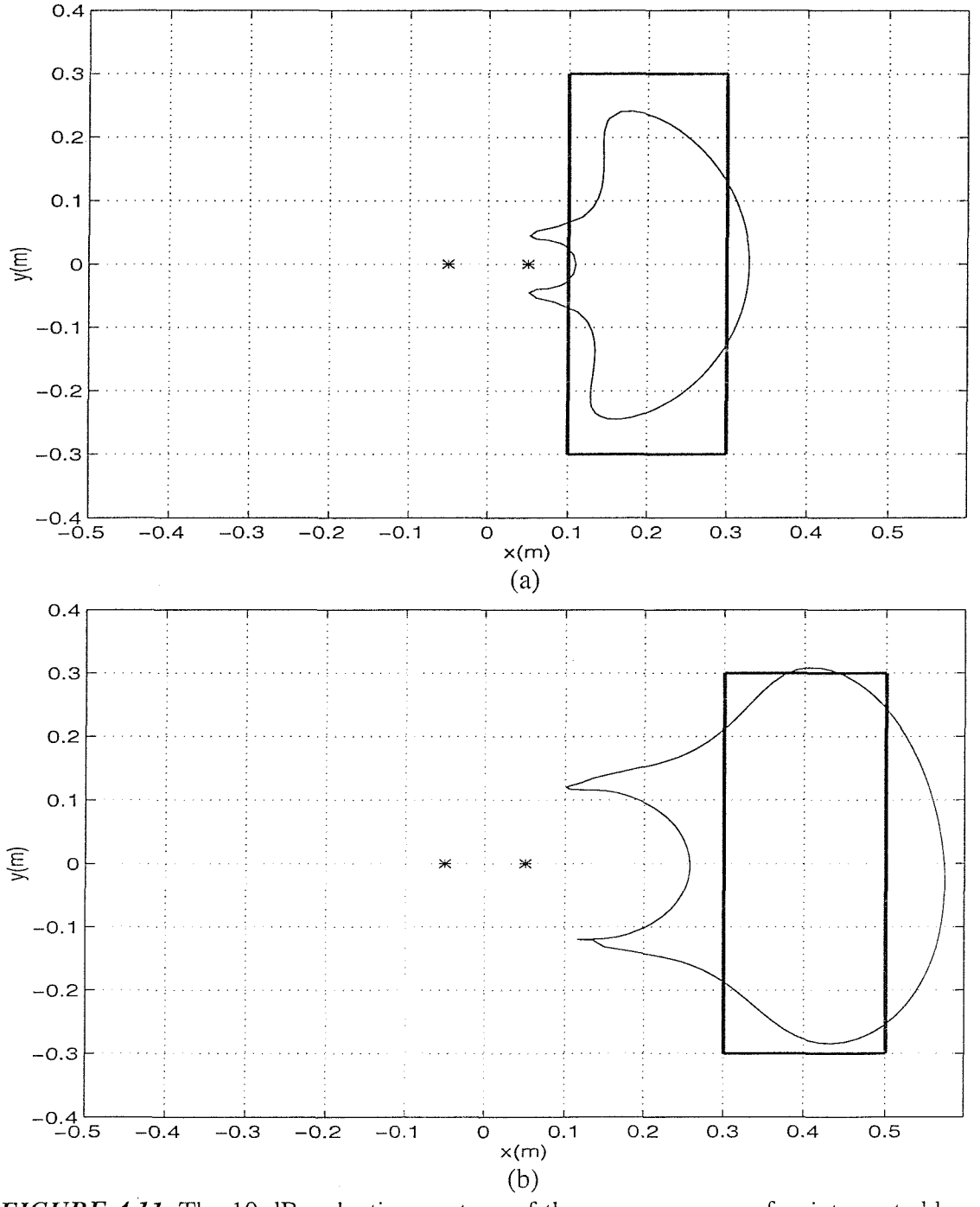

FIGURE 4.11. The 10 dB reduction contour of the average zones of quiet created by two secondary monopole sources located at positions (0.05,0) and (-0.05.0), minimising the acoustic pressure at different locations enclosed inside the rectangular frame (bold line). (a) The rectangular frame near the secondary monopoles. (b) The rectangular frame further away from the secondary monopoles.

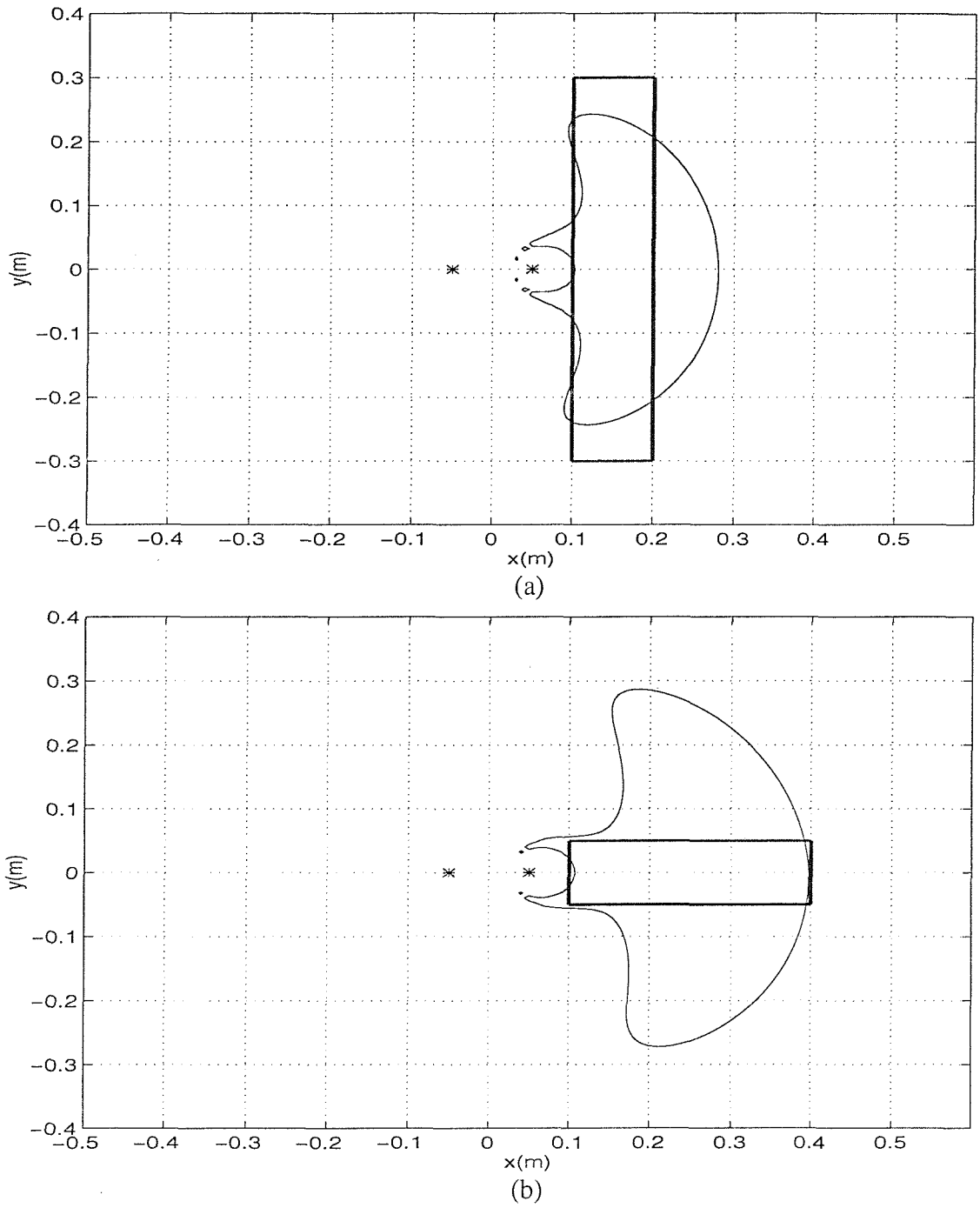

FIGURE 4.12. The 10 dB reduction contour of the average zones of quiet created by two secondary monopole sources located at positions (0.05,0) and (-0.05,0) minimising the acoustic pressure for different shapes represented by a bold rectangular frame. (a) The rectangular frame is narrow in the x-axis direction and longer in the y-axis direction. (b) The rectangular frame is narrow in the y-axis direction and longer in the x-axis direction.

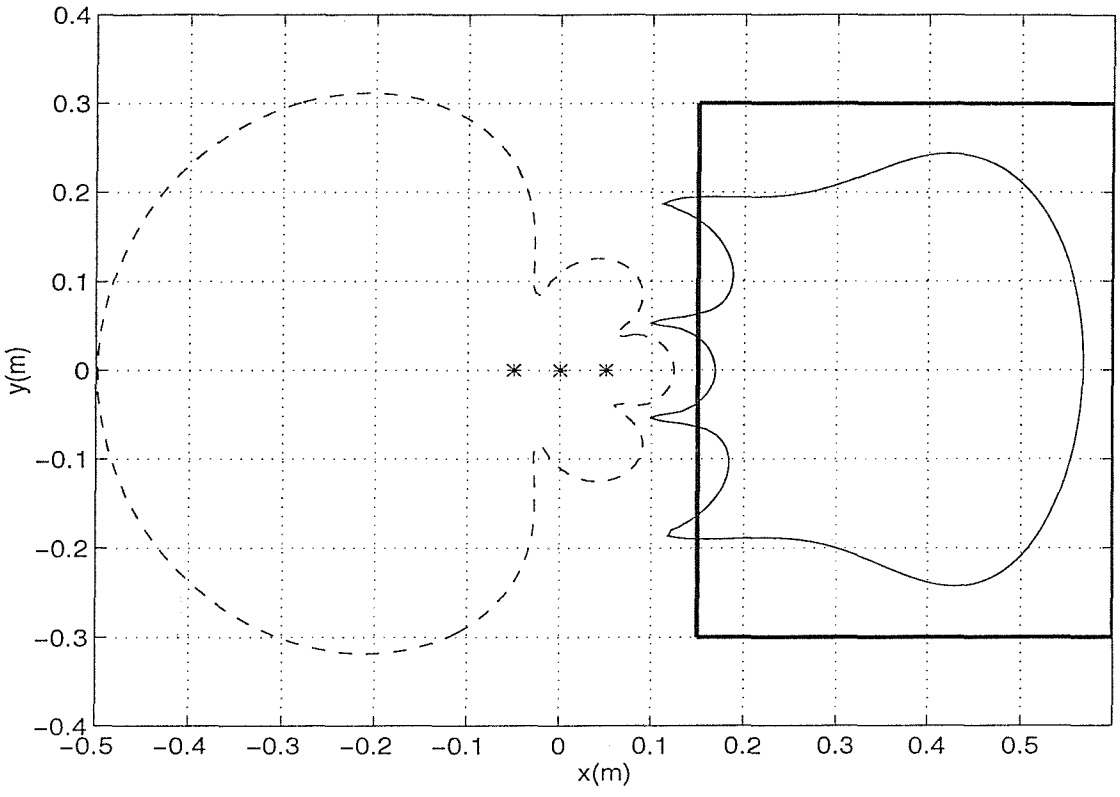

FIGURE 4.13. The 10 dB reduction contour of the average zone of quiet created by three secondary monopole sources located at positions (0,0), (0.05,0) and (-0.05,0) minimising the acoustic pressure at an area represented by a bold rectangular frame using 2-norm minimisation strategy (———), and the 10 dB increase in the primary field (- - - - -).

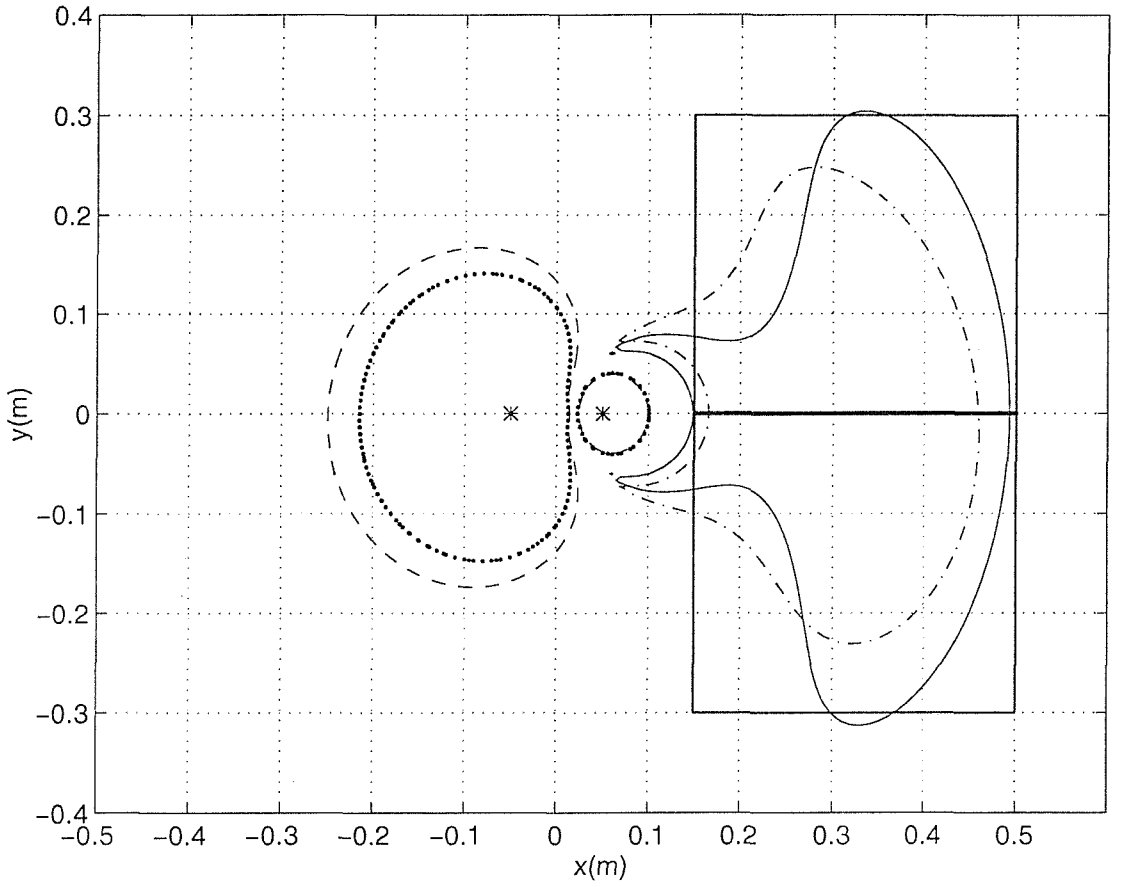

FIGURE 4.14. The 10 dB reduction contour of the average zones of quiet created by two secondary monopole sources located at positions (0.05,0) and (-0.05,0) minimising the acoustic pressure at a line from (0.15,0) to (0.5,0) represented by a bold line using 2-norm minimisation strategy (——) and minimising the acoustic pressure at an area represented by a bold rectangular frame using 2-norm minimisation strategy (-.-.-.), and the 10 dB increase in the primary field for line minimisation (- - - - -) and area minimisation (. . . . .).

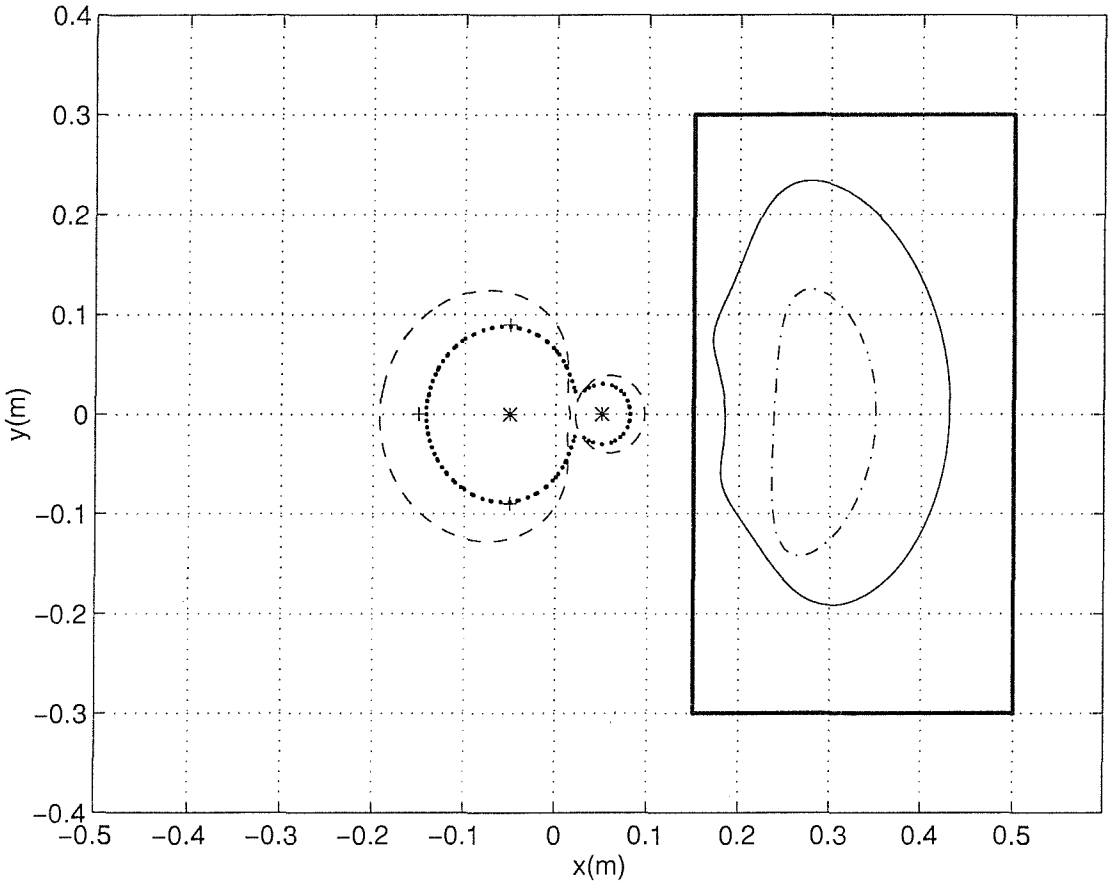

FIGURE 4.15 The 10 dB reduction contour of the average zones of quiet created by two secondary monopole sources located at positions (0.05,0) and (-0.05,0) minimising the acoustic pressure at an area represented by a bold rectangular frame using ∞-norm minimisation strategy without the constraint on 10dB pressure amplification (——) and with the constraint on 10dB amplification at (-0.15,0), (-0.05,0.09) and (-0.05,-0.09) points represented by '+' (-.-.-.), and the 10 dB increase in the primary field without the constraint (- - - - -) and with constraint (. . . . .).

4.4 Local control experiment

In this section we describe the experiment to validate the results of the local active noise control system using 2-norm and ∞-norm minimisation strategies to minimise the acoustic pressure over an area. The excitation frequency of 270Hz was chosen for the primary source, since the size of the quiet zones below 270Hz would be too large for the size of the microphone grid shown in Figure 4.16 to obtain the useful quiet zones. Figure 4.16 shows the experimental set-up used in the measurements. The secondary sources are two 110mm diameter loudspeakers placed separately and surrounded by a 30mm pitch grid made of 3mm diameter brass rod. The dimensions of the grid are 420×420 mm. A total of 139 electret microphones of 6mm diameter were located at the corresponding nodes of the grid, sampling a total area of 360×360 mm^2 around the loudspeakers. A 150mm diameter wooden sphere, divided in two halves was installed to simulate the effect of a diffracting head on the measured zone of quiet.

The size of the room where the experiment has been performed is 7m×6m×3m and it is a normal room. The primary source was located at 2m away from the microphone grid. The primary field can be assumed to be a slightly diffuse field due to the effect of reflection.

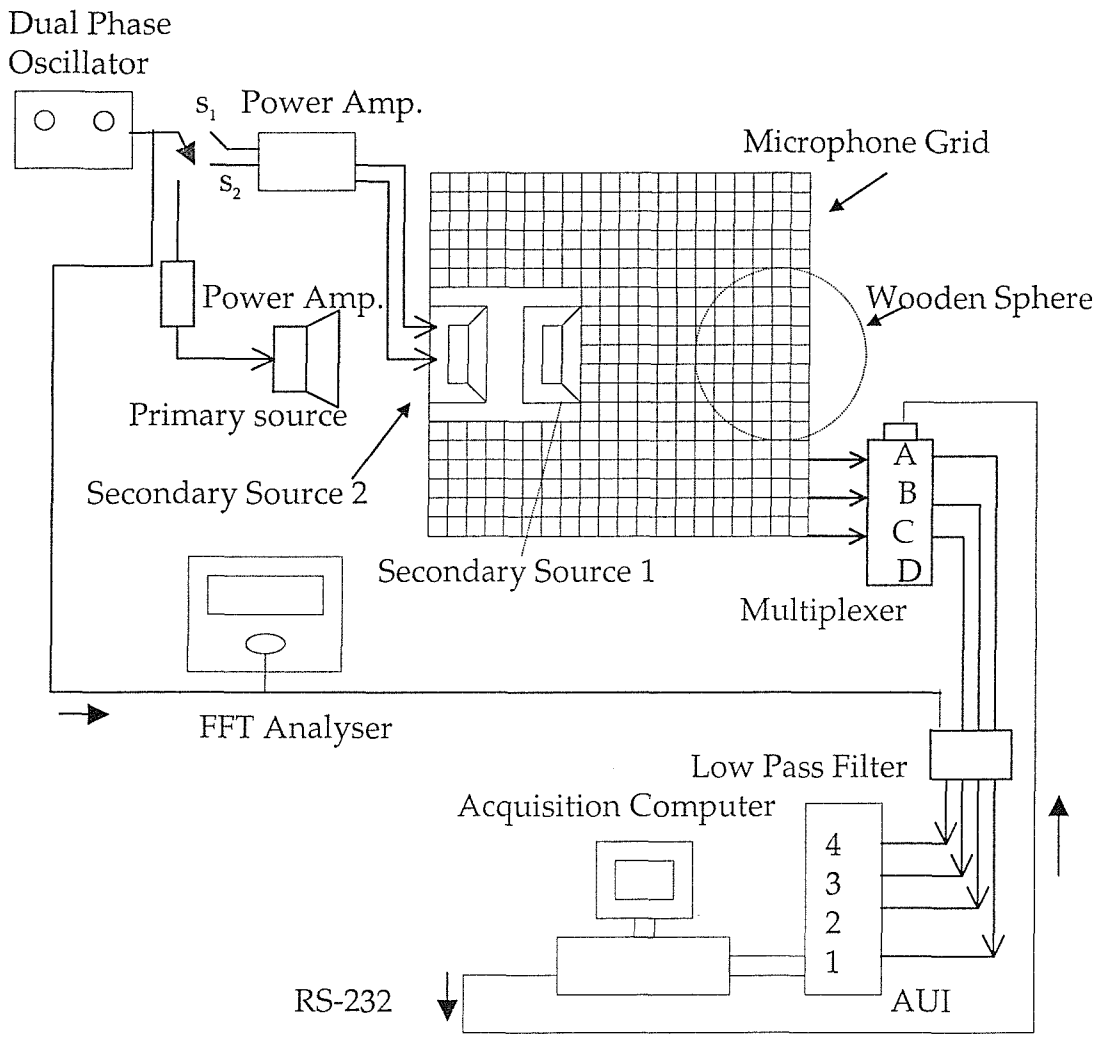

FIGURE 4.16. Configuration of experimental set-up

The primary and secondary sources are connected to a dual phase oscillator that allows the amplitude and phase of the secondary sources to be adjusted in order to minimise the acoustic pressure at a point or minimisation area. The reference signal necessary for the acquisition system to calculate the relative amplitude and phase of the complex acoustic pressure at the microphone positions is connected to a dual phase oscillator whose output can be selected with a switch that allows the signal fed

to the primary source or to the secondary source to be used as a reference. An FFT analyser is connected to the reference signal to measure the frequency of excitation accurately. All the microphones are connected to an electronic multiplexer which sequentially selects three microphone signals which are filtered by the low pass filter and then acquired by the Analogue Unit Interface (AUI). The sampling frequency is 1,000 Hz and 2,000 samples are acquired for every microphone. The input signal to the AUI through channel 4 is taken as a reference to calculate the relative amplitude and phase of all the signals measured by the microphones on the grid. The calculation of the relative amplitude and phase of the pressure signals was carried out by the computer by Fourier transforming the four input signals and calculating the amplitude and phase of the microphone signals at the excitation frequency with respect to the reference signal. After a complete cycle a matrix of complex pressure values at all the grid points is therefore obtained.

At this stage, the quiet zones created by one and two secondary loudspeakers were investigated through computer simulations using measured data for one sample of primary field at 270 Hz in a room. The primary field was measured first, and the transfer functions between the secondary loudspeakers and all the microphones on the microphone grid were then measured. The primary field and transfer functions were taken to calculate the optimal complex inputs to the secondary loudspeakers. The experimental set-up described above can be represented as the simplified block diagram of a 2 inputs n outputs feedforward control system shown in Figure 4.17, where the signals from n microphones at an area in front of secondary loudspeakers are taken as error signals to be minimised in the experiment. $\boldsymbol{y}$ is outputs of the controllers, i.e. the inputs to two secondary loudspeakers. $\boldsymbol{d}$ is the primary field, i.e. the signals from error microphones due to the primary field only. $\boldsymbol{P}$ is the plant response, i.e. the transfer function from the two secondary loudspeakers to microphones.

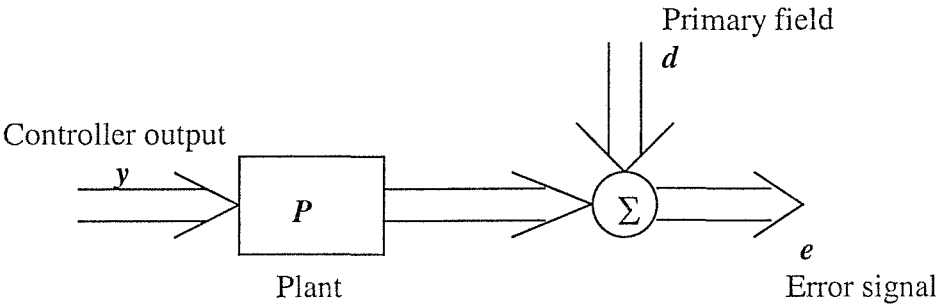

FIGURE 4.17 The simplified block diagram of two inputs n outputs feedforward control system.

If the system is assumed linear, then the total outputs from the *i*th error microphone can be expressed in its complex form as

$$e_i = d_i + P_{i1}(j\omega)\, y_1 + P_{i2}(j\omega)\, y_2, \qquad (4.6)$$

where P_{i1} is the transfer response between the signal driving the first secondary loudspeaker and the output from the *i*th microphone, at the frequency ω.

The cost function for 2-norm minimisation strategy can be expressed as

$$J_2 = \sum_{i=1}^{n} \left| d_i + P_{i1}(j\omega) y_1 + P_{i2}(j\omega) y_2 \right|^2 \qquad (4.7)$$

We can find the optimal values of y_1 and y_2 which minimise the cost function J_2 by using the function fmins( ) in MATLAB (Grace, 1995).

For ∞-norm minimisation, the following cost function is minimised:

$$J_\infty = \max_i \left| d_i + P_{i1}(j\omega) y_1 + P_{i2}(j\omega) y_2 \right| \qquad (4.8)$$

This ∞-norm minimisation can be rewritten as (see chapter 3):

$$\begin{aligned} &\textit{Minimise} \quad \sigma \\ &\textit{Subject to} \quad J_{\infty} < \sigma \end{aligned} \tag{4.9}$$

where σ is a real scale parameter used in the optimisation process.

The optimal values of y_1 and y_2 can be calculated using the function *constr( )* in MATLAB (Grace, 1995).

The zone of quiet is calculated as the ratio of the total (controlled) squared pressure and the primary squared pressure as in equation (3.32) in chapter 3. For the one secondary loudspeaker case, the zone of quiet created by using 2-norm pressure minimisation minimising the acoustic pressure in an area was investigated and compared to that created by cancelling the acoustic pressure at one point. The cost function of 2-norm pressure minimisation for one secondary source can be expressed as in equation (4.7) only with the first secondary loudspeaker.

Figure 4.18 (a) shows the 10 dB reduction contour line in the averaged zones of quiet created by introducing one secondary source in a diffuse primary field generated by computer using 2-norm pressure minimisation (solid line) to minimise the acoustic pressure in an area represented by the rectangular frame and cancelling the acoustic pressure (dash-dot line) at one point represented by a cross through the computer simulation. Figure 4.18 (b) shows the equivalent results as in Figure 4.18 (a) through computer simulations using the measured data for one sample of the primary field. The secondary loudspeaker is represented by a rectangular and the simulated head of the wooden sphere is represented by a dotted curve. It can be seen that 2-norm minimisation strategy creates a similar size of the quiet zone to that obtained by cancelling the pressure at one point. It can also be seen that the quiet zones created through computer simulations are similar to those created through the computer simulations with the measured data.

In two secondary loudspeakers case, the quiet zones created by using 2-norm and ∞-norm pressure minimisation to minimise the pressure in an area were investigated and compared to those created by cancelling the pressure and particle velocity at one point. The cost functions of 2-norm and ∞-norm pressure minimisation for two secondary sources are given in equations (4.7) and (4.8) respectively. Figure 4.19 (a) shows the averaged zones of quiet created by using 2-norm (solid line), ∞-norm (dash line) pressure minimisation to minimise the acoustic pressure over an area represented by the rectangular frame and cancelling the pressure and particle velocity (dash-dot line) at one point represented by "+" through computer simulations. Figure 4.19 (b) shows the equivalent results as in Figure 4.19 (a) through computer simulations with measured data for one sample of the primary field. It shows that 2-norm pressure minimisation to minimise the acoustic pressure over an area creates slightly longer extension in quiet zones in x-axis direction around the ear position of the wooden sphere than those created by cancelling the acoustic pressure and particle velocity at one point or using ∞-norm pressure minimisation minimising the acoustic pressure over an area.

In Figures 4.18 and 4.19 monopole sources were used as secondary sources in simulations. However loudspeakers were used as secondary sources in experiments. Although monopole sources are not an accurate model of loudspeakers, it simplifies the secondary source modelling and assists comparison between simulations and experiments.

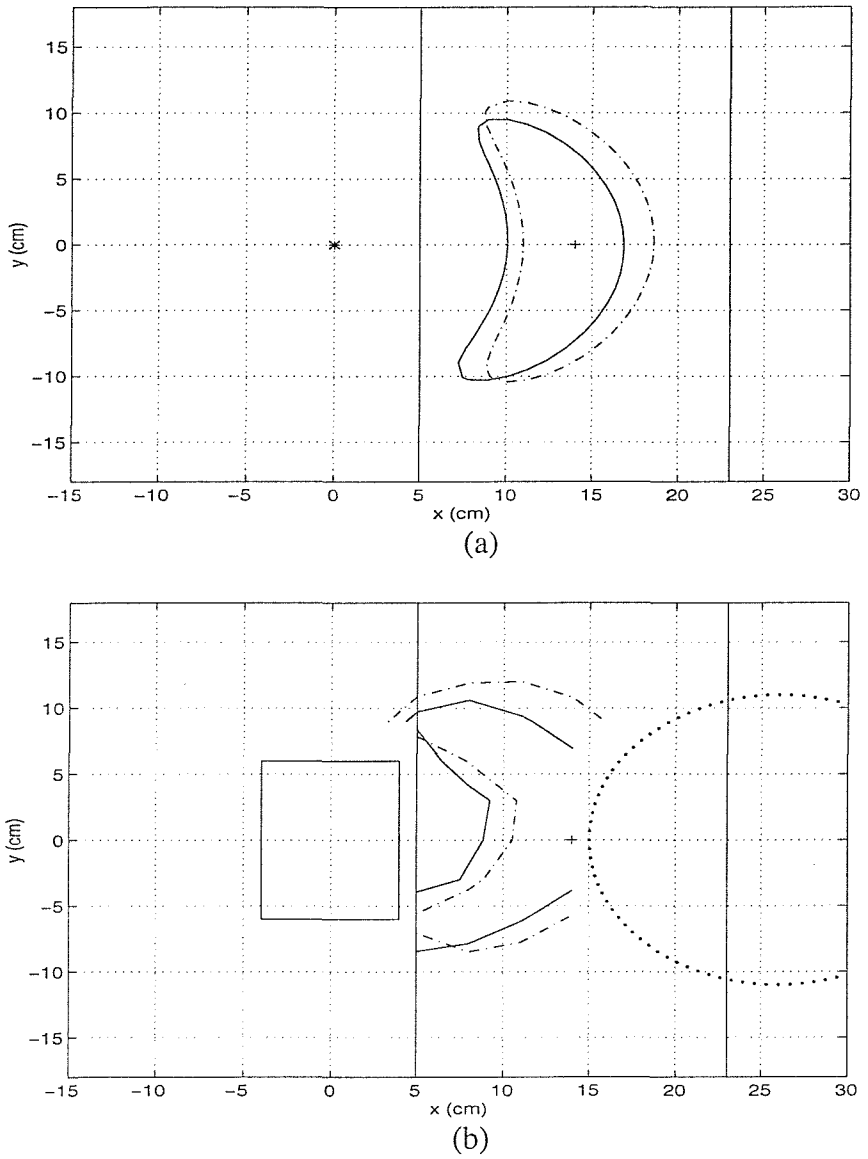

FIGURE 4.18. The zones of quiet created by introducing one secondary loudspeaker using 2-norm minimisation strategy (——) minimising the acoustic pressure in an area, and cancelling the pressure (-.-.-.-.) at a point. (a) Simulations. (b) Predictions from measured data.

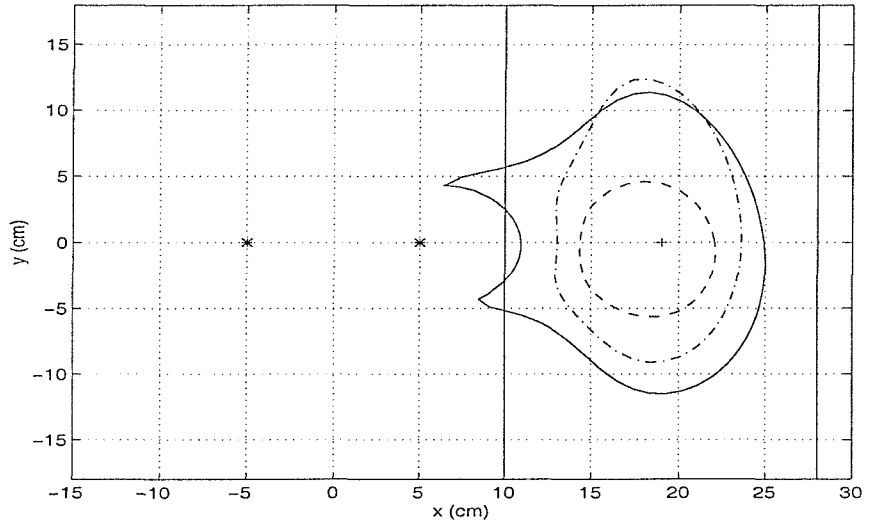

(a)

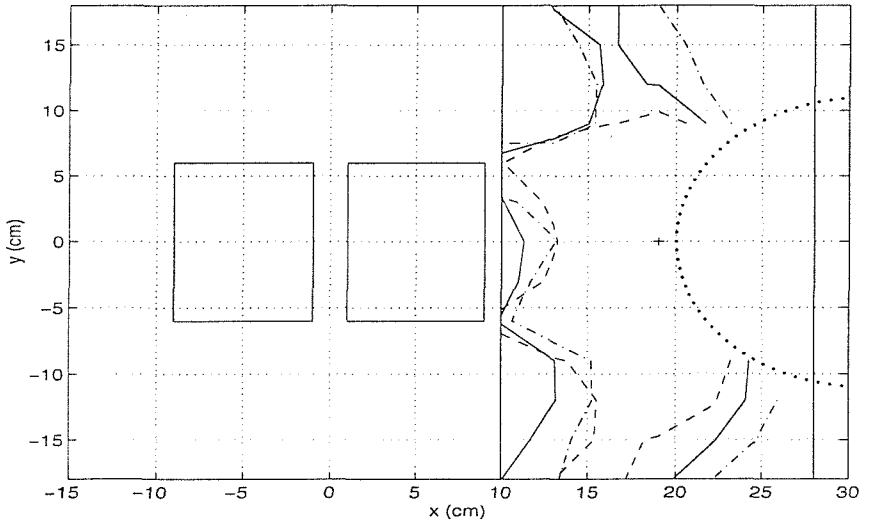

(b)

FIGURE 4.19. The zones of quiet created by introducing two secondary loudspeakers using 2-norm (——), ∞-norm (- - - -) minimisation strategies minimising the pressure in an area represented by a rectangular frame, and cancelling the acoustic pressure and the particle velocity (-.-.-.-.) at one point represented by a cross. (a) Simulations. (b) Predictions from measured data.

4.5 Conclusions

In this chapter the average zones of quiet created by introducing one, two and three secondary sources and using 2-norm and ∞-norm minimisation approaches to reduce the acoustic pressure at a specified area in a tone plane wave and diffuse primary fields have been explored through computer simulations. The results have been compared with the more traditional approaches of cancelling the acoustic pressure or the acoustic pressure and particle velocity at one point. It was shown that larger zones of quiet can be achieved with two or three secondary sources, since the secondary field is designed to better match the primary field at a large area, and not only at one point. An overall flatter secondary field and larger zone of quiet are achieved in this case. It was also shown that the ∞-norm minimisation approach created a smaller zone of quiet compared to that obtained by using 2-norm minimisation, due to the fact that it focuses on the more difficult areas to control. The effect of different minimisation locations and shapes on the zones of quiet has also been investigated in this work. It was shown that the locations and shapes of the quiet zones can be controlled by changing the minimisation area.

The initial results for zones of quiet created by using 2-norm and ∞-norm minimisation approaches for one sample of a primary field have also been investigated through computer simulations using measured data from an experimental system at 270 Hz. The results showed that 2-norm minimisation created slightly better zones of quiet at this frequency for two secondary sources.

Local active sound control using 2-norm minimisation could be applied to a practical application, such as a headrest system if the sum of the mean square pressure at an array of physical microphones was minimised (Nelson and Elliott, 1992) or by using a virtual microphone approach which may not require as many microphones (Garcia et al, 1997). In a practical system, a feedback controller could be designed to control a broadband noise. This would involve optimisation over both frequency and space (Rafaely, 1999). Although only a pure tone diffuse primary field was considered in this work, the expansion of this work to broadband noise will be studied in the next chapter.

Part III: Local active control of broadband sound fields

Chapter 5. Pressure minimisation over space and frequency

5.1 Introduction

This chapter presents the theory and simulations of active sound control for broadband disturbance using single-channel and two-channel systems, which is achieved by minimising the acoustic pressure over both space and frequency. This chapter is an extension of the paper presented by Rafaely (1999). In general the objective of active sound control systems is to control the noise at the dominant frequency range and at some specified region in space. Conventional methods of active sound control are to attenuate the noise at one point in space over some frequency range (Ross, 1980, Joseph, 1990, and Nelson and Elliott, 1992) or at many points in space for single tone disturbance (Miyoshi et al, 1994, and Guo et al, 1997). Cancelling the noise at one point would produce limited zone of quiet with no control over its shape. Although cancelling the noise at many points could create larger zones of quiet, the optimal spacing between the cancellation points varied with the frequency (Miyoshi et al, 1994, and Guo et al, 1997). Recent study showed that minimising the acoustic pressure over a desired region in space by using 2-norm strategy for a single tone disturbance could create larger zones of quiet (Tseng et al, 1999 and Tseng et al, 2000), and could achieve improved spatial performance. Therefore minimisation of the acoustic pressure over the space and frequency is desirable for achieving good performance, e.g. high attenuation of the broadband disturbance at a large spatial extent. The work presented in this chapter only concerns a plane wave primary field with one and two secondary sources for simplicity. Constrained minimisation of the pressure is introduced, to achieve control over the pressure in both frequency and space. The chapter is organised as follows. First, the theory of active sound control for a broadband disturbance is introduced in section 5.2. Second, simulations of actively controlling a broadband disturbance are presented in section 5.3. The chapter is concluded in section 5.4.

5.2 Theory of pressure minimisation for broadband disturbance

In this section we present the theory of actively controlling the broadband disturbance. The basic idea of this is to apply minimisation of acoustic pressure over both space and frequency. Figure 5.1 illustrates the configuration of the acoustic pressure minimisation over space and frequency.

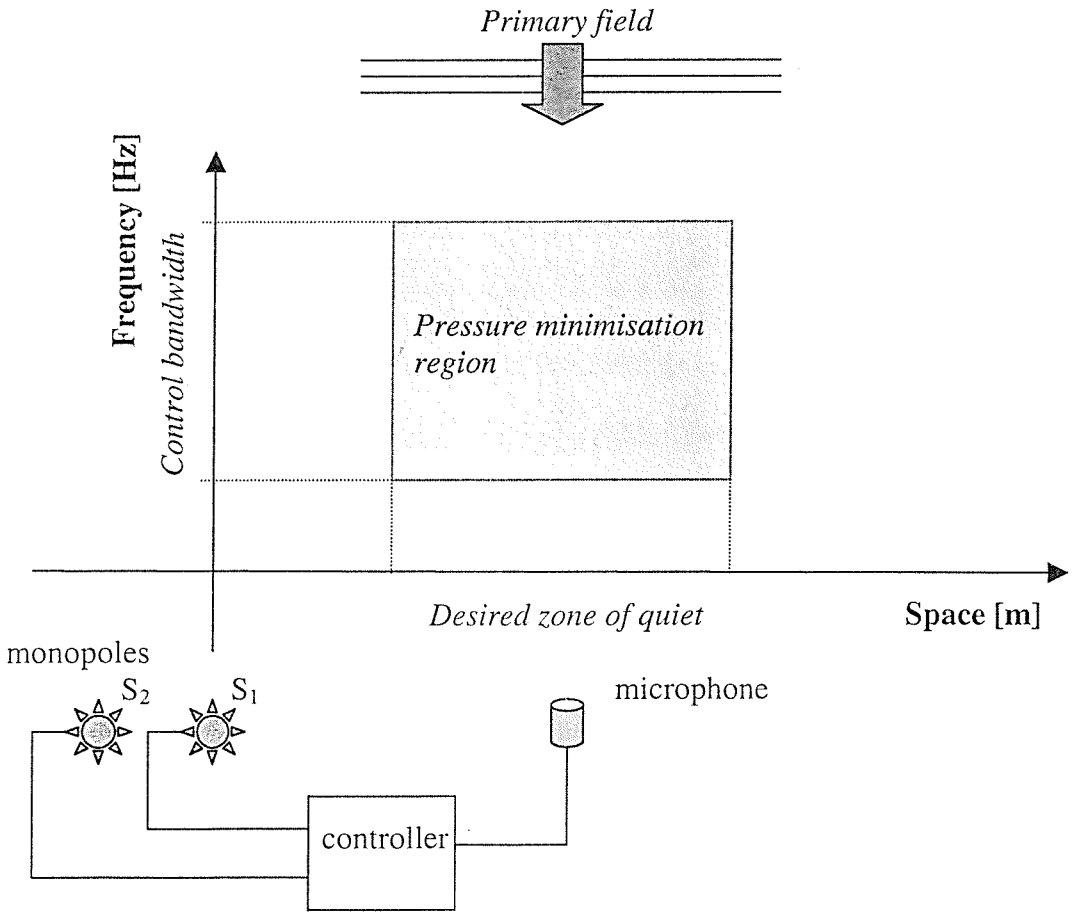

FIGURE 5.1 Configuration of acoustic pressure minimisation over space and frequency with a two-channel feedback system.

The x-axis in Figure 5.1 is a one-dimensional spatial axis, which could be extended in principle, to 2 or 3D. The desired zone of quiet can be defined on this axis where good attenuation is required. The y-axis is the frequency axis where the control bandwidth could be defined. The acoustic disturbance is assumed to be significant at the control frequency bandwidth. The shadow region is the pressure minimisation region. The region to the right of the pressure minimisation region is the far field of

the secondary sources, with low control effort, and thus small effect of the active system on the overall pressure. The region to the left of the pressure minimisation region is the near field of the secondary sources, which might result in amplification of the pressure at this region. To avoid significant pressure amplification a pressure amplification constraint is necessarily included in the design process using constrained optimisation. The regions above and below the pressure minimisation region represent the frequencies outside the bandwidth. Due to the waterbed effect (Skogestad and Postlethwaite, 1996), reduction of the disturbance at the control bandwidth will result in amplification outside the bandwidth. Therefore pressure amplification outside the bandwidth must be constrained in the design process.

In this work the case of one-dimensional space and a plane wave primary field propagating in the direction perpendicular to the spatial dimension is considered for simplicity and the secondary sources are located at the origin and (-0.1m, 0) point. Therefore the primary field is constant along the spatial axis. A microphone can be placed at the desired zone of quiet or other locations close to the secondary monopoles. The secondary sources are driven by feedback controllers connected to the microphone. The microphone detects the signal of the primary field, which is then filtered through the controllers to drive the secondary sources. The signals from the secondary sources are then used to attenuate the primary disturbance at the pressure minimisation region. The feedback system used in this work is shown in Figure 5.2 and is configured using Internal Model Control (Morari and Zafiriou, 1989) as shown in Figure 5.3, where P_1 is plant 1, the response between the input to the first monopole and the output of the microphone, P_{1o} is the internal model of plant 1, P_2 is plant 2, the response between the input to the second monopole and the output of the microphone, P_{2o} is the internal model of plant 2, P_{s1} and P_{s2} are the secondary fields at the field point away from the first and second monopoles respectively, d is the disturbance at the microphone, d_s is the disturbance at the field point away from the microphone, and e is the error signal. In this work P_{1o} is assumed to be equal to P_1 and P_{2o} is equal to P_2. Therefore the feedback system turns to a feedforward system with $x=d$.

It is also assumed that the secondary and primary fields in both space and frequency, are known, and although a microphone is used for the feedback signal, the pressure

elsewhere is assumed to be known and this knowledge is used in the minimisation formulation. Although it is not always practical to have a good estimate of the pressure far from the microphone, this still can be done in some cases using virtual microphone techniques (Garcia-Bonito et al, 1997).

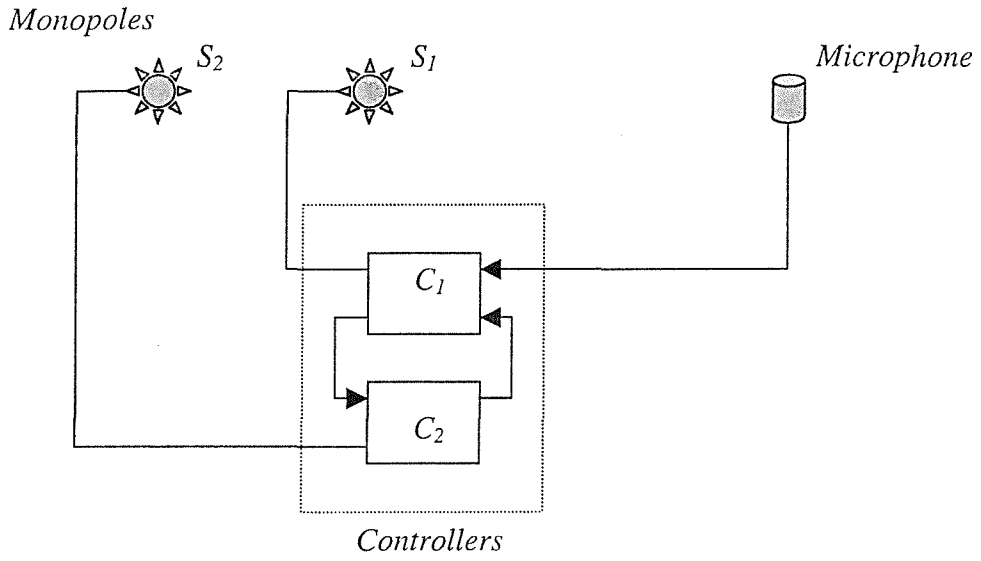

FIGURE 5.2 The two-channel feedback control system used to control the broadband disturbance.

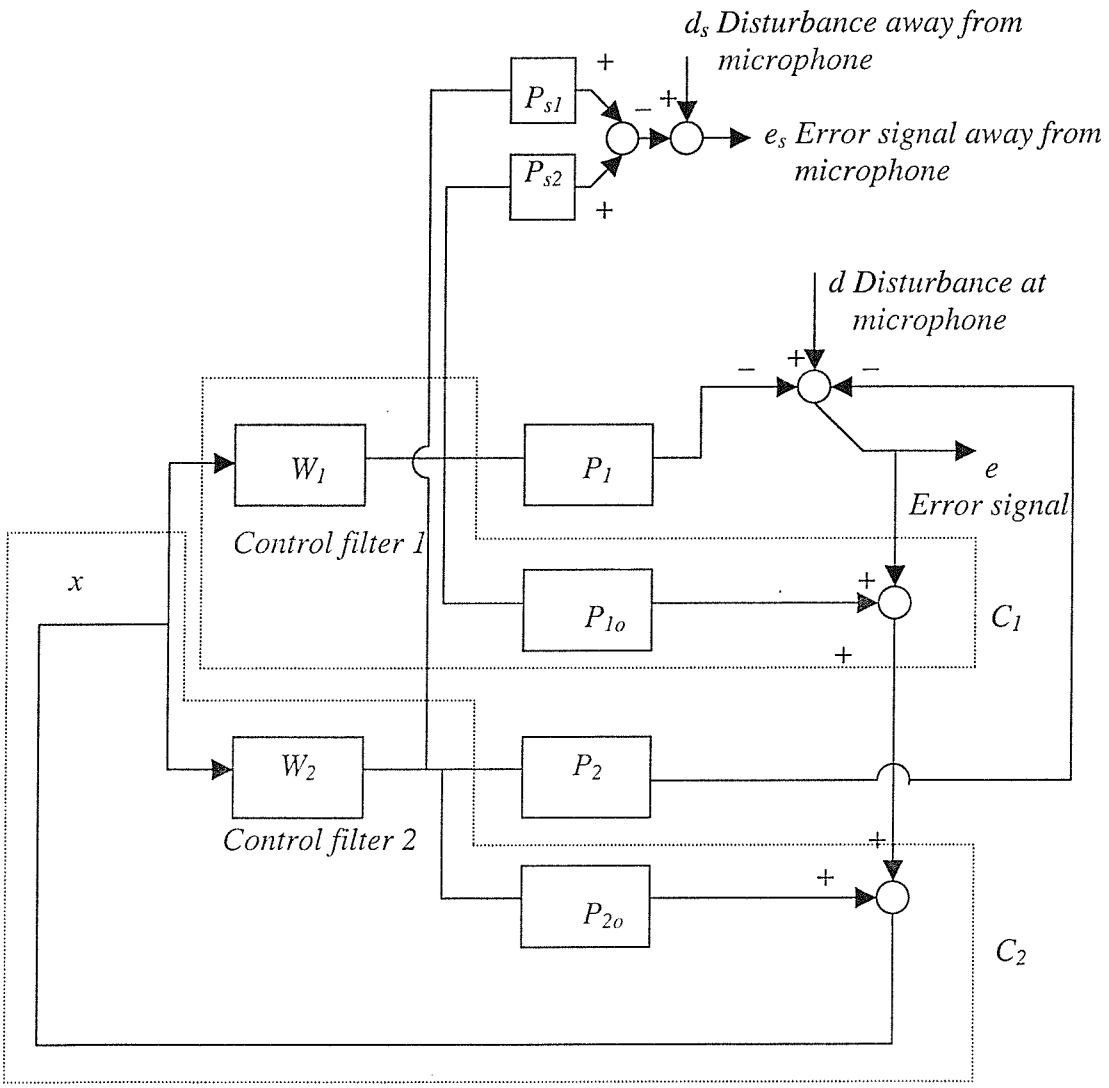

FIGURE 5.3 The two-channel feedback control system with two internal model controllers.

The secondary fields at the field point away from the secondary monopoles could be written as (Nelson and Elliott, 1992):

$$P_{s1}(r_1, f) = \frac{A_1}{r_1} e^{-j2\pi f r_1 / c} \tag{5.1}$$

$$P_{s2}(r_2, f) = \frac{A_2}{r_2} e^{-j2\pi f r_2 / c} \tag{5.2}$$

where r_1, r_2 are the distance from the field point to the first and second monopoles, A_1, A_2 are the amplitude constant, f is frequency and c is the speed of sound.

The plant responses can be written as:

$$P_1(r_{1o}, f) = \frac{A_{1o}}{r_{1o}} e^{-j2\pi f r_{1o} / c} \tag{5.3}$$

$$P_2(r_{2o}, f) = \frac{A_{2o}}{r_{2o}} e^{-j2\pi f r_{2o} / c} \tag{5.4}$$

where r_{1o}, r_{2o} are the distance from the microphone to the first and second monopoles, A_{1o}, A_{2o} are the amplitude constant.

The error signal could be expressed as:

$$\begin{aligned} e_s &= d_s - d_s W_1 P_{s1} - d W_2 P_{s2} \\ &= d_s (1 - W_1 P_{s1} - W_2 P_{s2}) \\ &= d_s (1 - W_1 \frac{A_1}{r_1} e^{-j2\pi f r_1 / c} - W_2 \frac{A_2}{r_2} e^{-j2\pi f r_2 / c}) \end{aligned} \tag{5.5}$$

The term $(1 - W_1 \frac{A_1}{r_1} e^{-j2\pi f r_1 / c} - W_2 \frac{A_2}{r_2} e^{-j2\pi f r_2 / c})$ is the sensitivity function (Franklin et al, 1994). The formulation of the cost function to be minimised can be written as.

$$J(r_1, r_2, f) = \left\| \sqrt{S_{dds}} (1 - W_1 \frac{A_1}{r_1} e^{-j2\pi f r_1 / c} - W_2 \frac{A_2}{r_2} e^{-j2\pi f r_2 / c}) \right\|_2^2 \tag{5.6}$$

where $\sqrt{S_{dds}}$ is the square root of the power spectral density of the disturbance pressure at the field points.

For robust stability the closed-loop of the feedback system must satisfy the following condition.

$$\left\| W_1 B_1 \frac{A_{1o}}{r_{1o}} e^{-j2\pi f r_{1o}/c} + W_2 B_2 \frac{A_{2o}}{r_{2o}} e^{-j2\pi f r_{2o}/c} \right\|_\infty < 1 \qquad (5.7)$$

where B_1, B_2 are the multiplicative plant uncertainty bounds for plants 1 and 2 (Franlin et al, 1994) and r_{1o}, r_{2o} are the distance from the microphone to the first and second monopoles respectively. The terms $e^{-j2\pi f r_{1o}/c}$ and $e^{-j2\pi f r_{2o}/c}$, the plant responses, therefore follow the robust stability condition, $\|WPB\|_\infty < 1$, introduced in chapter 2. For amplification limit a constraint could be added into the optimisation process as follows.

$$\left\| (1 - W_1 \frac{A_1}{r_1} e^{-j2\pi f r_1/c} - W_2 \frac{A_2}{r_2} e^{-j2\pi f r_2/c}) D \right\|_\infty < 1 \qquad (5.8)$$

where $1/D$ is the desired enhancement bounds.

Therefore the overall design objective can now be written as:

$$\textit{min} \quad \left\| \sqrt{S_{dds}} (1 - W_1 \frac{A_1}{r_1} e^{-j2\pi f r_1/c} - W_2 \frac{A_2}{r_2} e^{-j2\pi f r_2/c}) \right\|_2^2$$

$$\textit{subject to} \quad \left\| W_1 B_1 \frac{A_{1o}}{r_{1o}} e^{-j2\pi f r_{1o}/c} + W_2 B_2 \frac{A_{2o}}{r_{2o}} e^{-j2\pi f r_{2o}/c} \right\|_\infty < 1$$

$$\left\| (1 - W_1 \frac{A_1}{r_1} e^{-j2\pi f r_1/c} - W_2 \frac{A_2}{r_2} e^{-j2\pi f r_2/c}) D \right\|_\infty < 1 \qquad (5.9)$$

Equation (5.9) can be reformulated by approximating f and r at discrete points only, similar to the formulation presented in chapter 7. The discrete frequency and space constrained optimisation problem can now be written as:

$$
\begin{aligned}
\textit{min} \quad & \sum_{f}\sum_{r}\left|\sqrt{S_{dds}}\left(1-W_1\frac{A_1}{r_1}e^{-j2\pi f r_1/c}-W_2\frac{A_2}{r_2}e^{-j2\pi f r_2/c}\right)\right|^2 \\
\textit{subject to} \quad & \left|W_1B_1\frac{A_{1o}}{r_{1o}}e^{-j2\pi f r_{1o}/c}+W_2B_2\frac{A_{2o}}{r_{2o}}e^{-j2\pi f r_{2o}/c}\right|<1 \quad \text{for all } f,\ r_{1o} \text{ and } r_{2o} \\
& \left|\left(1-W_1\frac{A_1}{r_1}e^{-j2\pi f r_1/c}-W_2\frac{A_2}{r_2}e^{-j2\pi f r_2/c}\right)D\right|<1 \quad \text{for all } f,\ r_1 \text{ and } r_2
\end{aligned}
\tag{5.10}
$$

It should be noted that only constraints on the amplification will be used in the simulations below, since these are easier to present on a frequency-space plot, although they can both be used in practice. In the next section we will present simulations of the pressure minimisation over space and frequency.

5.3 Simulations of pressure minimisation for broadband disturbance

In this section the performance of active sound control for a broadband disturbance using single-channel and two-channel systems is investigated through computer simulations. The primary field is a plane wave propagating in the direction perpendicular to the spatial axis. One and two monopoles are used as the secondary field in the work. A microphone is placed at the point (0.1m, 0), i.e. 10cm from the secondary monopole source. A series of simulations are performed to evaluate the performance of active broadband noise control. The theory in section 5.2 is used for the simulations.

In the first example a single-channel system is used and a constant gain controller is implemented. The secondary monopole is located at the origin. Therefore only the first two terms in equation (5.5) are used. The control filter W_1 in equation (5.5) is set to the constant r_{1o}/A_1, where r_{1o} is the distance between the microphone and the first monopole. Therefore the attenuation can be shown to be:

$$Att1(f, r_1) = -20\log_{10}\left|1 - \frac{r_{1o}}{r_1} e^{-j2\pi f r_1 / c}\right| \tag{5.11}$$

Figure 5.4 shows the resulting attenuation of the controller as a function of both frequency and space. A good attenuation is obtained at the microphone position and at very low frequencies. This is since the control filter is a simple form of a prediction filter, which performed well at the very low frequencies. This is equivalent to producing a secondary field at the microphone location that is equal to the primary field but delayed with the plant delay (Rafaely, 1999). It also shows the amplifications at high frequencies and at locations near the secondary source, due to the waterbed effect discussed above. This example showed that high attenuation is achieved at the microphone location and at the very low frequencies. However in some cases good performance at other locations and other frequencies might be required.

In the second example a single-channel system is used and the controller is designed to minimise the acoustic pressure at a specified area over space and frequency. An

FIR filter W_1 with 4 coefficients is designed to minimise the acoustic pressure at the region as enclosed by the rectangle in Figure 5.5. The optimal values of the filter coefficients were calculated using the function *fmins()* in MATLAB to minimise the cost function as in equation (5.4) only with the first two terms. The attenuation can be expressed as:

$$Att2(f, r_1) = 20\log_{10}\left|1 - W_1 \frac{A_1}{r_1} e^{-j2\pi f r_1 / c}\right| \tag{5.12}$$

From Figure 5.5 it can be seen that good performance is achieved at the minimisation area as expected. This suggests that we could minimise the acoustic pressure at the desired range in both space and frequency.

In the third example an FIR filter with 16 coefficients is used. The configuration is the same as in the second example. Figure 5.6 shows the attenuation contour over space and frequency for an FIR filter with 16 coefficients without constraint on amplification. We can see that higher attenuation is achieved in the desired region compared to Figure 5.5 and a more rectangle-like shape is formed, i.e. similar to the minimisation region shape. This is because more coefficients of the control filter can better control the disturbance at the control bandwidth. It can also be seen that high amplification appears at high frequencies and at the regions close to the secondary monopole. Therefore a constraint on amplification could be added in the design process.

In the fourth example an amplification constraint is included in the optimisation process. Equations (5.6) and (5.8) with the first monopole only were used in the optimisation process and the coefficients of the control filter can be found using the function *constr()* in MATLAB. Figure 5.7 shows the attenuation contour over space and frequency with the same configuration as in Figure 5.6 and with a constraint on amplification not to exceed 6dB at the spatial axis from r=0.04m to r=0.2m for all the frequencies. It shows that the lower attenuation is achieved in the desired region compared to the design without the amplification constraint. This is since the controller tried to reduce the amplification at high frequencies and at the region close

to the secondary source resulting in lower control effort. Therefore the performance with the amplification constraint is slightly worse than that without the amplification constraint. The examples described above used one secondary monopole, where only a simple secondary field could be produced. If two secondary monopoles are used more complicated secondary fields could be obtained and better performance might be achieved.

In the fifth example two secondary monopoles are used to control the broadband disturbance. Equation (5.6) is used as the cost function to be minimised. The coefficients of the control filters with 16 coefficients were calculated using the function *fmins()* in MATLAB. The attenuation contour over space and frequency for two-channel system is shown in Figure 5.8. The secondary monopoles are located at the origin and (-0.05m, 0) point and the minimisation region is the same as in previous examples. From the figure we can see that high attenuation is achieved in the desired region which is larger than that in the one secondary monopole case as shown in Figure 5.6. It can also be seen that the shape of the high attenuation area is similar to that of the minimisation region. This is because two monopoles created more complicated secondary fields. Thus better performance over the minimisation region was obtained as expected. High amplification also appears at high frequencies and at the region close to the secondary monopoles.

In the sixth example a constraint on amplification is added in the optimisation process to avoid high amplification. Equations (5.4) and (5.6) were used in the design process and the coefficients of the control filters were calculated using the function *constr()* in MATLAB. Figure 5.9 shows the attenuation contour over space and frequency with an amplification constraint not to exceed 6dB at the spatial axis from r=0.04m to r=0.2m for all frequencies. As can be seen the attenuation area becomes smaller than that without the amplification constraint as discussed above.

5.4 Conclusions

The theory of active control for broadband disturbance using single-channel and two-channel systems has been presented and the performance has been investigated through computer simulations. The acoustic pressure was minimised at the specified area over space and frequency. A constraint on the amplification was also included in the design process. The results showed that good attenuation could be achieved at the microphone location or desired range over space and frequency using a single-channel system. However better performance was achieved using a two-channel system. When limits on amplification were introduced, the performance began to degrade. It has also been shown that the acoustic pressure could be minimised at a specific frequency range and at a specific location in space away from the microphone location. This could be realised by using virtual microphone methods (Garcia et al, 1997). Also the shape of the attenuation area could be controlled by using a two-channel system.

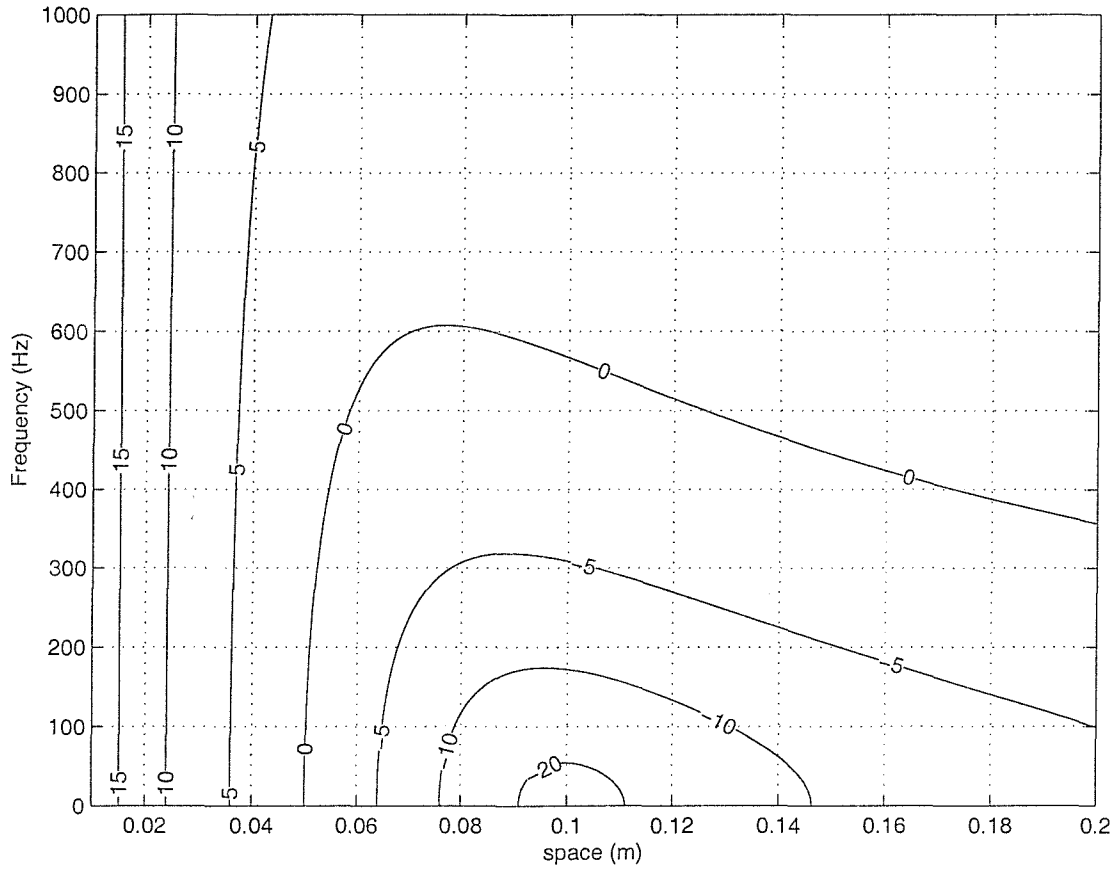

FIGURE 5.4 Attenuation in decibels as a function of space and frequency for the constant gain controller with a single-channel system.

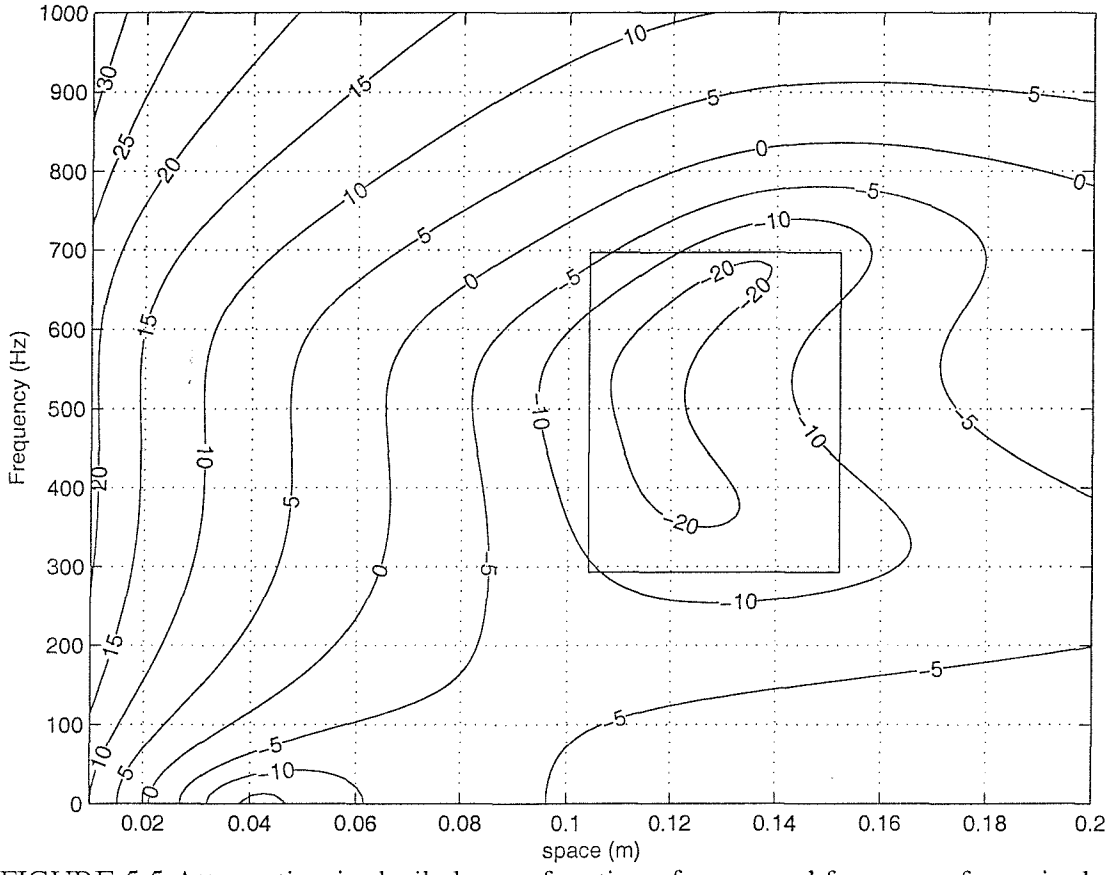

FIGURE 5.5 Attenuation in decibels as a function of space and frequency for a single-channel system with an FIR filter having 4 coefficients.

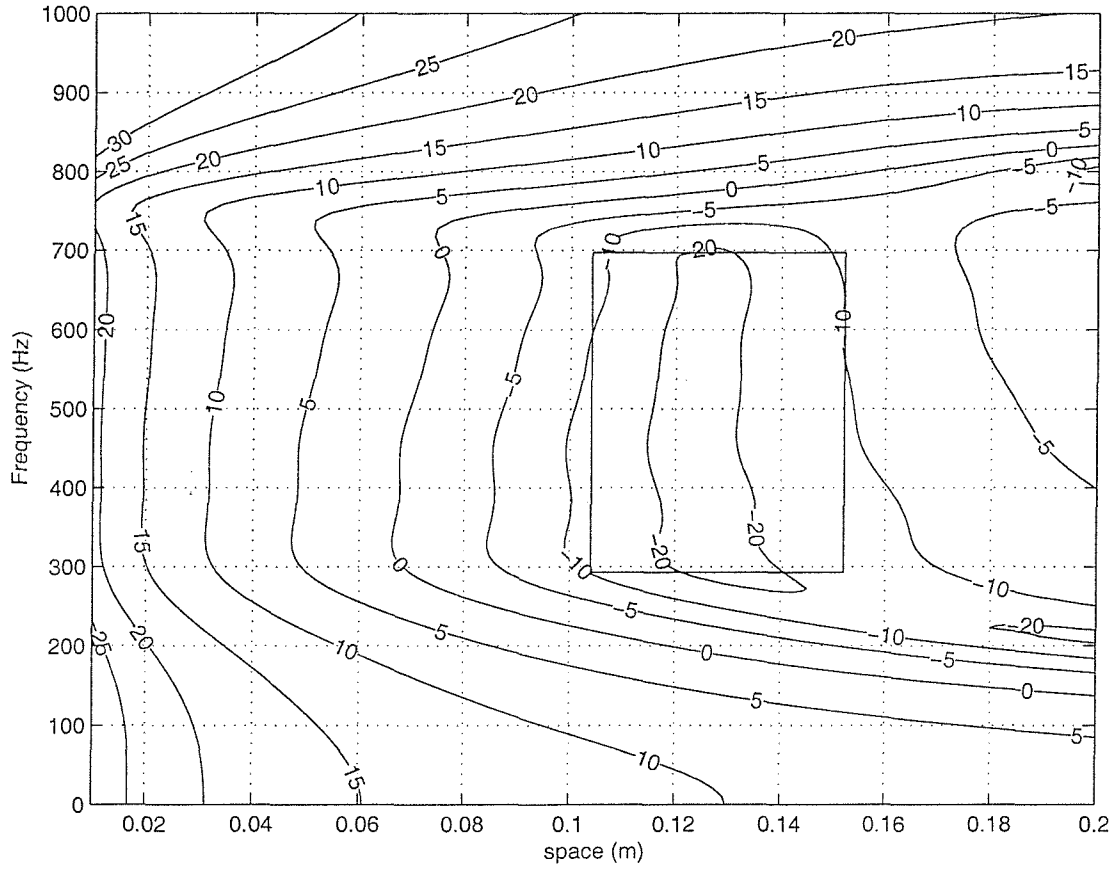

FIGURE 5.6 Attenuation in decibels as a function of space and frequency for a single-channel system with an FIR filter having 16 coefficients, without constraints.

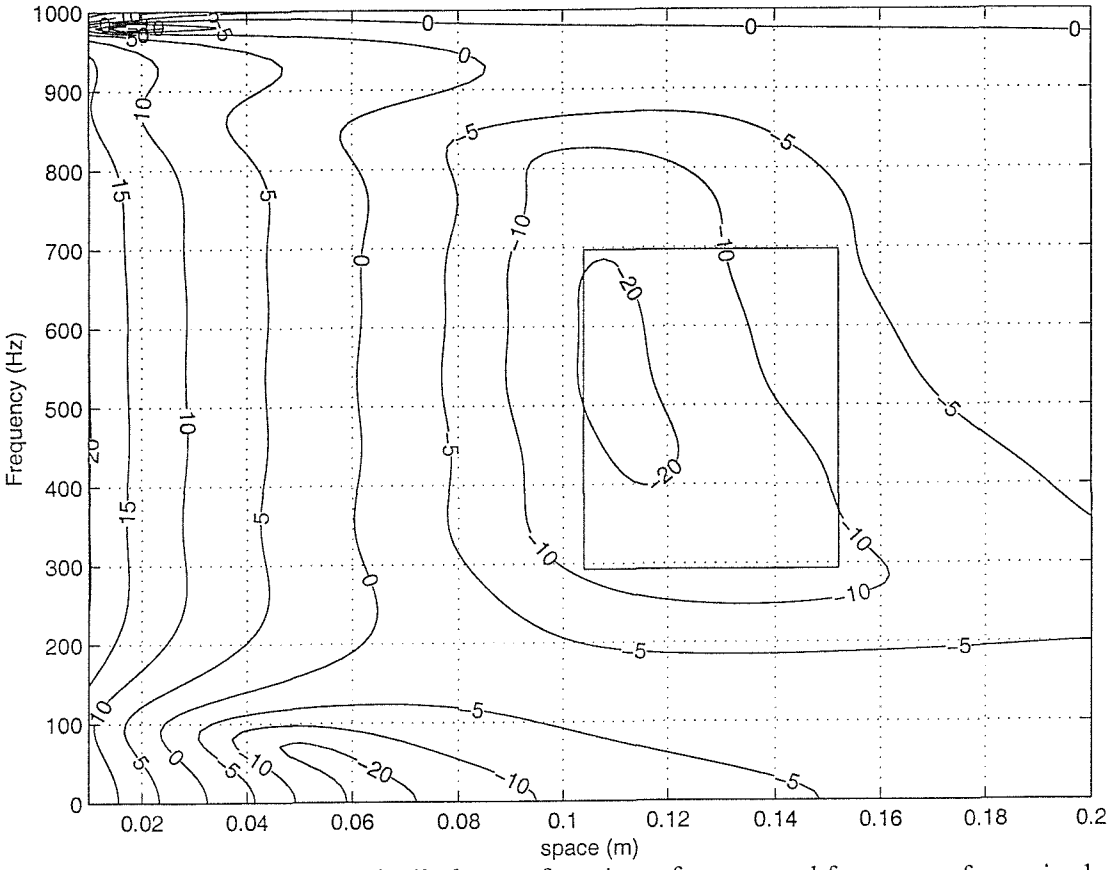

FIGURE 5.7 Attenuation in decibels as a function of space and frequency for a single-channel system with an FIR filter having 16 coefficients and constraints on amplification not to exceed 6dB at the spatial axis from r=0.04m to r=0.2m for all the frequencies.

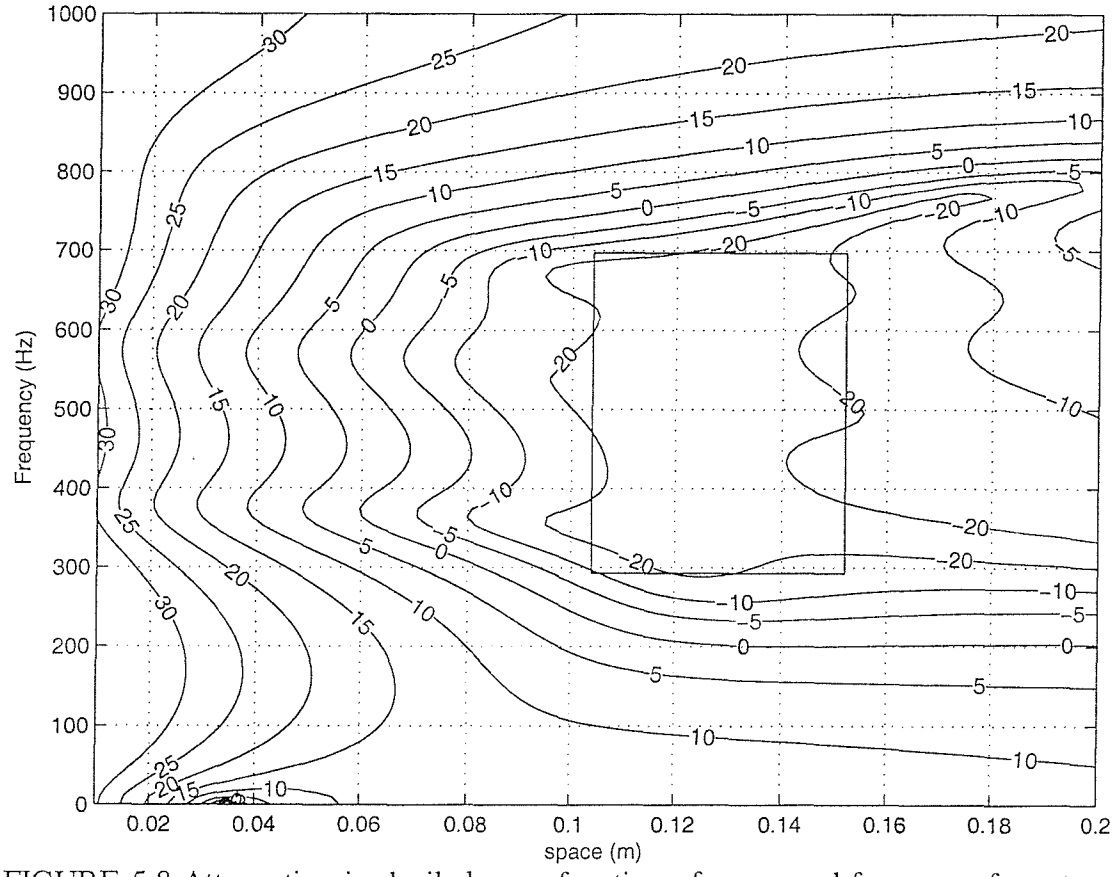

FIGURE 5.8 Attenuation in decibels as a function of space and frequency for a two-channel system with an FIR filter having 16 coefficients, without constraints.

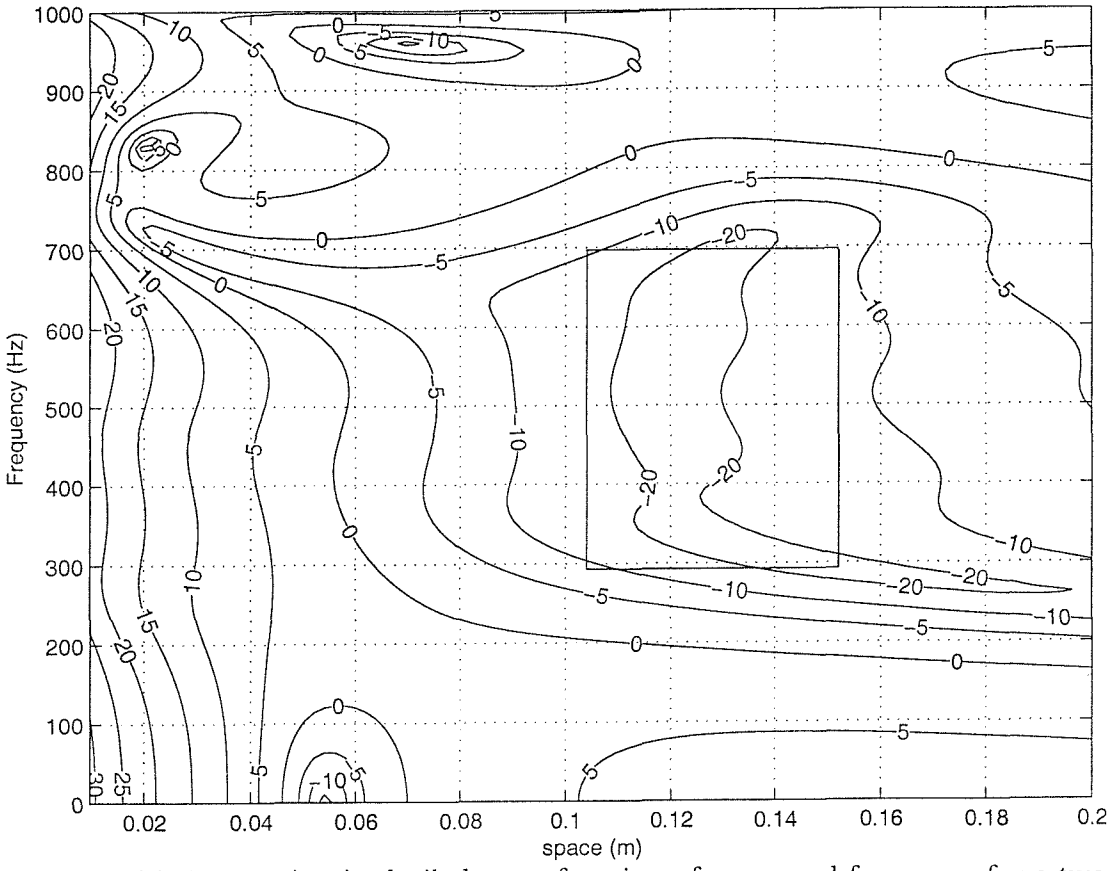

FIGURE 5.9 Attenuation in decibels as a function of space and frequency for a two-channel system with an FIR filter having 16 coefficients and constraints on amplification not to exceed 6dB at the spatial axis from r=0.04m to r=0.2m for all the frequencies.

Part IV: Application in a headrest system

Chapter 6. Design of a SISO virtual microphone feedback controller

6.1 Introduction

Active control of sound in an enclosure can be divided into two categories. One is global control, where the sound is attenuated in the entire enclosure. The other is local control, where the sound is attenuated at restricted areas called zones of quiet. It is more desirable that global control is achieved. However it is not always possible, due to the complexity of the sound field at high frequencies. Under this circumstance, local control is more practical. Previous work on local active control of diffuse sound fields showed that the zones of quiet are limited in diameter to about a tenth of a wavelength (Joseph *et al*, 1992 and Elliott *et al*, 1998). Therefore local control is useful at low frequencies only. In order to achieve more effective local control it is necessary to centre the zones of quiet close to the listener's ears. To achieve this without physically placing a microphone near the listener's ears, a virtual microphone arrangement could be used, where the sound is attenuated at a location remote from the microphone, towards the ears, to increase the attenuation at listener's ears (Elliott and David, 1992). In this chapter we present the design formulation of a single-input single-output feedback controller used to attenuate the noise at the virtual microphone. The design methods are formulated as H_2 and H_2/H_∞ optimisations, where H_2 objective is used to achieve reduction in the noise, and H_∞ constraints are used to guarantee robust stability in the face of plant uncertainties, and to prevent the noise enhancement at any frequency. The H_2 and H_2/H_∞ methods are formulated as convex problems using FIR filters, and solved numerically. The reason for choosing these methods is that H_2 method is used to estimate the performance, since H_2 formulation is easy to solve and takes less computational effort. Once the performance has been estimated H_2/H_∞ method could be used to obtain better performance.

The H_2/H_∞ design method follows that described in Rafaely, 1997, Rafaely and Elliott, 1999, and the formulation using a virtual microphone follows that for Rafaely *et al*, 1999. Although the design method has been previously presented and is therefore not novel, the detailed study of its use for active headrest and its real-time implementation are novel, and will be discussed in the following chapters.

6.2 Internal model control configuration

In this section we present the digital feedback controller configuration, which employed an Internal Model Control (IMC) structure for the feedback controller, and a multiplicative uncertainty model for the plant (Doyle *et al*, 1992), as illustrated in Figure 6.1. The frequency response of the plant can be written in terms of the plant model and the multiplicative uncertainty as (Franklin *et al*, 1994):

$$P = P_0 (1+L), \tag{6.1}$$

where P_0 is a parameterised model of the plant and L is an unstructured uncertainty and is limited in magnitude to

$$|L| \leq B, \tag{6.2}$$

where B is the uncertainty bound.

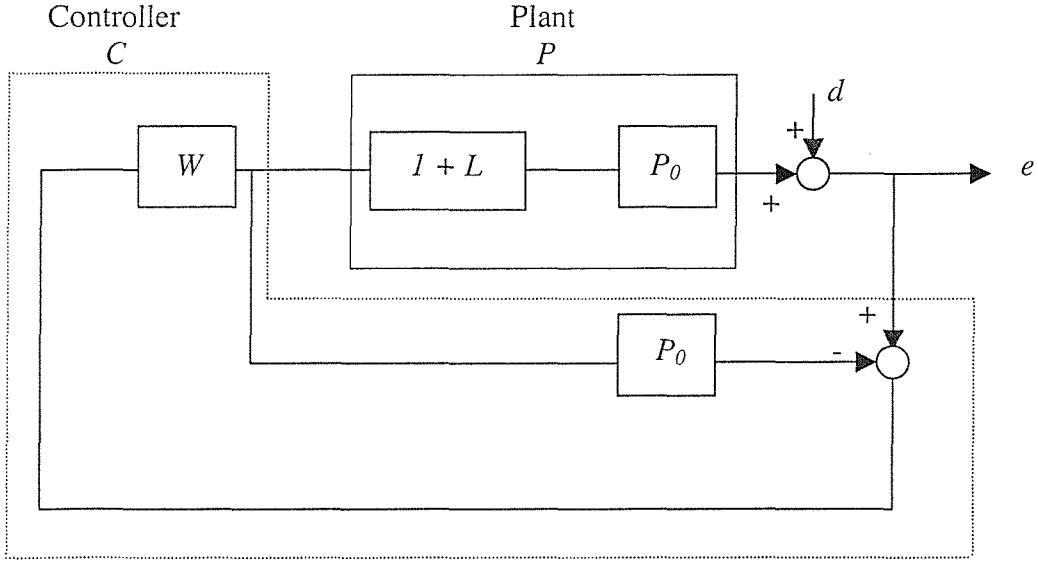

FIGURE 6.1. An Internal Model Controller with C the feedback controller, W the control filter, P_0 the plant model, and P the true plant, which is described by multiplicative uncertainty around the plant model.

The feedback controller C can be written in the frequency domain as:

$$C = \frac{W}{1 + WP_0} \tag{6.3}$$

If the plant model P_0 is equal to the true plant P, the nominal sensitivity function S_0, which is the response from the disturbance d to the error e, can be written as:

$$S_0 = \left.\frac{1 + WP_0}{1 + W(P_0 - P)}\right|_{P_0 = P} = 1 + WP_0 \tag{6.4}$$

It should be noted that in some circumstances, the controller itself, C, may not be stable, and so the open-loop control system is unstable, even though the closed-loop system, whose transfer function is given by S_0, is stable provided W and P_0 are stable (Morari and Zafiriou, 1989).

The nominal complementary sensitivity function T_0 can also be written as:

$$T_0 = 1 - S_0 = \left.\frac{-WP}{1 + W(P_0 - P)}\right|_{P_0 = P} = -WP_0 \tag{6.5}$$

In this work the power spectral density of the error signal is minimised and can be written as:

$$S_{ee} = \left|S_0\right|^2 S_{dd}, \tag{6.6}$$

where S_{ee} is the power spectral density of the error signal, S_0 is the nominal sensitivity function and S_{dd} is the power spectral density of the disturbance.

The nominal sensitivity function also plays an important role in the amplification limitation of the disturbance as follows.

$$|S_0 A| < 1 \text{ for all frequency,} \tag{6.7}$$

where S_0 is the sensitivity function and $1/A$ is the desired enhancement bounds.

For robust stability the closed-loop system must remain stable for changes or uncertainties in the response of the plant. A multiplicative uncertainty plant model is assumed here. A robust stability condition can be derived for the multiplicative plant uncertainty (Doyle *et al*, 1992) by constraining the uncertainty circles, plotted on a Nyquist diagram, from enclosing the instability point (-1,0). This leads to the following robust stability constraint:

$$\|T_0 B\|_\infty < 1, \tag{6.8}$$

where T_0 is the complementary sensitivity function with the nominal plant, and B is the multiplicative uncertainty bound. With an Internal Model Control configuration the robust stability constraint reduces to:

$$\|W P_0 B\|_\infty < 1. \tag{6.9}$$

In order to achieve the maximum error reduction the sensitivity function should be close to zero, and the complementary sensitivity function needs to be close to zero for the maximum robust stability. However the sensitivity and complementary sensitivity functions must obey the following relation (Franklin *et al*, 1994).

$$S_0 + T_0 = 1. \tag{6.10}$$

Therefore there is a trade-off between the performance and the robust stability.

6.3 Virtual microphone controller design

In this section the methods used to design the feedback controller to minimise the acoustic pressure at a virtual microphone are presented. The methods involve H_2 and H_2/H_∞ design as described in Rafaely *et al* (1999). The H_2 method is used for the initial design process to estimate the performance, due to its simplicity and efficiency. However the H_2/H_∞ design method is used for the final design stage to achieve a better performance/robustness trade-off, although it is more computationally complex. Consider a feedback control system with a virtual microphone arrangement as shown in Figure 6.2, where the controller is designed to minimise the acoustic pressure at the virtual microphone. However it is the signal from the physical microphone that is fed into the controller.

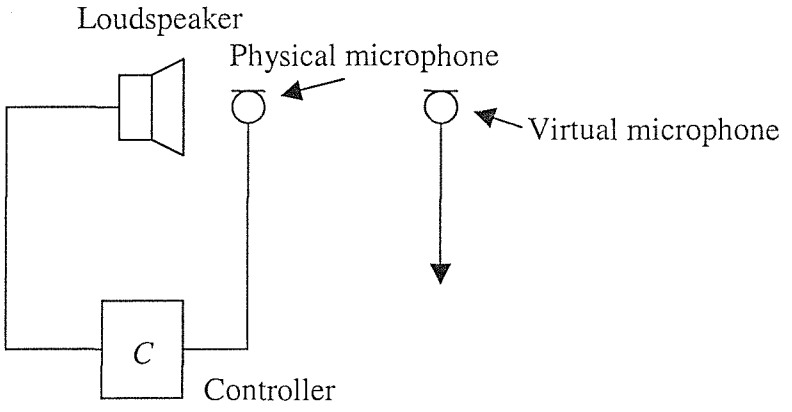

FIGURE 6.2. A feedback system with a virtual microphone arrangement

The equivalent block diagram of this feedback control system can be drawn in Figure 6.3, where C is the controller, P_{mic} is the physical plant (the response from loudspeaker input to physical microphone output), P_{vir} is the virtual plant (the response from loudspeaker input to virtual microphone output), e_{mic} is the error signal from the physical microphone output, e_{vir} is the error signal from the virtual microphone output, d_{mic} is the disturbance at the physical microphone, d_{vir} is the disturbance at the virtual microphone and is equivalent to filtering d_{mic} with F, which is the response between the physical and virtual microphones. This represents the relation between the primary signals at the two microphone locations and will depend on the acoustic environment. If the microphones are located closely enough, $F \cong 1$.

The idea behind a virtual microphone design is to place a physical microphone at the virtual microphone position in the controller design phase, using a prototype system and measure the responses P_{vir} and F needed in the design process. However, once the controller is designed, only the physical microphone as in Figure 6.2 is used in practice. When the controller is operating the best attenuation should then be achieved at the virtual microphone location.

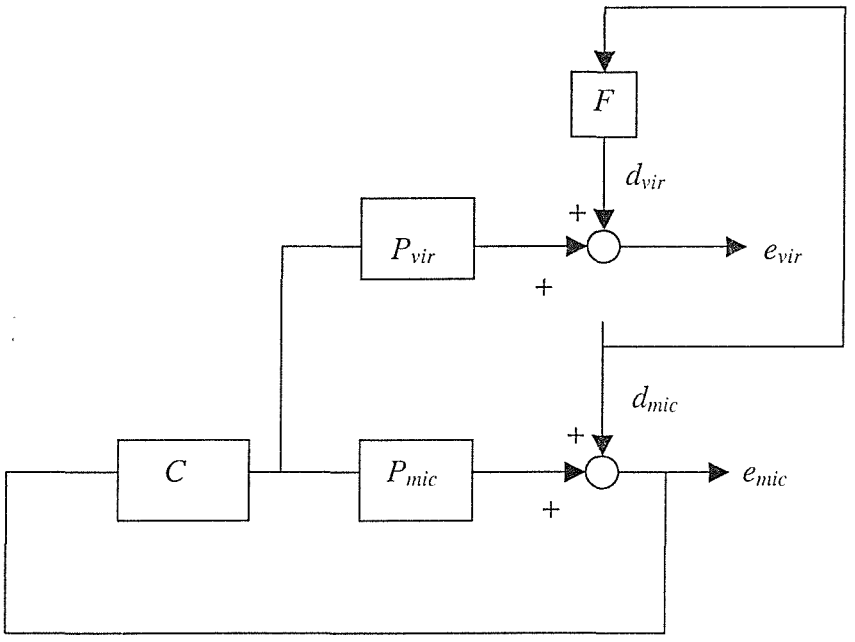

FIGURE 6.3. The equivalent block diagram of a feedback control system with a virtual microphone arrangement.

The feedback system shown in Figure 6.3 can be implemented differently, if we use an internal model of the physical plant within the controller which is driven by the same signal as the physical plant, as shown in Figure 6.4, where W is the control filter and P_{mic0} is the model of the nominal physical plant. Therefore the controller can be written as

$$C = \frac{W}{1 + WP_{mic0}} \tag{6.11}$$

If the model of the physical plant is perfect so that $P_{mic0}=P_{mic}$, then the input to W is equal to d_{mic}, and the IMC (internal model control) controller configuration reduces to a pure feedforward system as shown in Figure 6.5. We assume the system is linear, then the position of the control filter and the virtual plant can be exchanged as shown in Figure 6.6, where the x is the signal by filtering the disturbance d_{mic} with the virtual plant.

Although in a practical system $P_{mic0} \neq P_{mic}$, the controller is designed with the nominal plant, so the assumption that $P_{mic0}=P_{mic}$ holds for the design phase only. The controller is also designed to be robustly stable for the given variation of P_{mic} around P_{mic0}.

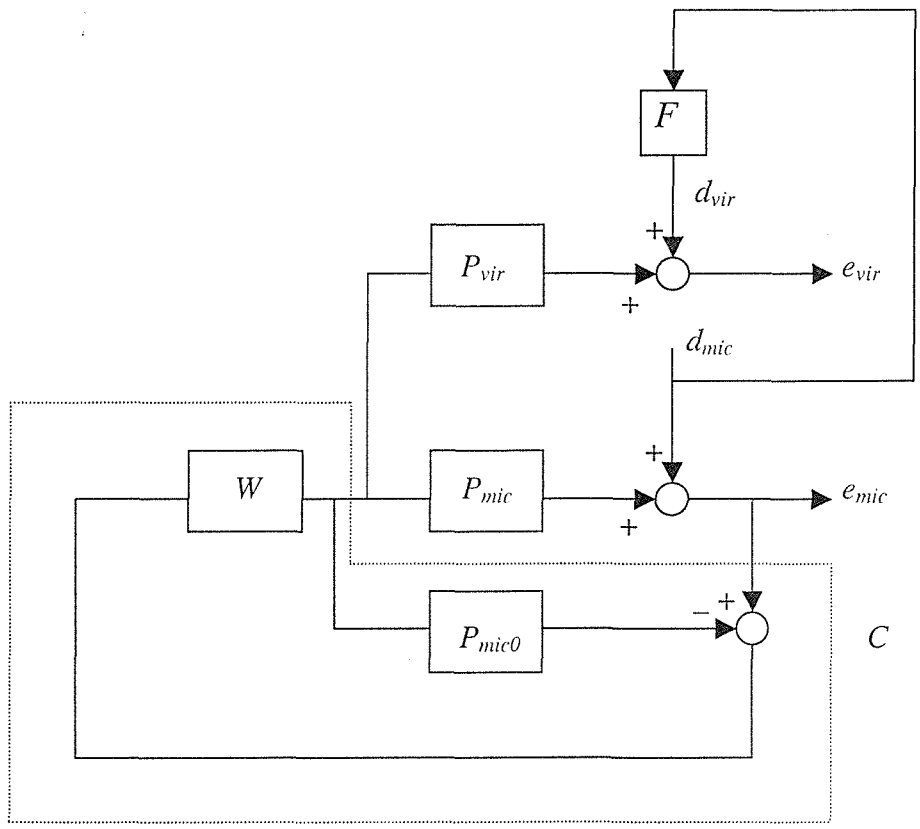

FIGURE 6.4. A internal model control system configuration.

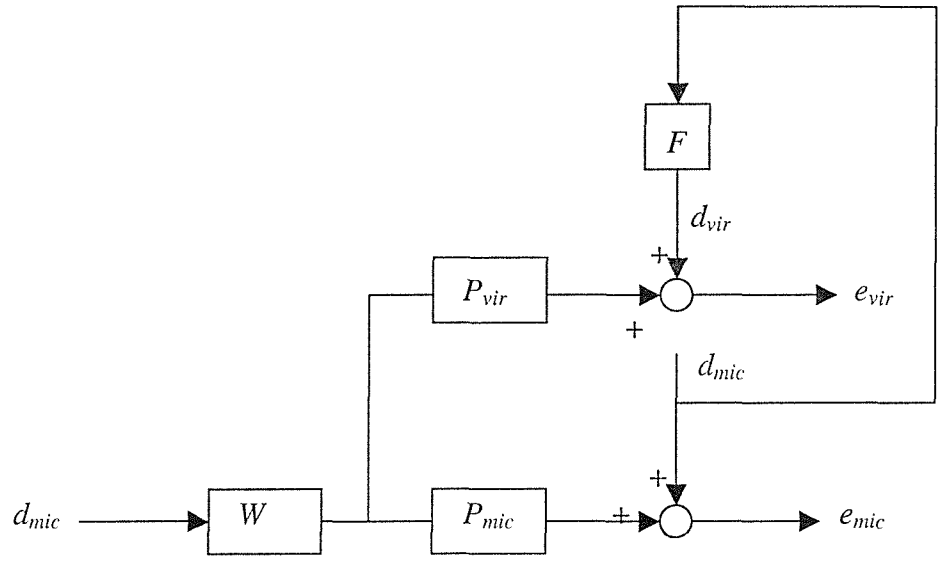

FIGURE 6.5. The pure feedforward system for the internal model control configuration.

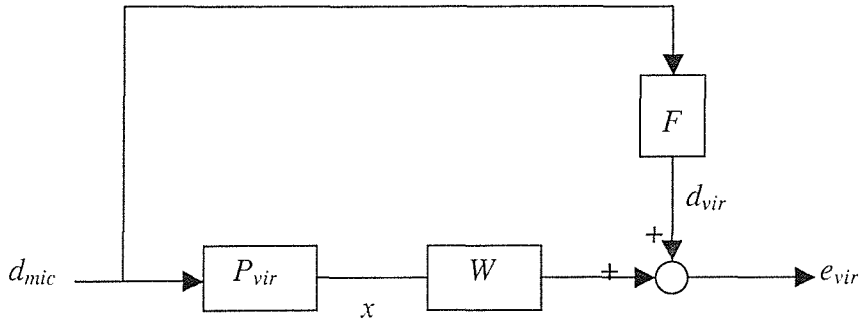

FIGURE 6.6. The pure feedforward system with exchanging the position of the control filter and the virtual plant.

In this work H_2 and H_2/H_∞ controllers are designed to minimise the error signal from the virtual microphone output. For the H_2 controller design, the cost function is of the form

$$J = E[e_{vir}^2] + \beta \boldsymbol{w}^T \boldsymbol{w}. \tag{6.12}$$

Although other H_2 cost functions could be used (see, for example, Rafaely, 1997), the cost function in equation (6.12) is simple to solve and provides a straightforward trade-off between the performance and robustness via the parameter β.

In order to find the optimal set of filter coefficients, that minimise this quadratic cost function, we can set the differential of this cost function with respect to each w_i to zero simultaneously, and the optimal filter can be written as (Elliott and Sutton, 1996):

$$\boldsymbol{w}_{opt} = -(\boldsymbol{A} + \beta \boldsymbol{I})^{-1} \boldsymbol{b}, \tag{6.13}$$

where $\boldsymbol{A}$ is the auto-correlation matrix of the reference signal x created by filtering the signal d_{mic} with the P_{vir} as shown in Figure 6.6, and $\boldsymbol{b}$ is the cross correlation vector of the reference signal x and disturbance signal d_{vir}. Therefore the power spectral density of the filtered reference signal can be written as

$$S_{xx} = S_{ddmic} \mid P_{vir} \mid^2, \tag{6.14}$$

where S_{xx} is the power spectral density of the filtered reference signal, S_{ddmic} is the power spectral density of the disturbance signal at the physical microphone and P_{vir} is the virtual plant. The cross spectral density of the reference signal x and the disturbance signal d_{vir} can also be written as

$$S_{xdvir} = S_{xx} F/P_{vir}. \tag{6.15}$$

Substituting equation (6.14) into equation (6.15) we can obtain

$$S_{xdvir} = S_{ddmic} P_{vir}^* F, \tag{6.16}$$

where P_{vir}^* is the conjugate of the response of the virtual plant.

For robust stability equation (6.9) can be used as the stability constraint as follows.

$$\left\| WP_{mic0}B \right\|_{\infty} < 1 \qquad (6.17)$$

Equations (6.13) and (6.17) can be used to design the H_2 feedback controller as follows:

a.Design W using $\boldsymbol{w}_{opt} = -(A+\beta I)^{-1}\boldsymbol{b}$ with small β.

b.Repeat (a) with increased β until the robust stability condition, $\left\| WP_{mic0}B \right\|_{\infty} < 1$, is satisfied with the smallest β.

For H_2/H_∞ controller design, the performance objective is written as

$$min \left\| S_0 \sqrt{S_{ddvir}} \right\|_2^2, \qquad (6.18)$$

where S_0 is the sensitivity function, $(1+ W P_{vir0} / F)$, with P_{vir0} the nominal virtual plant, F is the response between the physical and virtual microphones and $\sqrt{S_{ddvir}}$ is the square root of the power spectral density of the disturbance pressure at the virtual microphone.

For robust stability, the condition for closed-loop stability in face of plant perturbations can be written as (see equation (6.9) in section 6.2)

$$\left\| WP_{mic0}B \right\|_{\infty} < 1 \qquad (6.19)$$

where W is the control filter, P_{mic0} is the response of the nominal physical plant and B is the plant uncertainty bound.

The constraint of disturbance enhancement is equivalent to setting an upper limit on the amplitude of the sensitivity function, and is thus written as

$$\left\|(1+WP_{vir0}/F)D\right\|_{\infty}<1, \tag{6.20}$$

where *1/D* is the desired enhancement bounds. This constraint is important in active sound control, since high disturbance amplification outside the control bandwidth can increase the sound audibility.

Therefore the overall design objective can now be written as

$$\begin{aligned} &min \left\|(1+WP_{vir0}/F)\sqrt{S_{ddvir}}\right\|_2^2 \\ &subject\ to \left\|WP_{mic0}B\right\|_{\infty}<1, \\ &\left\|(1+WP_{vir0}/F)D\right\|_{\infty}<1. \end{aligned} \tag{6.21}$$

The design objective described above used continuous functions of the frequency ω, however, to facilitate the solution method, all the frequency response functions were evaluated at *N* discrete frequencies, linearly spaced from zero frequency to the sampling frequency. Therefore, all the continuous functions of the frequency are sampled to produce vectors of the frequency index *k* (*k=0,...,N-1*, which corresponds to frequencies of kf_s/N, where f_s is the sampling frequency) (see Boyd *et al*, 1988, and Rafaely and Elliott, 1999 for consideration on the frequency discretisation). The 2-norm performance objective in equation (6.21) becomes the average over all discrete frequencies, and the ∞-norm constraints are separated to individual constraints for each discrete frequency.

The control filter *W* is now defined to be an FIR filter of length *I*, with coefficients vector *w* written as:

$$w = (w_0 \ w_1 \ \ldots \ w_{I-1})^T \tag{6.22}$$

Thus equation (6.21) can be approximated as:

$$\begin{aligned} \textit{min} \quad & \frac{1}{N}\sum_{k=0}^{N-1}\left|(1+W(k)P_{vir0}(k)/F(k))\sqrt{S_{ddvir}(k)}\right|^2 \\ \textit{subject to} \quad & \left|W(k)P_{mic0}(k)B(k)\right|<1, \text{ for } k=0,...,N-1 \\ & \left|(1+W(k)P_{vir0}(k)/F(k))D(k)\right|<1. \text{ for } k=0,...,N-1 \end{aligned}$$

$$\textit{where } W(k)=\frac{1}{N}\sum_{i=0}^{I-1}w_i e^{-j2\pi ik/N} \qquad I\le N/2 \tag{6.23}$$

where $I \le N/2$ corresponds to the causality constraint on the control filter W. The size of I should be chosen large enough that the impulse response of the optimal continuous filter W will have negligible amplitude beyond I/f_s, and thus will be accurately represented by the FIR control filter W, which is the solution to equation (6.23) (see Rafaely, 1997 for more details).

Equation (6.23) will accurately represent the design problem in equation (6.21) if N is sufficiently large. However smaller N will reduce the computation complexity and an engineering choice must be made for the value of N used. The size of N can be determined by considering the frequency-sampling process using the tools of time-domain sampling. The reader is referred to Rafaely, 1997, for more details. Equation (6.23) is a convex programming problem (with a unique, global minimum), as a function of the parameters vector w, since both objective and constraints function are quadratic (and convex) functions of w (Rafaely and Elliott, 1996). The optimal filter W can be calculated by solving equation (6.23) using the function *constr( )* in MATLAB (Grace, 1995), with the optimisation parameters being the coefficients of the FIR filter W. The method used in the function *constr( )* is sequential quadratic programming (Grace, 1995).

6.4 Conclusions

Design methods for a feedback controller using robust H_2 and H_2/H_∞ approaches for active control of sound have been presented in this chapter. The feedback controller is configured using Internal Model Control, which simplifies the design formulation. These methods have been previously used successfully in the design of an active controller (Rafaely and Elliott, 1999) and were therefore used in this work. An H_2 method can be initially used to estimate the performance in the design process since it has a simple and efficient solution, however, a better performance/robustness trade-off can be achieved by using an H_2/H_∞ method and so this method can be used in the final design stage. Nevertheless, the latter is more computationally complex. In the next chapter we will discuss some stability issue in the H_2 and H_2/H_∞ virtual microphone controllers, which limit the performance of active control of sound.

Chapter 7. Performance and stability of a SISO virtual microphone feedback controller

7.1 Introduction

In this chapter the limitation on performance of an active headrest system due to the use of virtual microphone feedback controllers is presented. Practical aspects of headrest performance will be presented in chapters 8 and 9. The performance and stability of a feedback controller with Internal Model Control configuration to cancel the noise at a virtual microphone is investigated. The attenuation using an open-loop stable feedback controller is also compared with that using an open-loop unstable feedback controller. The results show that the controller which was open-loop unstable gave the best performance. Therefore there is a trade-off between the performance and controller open-loop stability. This is found to be due to the fact that the magnitude of the response of the virtual plant is lower than that of the physical plant. The feedback controller in this work is designed to minimise the noise at the virtual microphone, with a virtual plant response used in the performance objective. However the physical plant is used in the stability constraint. This results in conflicting requirement from the control filter and good performance is only achieved with an unstable feedback controller.

7.2 Headrest system arrangement

The performance and stability of a virtual microphone feedback system is demonstrated in this chapter by examples from a laboratory active headrest system. The arrangement of the system is described in this section. Figure 7.1 shows the arrangement of the headrest system, which includes primary and secondary loudspeakers, a physical microphone, a virtual microphone and a manikin head. The distance between the physical and virtual microphone is about 10cm. The physical microphone and the secondary loudspeaker are connected via a feedback controller. The primary loudspeaker is 1.5m away from the physical and virtual microphones. The headrest system is designed to attenuate the acoustic noise at the virtual microphone, which is used in the design process only. However the physical microphone is used to detect the error signal which is filtered by the feedback controller and then fed to the secondary loudspeaker. In this work the physical and virtual plants were measured and used to design the controller. The physical plant is the response from the input of the secondary loudspeaker to the output of the physical microphone and the virtual plant is the response from the input of the secondary loudspeaker to the output of the virtual microphone.

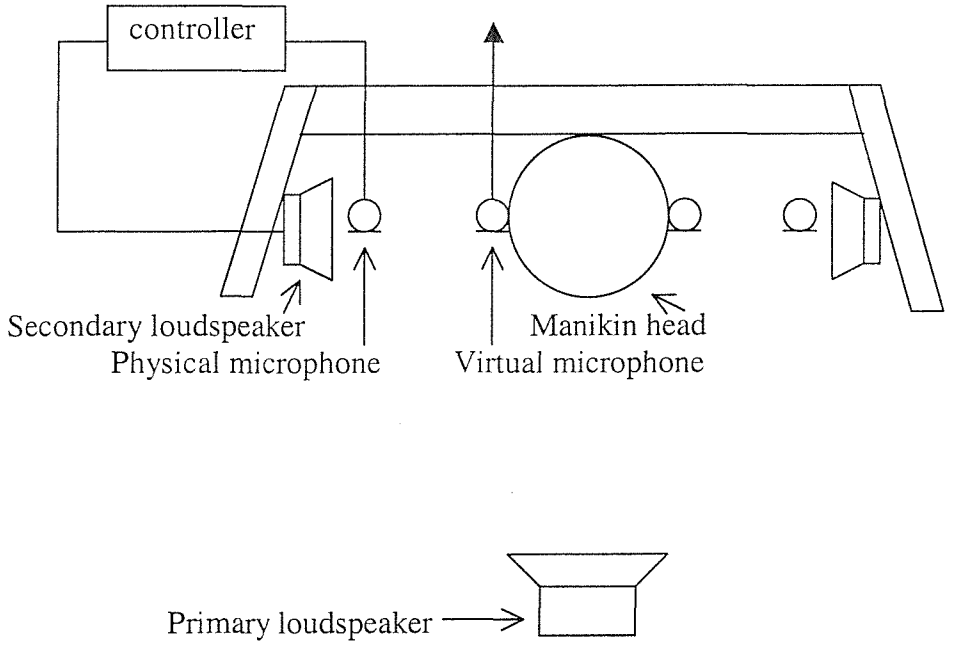

FIGURE 7.1 The active headrest system with physical and virtual microphones arrangement.

7.3 Controller stability vs. performance in a virtual microphone feedback controller with Internal Model Control configuration

In this section we discuss the stability problem of a virtual microphone feedback controller with Internal Model Control configuration. The performance of an unstable feedback controller is compared to that of a stable feedback controller.

Figure 7.2 shows the power spectral density of the disturbance used in the design process. The disturbance is created by filtering the white noise via the shaping filter which is modelled as an 8-pole Butterworth low-pass filter with a cut-off frequency of 400 Hz, combined with an 8-pole Butterworth high-pass filter with a cut-off frequency of 200 Hz. We chose 200 Hz for the bandwidth of the disturbance, since when the bandwidth of the disturbance is increased the performance will be too poor. Figures 7.3 and 7.4 show the frequency responses of the physical and virtual plants respectively. It can be seen that the magnitude of the frequency response of the physical plant is about 10 dB higher than that of the virtual plant. The reason for this is because the virtual microphone is about 10 cm further away from the secondary loudspeaker than the physical microphone. Therefore the acoustic pressure at the virtual microphone is lower than that at the physical microphone. This difference can be reduced by placing the headrest close to the ears. However this would restrict the movement of the head.

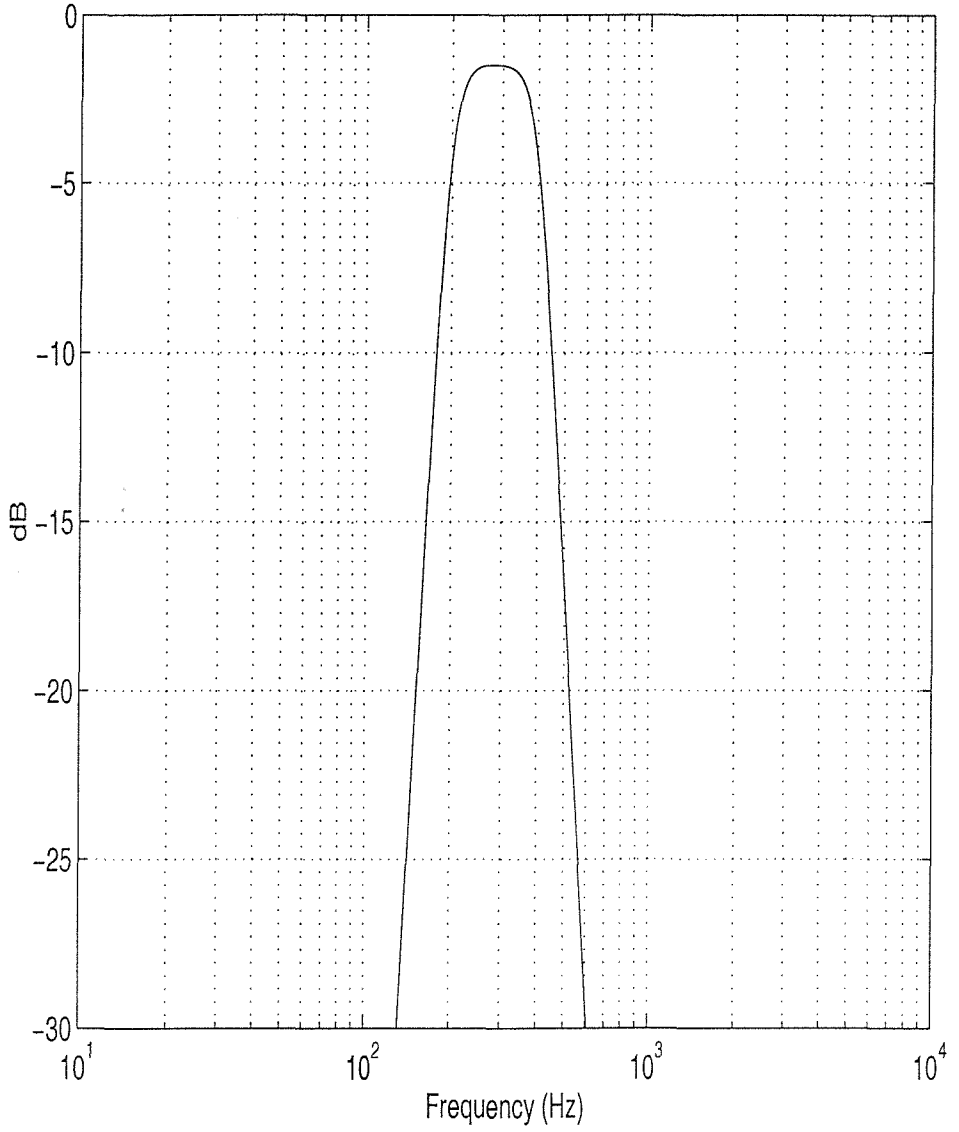

FIGURE 7.2 The power spectrum of the random disturbance.

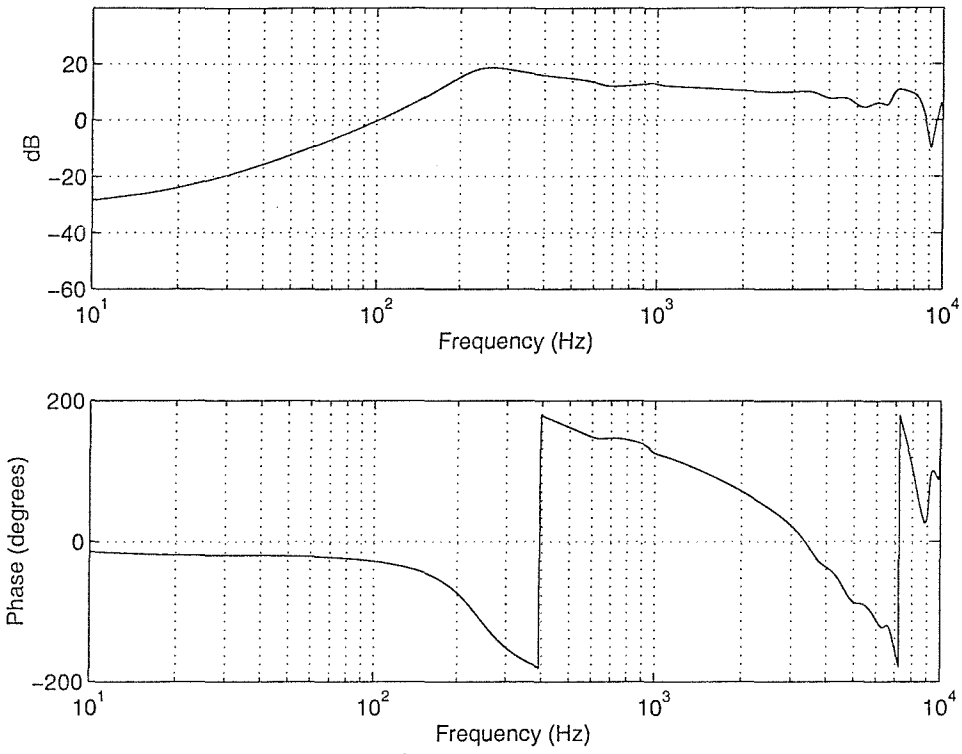

FIGURE 7.3 Frequency response of the physical plant.

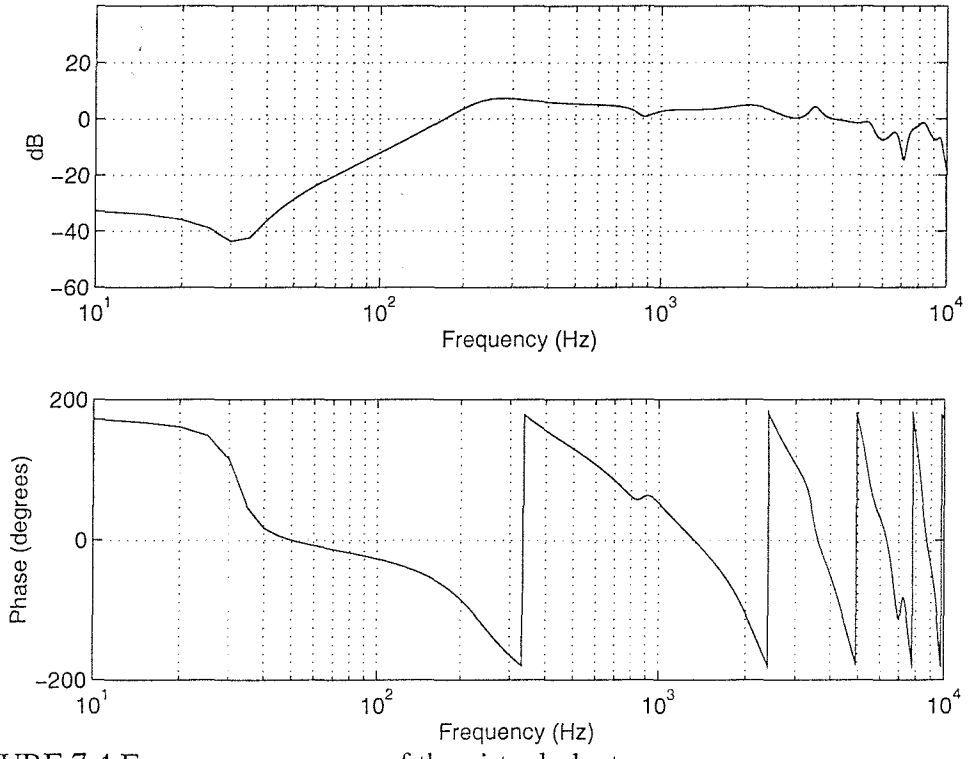

FIGURE 7.4 Frequency response of the virtual plant.

In this work we design the controller to minimise the acoustic pressure at the virtual microphone and subject to the stability and enhancement constraints (see chapter 6 for more details). We assume that the primary field at the physical and virtual microphones is equal, since the distance between the two microphones is small compared to a wavelength in this frequency range. Therefore F, the response between the physical and virtual microphones, is assumed to be unity. The performance, stability and enhancement constraints can now be written as follows.

$$\begin{aligned} &\textbf{\textit{performance}} && \left\|(1+WP_{vir0})\sqrt{S_{ddvir}}\right\|_2^2 \\ &\textbf{\textit{closed-loop stability}} && \left\|WP_{mic0}B\right\|_\infty < 1, \\ &\textbf{\textit{enhancement}} && \left\|(1+WP_{vir0})D\right\|_\infty < 1, \end{aligned} \tag{7.1}$$

where the constraints only guarantee the stability of the closed-loop system and does not guarantee the stability of the feedback controller itself.

The transfer function of the feedback controller can be written as (see chapter 6)

$$C = \frac{W}{1+WP_{mic0}} \tag{7.2}$$

For controller stability the Nyquist plot of (WP_{mico}) must not enclose (-1,0) point. We should notice that the virtual plant is used in the performance objective; however, the physical plant is used in the stability constraint. For good performance the following condition must be satisfied.

$$WP_{vir0} = -1 \quad \text{at the disturbance frequencies} \tag{7.3}$$

However the magnitude of the physical plant is about 10 dB higher than that of the virtual plant, i.e.

$$P_{mic0} \cong 3P_{vir0} \tag{7.4}$$

so that

$$WP_{mic0} = -3 \quad \text{at the disturbance frequency.} \tag{7.5}$$

This result has important consequences on the open-loop stability of the controller C in equation (7.2). The stability of this controller and hence of the open-loop response of the complete control system is determined by the Nyquist plot of WP_{mic0}, as shown in Figure 7.5.

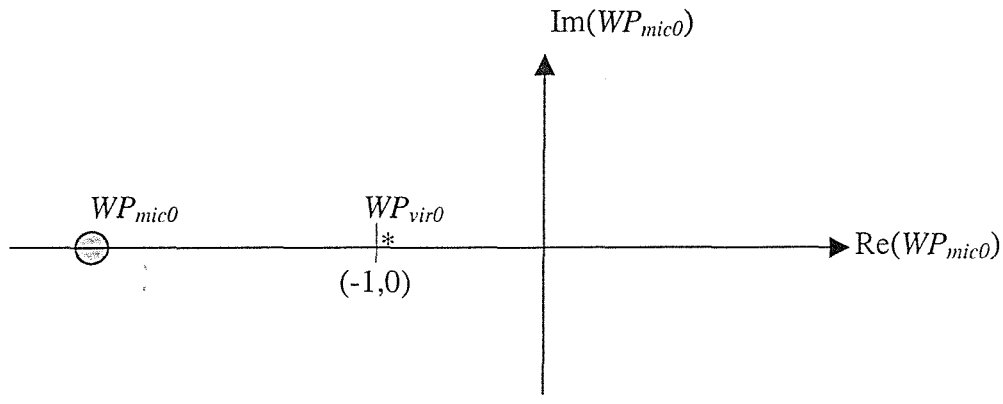

FIGURE 7.5 Performance and controller stability condition. Good performance with an unstable controller.

If the Nyquist plot of WP_{mic0} passes through the point (-3,0), as required for good performance in equation (7.2), the controller is likely to be unstable. In order to obtain a stable controller C the gain of W must generally be reduced to achieve the following condition.

$$WP_{mic0} < -1 \tag{7.6}$$

in which case

$$WP_{vir0} \leq -0.33 \tag{7.7}$$

which can be represented as in figure 7.6.

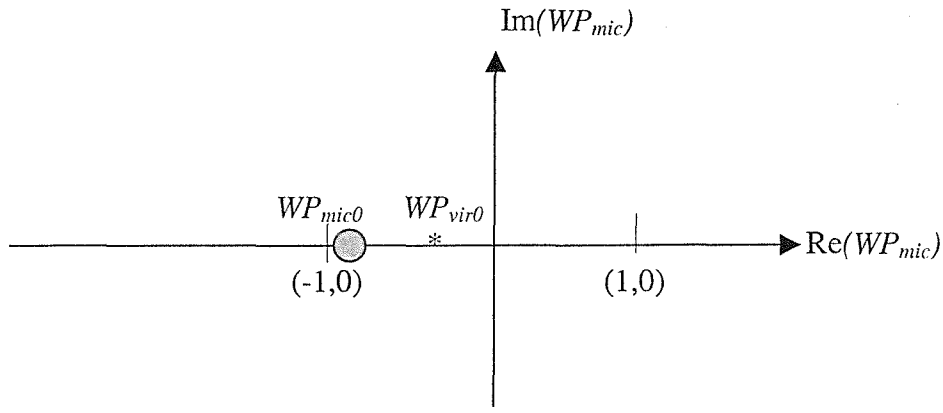

FIGURE 7.6 Performance and controller stability condition. Poor performance with a stable controller.

This will result in poor performance because equation (7.3) can not be satisfied. Therefore there is a trade-off between the performance and the stability of the feedback controller C in the case of using a virtual microphone in a headrest system. In real-time implementation of practical systems we usually need to measure the frequency response of the controller before the controller is implemented, in order to ensure that the expected performance is achieved. If an unstable controller is used, we will not be able to measure the frequency response of the controller. In the next section we will discuss how to design stable controllers by using another constraint for the controller stability in the design process.

7.4 Design of stable feedback controllers

In this section we present the design method of stable feedback controllers. The performance of stable and unstable controllers will be compared in the next section. For a ''fair'' comparison, the best attenuation with stable controller is required. This can be done by adding a controller stability constraint in the design process. If Nyquist stability criterion, which ensures that the frequency response of (WP_{mic0}) does not encircle the point (-1,0) on the Nyquist plane, is applied directly to the design process, the formulation might not be simple, in particular if a convex formulation is required. Another method of designing a stable controller is to apply the small gain theory, which ensures that all the frequency response (WP_{mic0}) is inside the unit circle. This is a very conservative method. A slightly less conservative criterion, which is also easily applied, is to avoid any response of the left hand side of the point (-1,0) on the Nyquist plane. Therefore another constraint could be added into the design process to ensure that the controller is stable as follows.

$$\left\| \mathrm{Re}\left\{ WP_{mic0} \right\} \right\|_{\infty} > -1. \tag{7.8}$$

This constraint will guarantee that the Nyquist plot of the frequency response of (WP_{mic0}) is on the right hand side of the point (-1,0), which results in stable controller. This is less conservative than small gain theory and appears to be a novel formulation of the design process to ensure open-loop stability. The reason for choosing this method rather than other methods to guarantee the controller stability is because it is more efficient in the optimisation process. Therefore the design objectives can now be written as follows.

performance	$\left\| (1 + WP_{vir0} / F)\sqrt{S_{ddvir}} \right\|_2^2$
closed-loop stability	$\left\| WP_{mic0} B \right\|_{\infty} < 1,$
enhancement	$\left\| (1 + WP_{vir0} / F) D \right\|_{\infty} < 1$
open-loop controller stability	$\left\| \mathrm{Re}\left\{ WP_{mic0} \right\} \right\|_{\infty} > -1.$ (7.9)

In this case the controller stability constraint can be written as:

$$\left|\mathrm{Re}\left\{\frac{1}{N}\sum_{i=0}^{I-1} w_i e^{-j2\pi ik/N}(P_R(k)+P_I(k))\right\}\right| > -1, \text{ for } k=0,\ldots, N-1 \qquad (7.10)$$

where w_i is the coefficients vector of the FIR filter W, P_R is the real part of the response P_{mic0} and P_I is the imaginary part of the response P_{mic0}.

Expanding the equation (7.10) we obtain

$$\left|\frac{1}{N}\sum_{I=0}^{I-1} w_i C(k)\right| > -1, \qquad \text{for } k=0,\ldots, N-1 \qquad (7.11)$$

where $C(k)$ is the constant $cos(2\pi ik/N)P_R(k) - sin(2\pi ik/N)P_I(k)$.

Equation (7.11) is linear, since its second derivative is equal to zero. Therefore the optimisation problem in equation (7.9) is still convex (Rafaely, 1997, Roberts and Varberg, 1973).

In the next section some design examples will be shown to compare the performance of the active headrest using stable and unstable controllers.

7.5 Design example

In this section we present active headrest controller design examples using a controller open-loop stability constraint, and compare the result to that without a controller open-loop stability constraint. In this work B, physical plant uncertainty bound, is calculated from the measurements on the laboratory headrest system with the manikin moved to 5 positions (see next chapter). D, the enhancement bound, is set to 6dB, and F, the response between the physical and virtual microphones, is assumed to be unity. A sampling frequency of 20 kHz is used and 2000 points between 0 and half sampling frequency are taken in the frequency responses. The length of filter W is 64.

Figure 7.7 shows the attenuation of the disturbance using the H_2/H_∞ controller designed without the constraint of the controller stability as in equation (7.1). Figure 7.8 shows the attenuation of the disturbance using the H_2/H_∞ controller designed with the constraint of the controller stability as in equation (7.9). It can be seen that the performance without the constraint of the controller stability is better than that with the constraint of the controller stability. This is because the gain of the control filter W without the constraint of the controller stability can be higher than that with the constraint of the controller stability as explained in section 7.3. However the controller is open-loop unstable for the case without the stability constraint as seen in figures 7.9 and 7.10 which show the Nyquist plots of the frequency responses of (WP_{mic0}) in the two cases. It should be remembered that since the internal model controller response has the form given by equation (6.11), then the stability of the controller is determined by the Nyquist plot of WP_{mic0}. In this case the controller stability constraint is set to greater than -0.96 rather than -1 in order to keep the Nyquist plot of the response of (WP_{mic0}) away from the stability critical point (-1,0). The controller is unstable if the constraint of the controller stability is not included in the design process. Figure 7.10 shows that the controller stability is maintained, as expected, because the constraint in equation (7.8) is maintained.

Figures 7.11 and 7.12 show the Nyquist plot of the frequency response of (WP_{vir0}) without and with the constraint of the controller stability, where the solid line represents the response of (WP_{vir0}) between 200 Hz and 400 Hz. As can be seen the

magnitude of (WP_{vir0}) with the controller stability constraint is further away from the point (-1,0) than that without the controller stability constraint at the frequency range from 200 Hz to 400 Hz. Therefore the performance with the controller stability constraint is poor as expected.

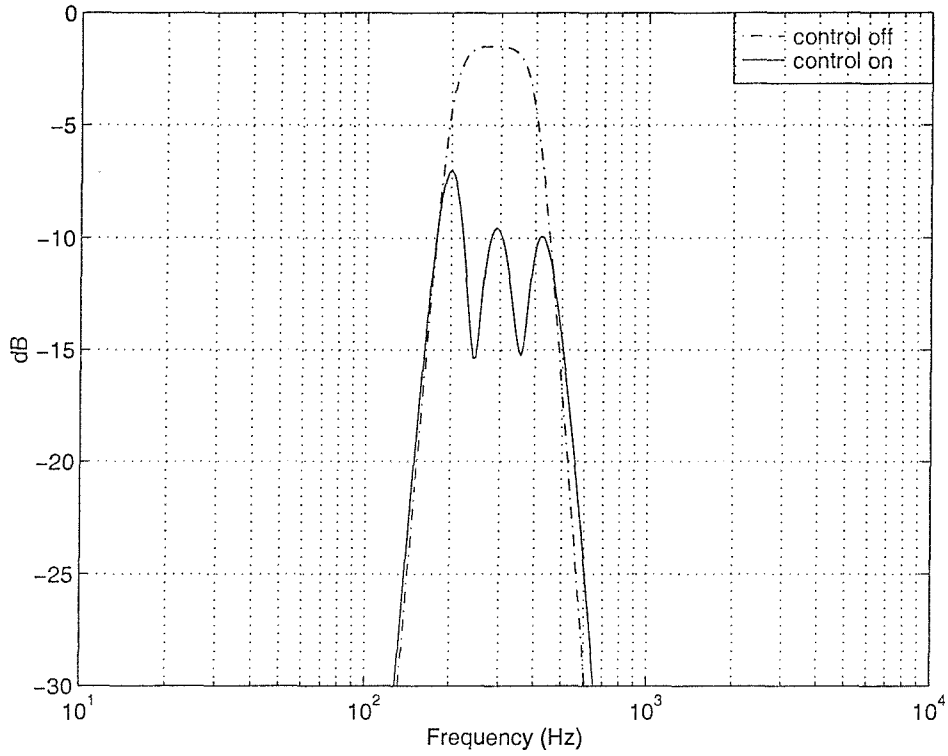

FIGURE 7.7 The power spectrum of the random disturbance before control (---) and after control (—) by using H_2/H_∞ method without the constraint of the controller stability.

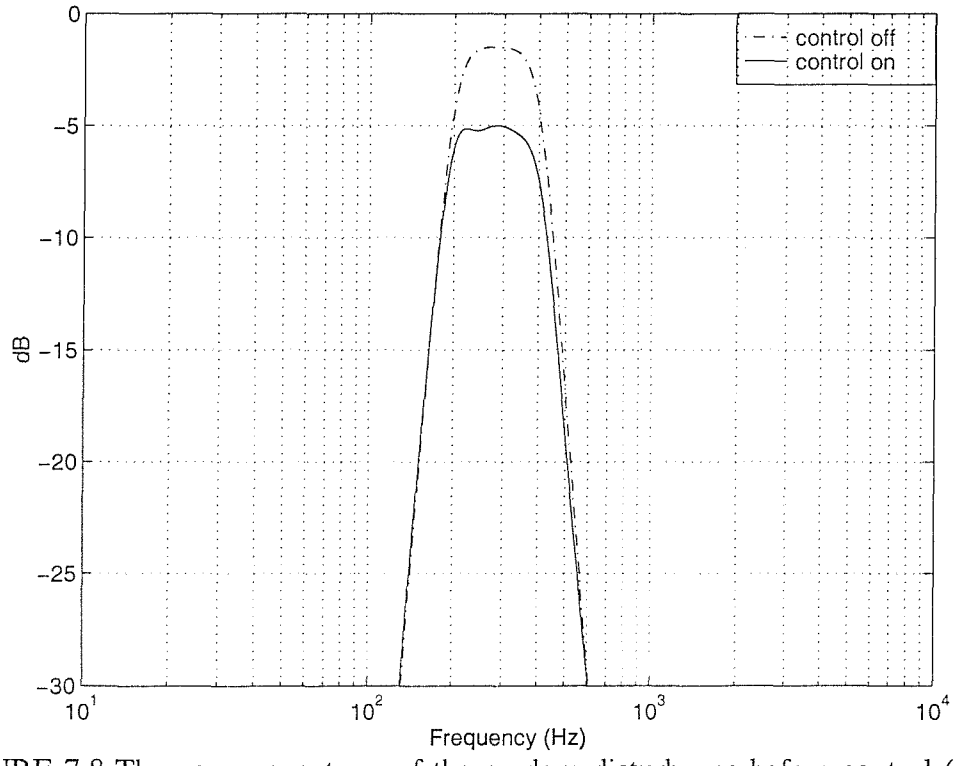

FIGURE 7.8 The power spectrum of the random disturbance before control (---) and after control (——) by using H_2/H_∞ method with the constraint of the controller stability.

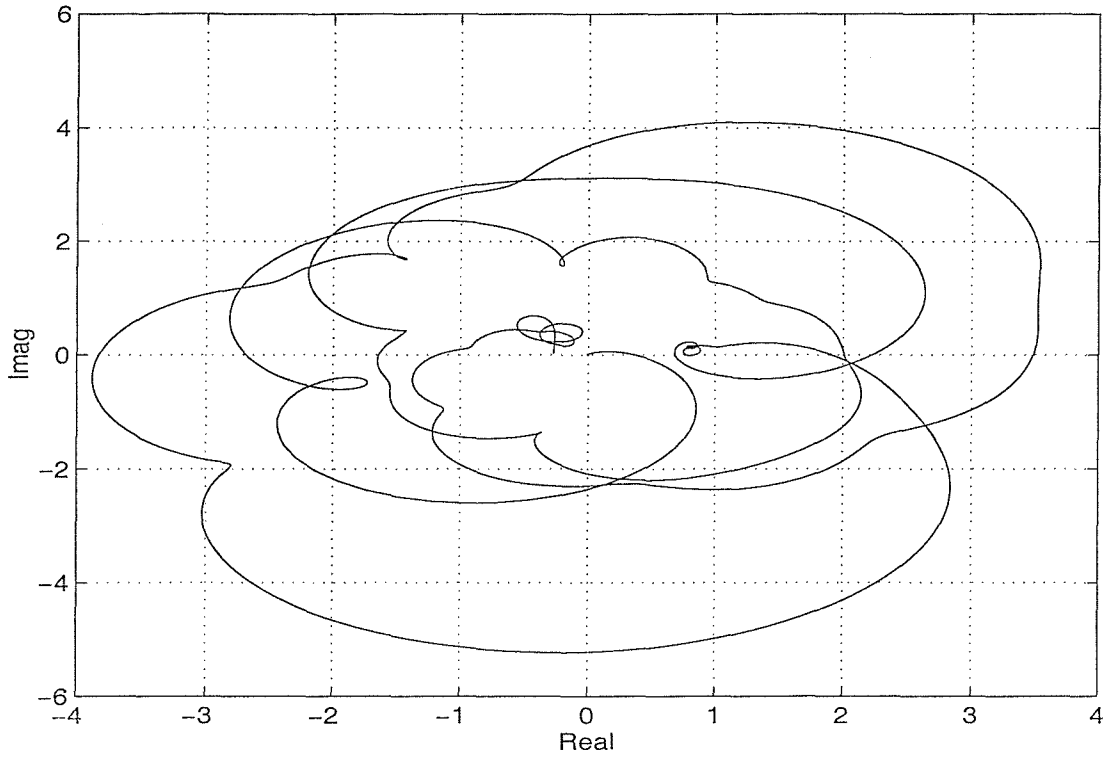

FIGURE 7.9 Nyquist plot of the frequency response of (WP_{mic0}) without the constraint of the controller stability.

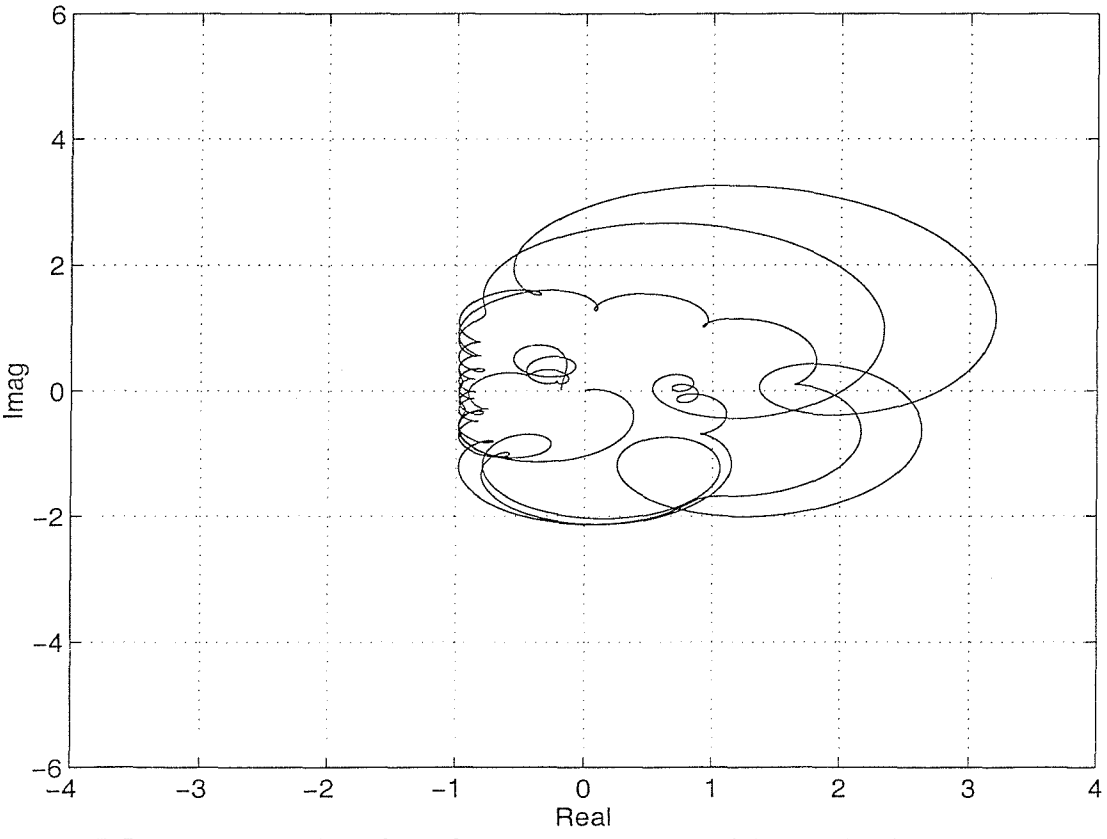

FIGURE 7.10 Nyquist plot of the frequency response of (WP_{mic0}) with the constraint of the controller stability.

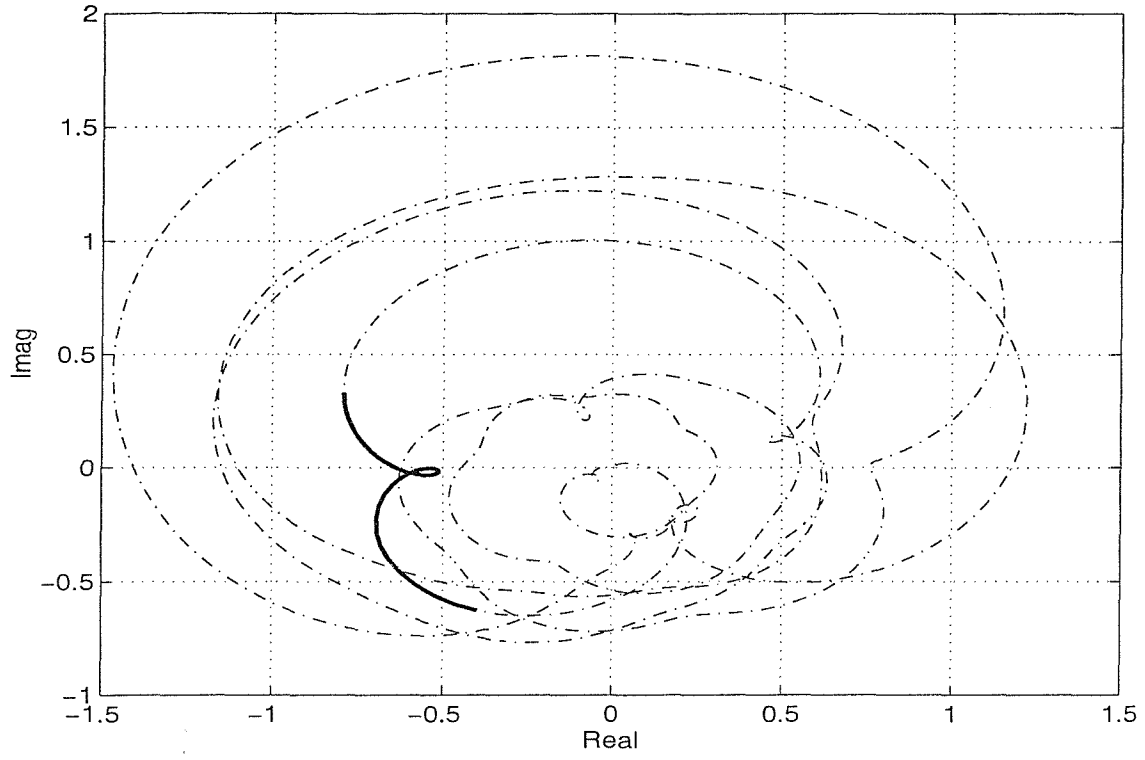

FIGURE 7.11 Nyquist plot of the frequency response of (WP_{virc0}) without the constraint of the controller stability.

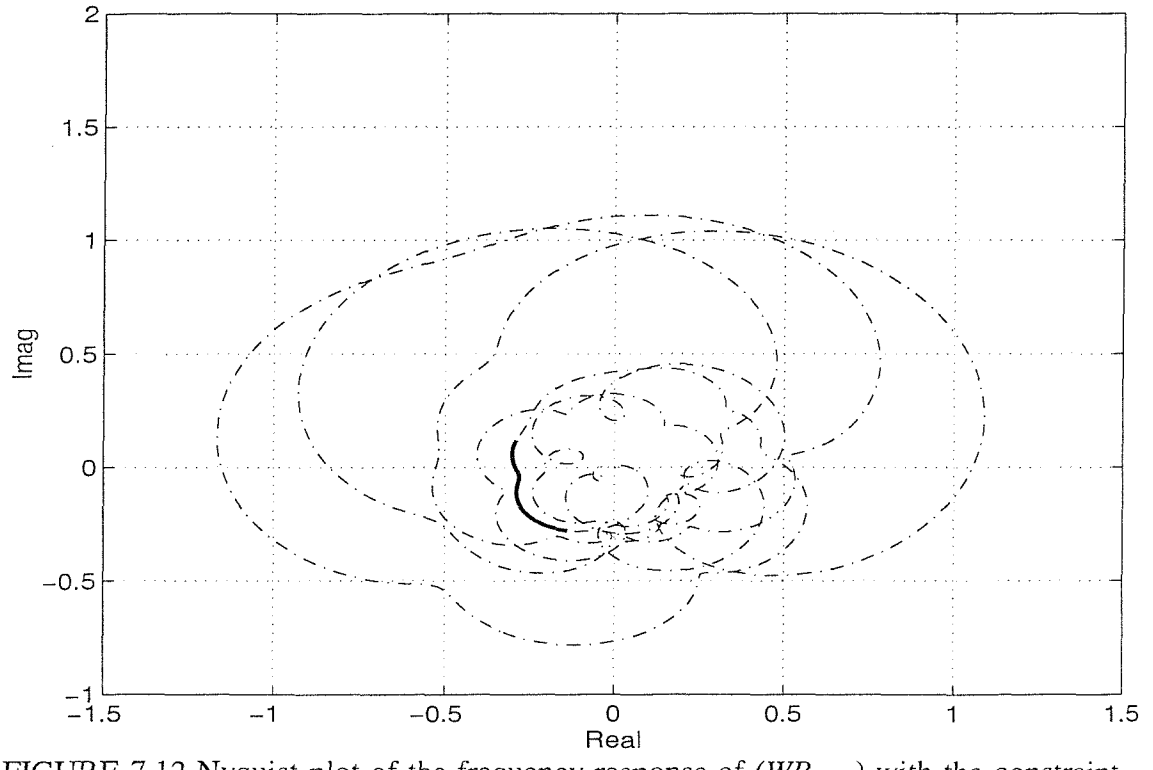

FIGURE 7.12 Nyquist plot of the frequency response of (WP_{virc0}) with the constraint of the controller stability.

7.6 Conclusions

In this chapter we introduced a novel analysis of the stability issue of the internal model feedback controller designed to minimise the acoustic pressure at a virtual microphone. The results showed that if a good performance was to be achieved the controller would be unstable. Therefore there is a trade-off between performance and controller stability. Also, a novel method has been developed to design stable feedback controllers which were used in the design of a virtual microphone controller.

Chapter 8. Real-time implementation of an active headrest system

8.1 Introduction

The aims of the work presented in this chapter were to investigate the performance of an active headrest system using H_2 and H_2/H_∞ methods presented in chapter 6 and to implement real-time feedback controllers in an experimental headrest system. The headrest system is designed to attenuate a broadband disturbance at a point near the listener's ear, rather than at the control microphone. Previous chapters concluded that good performance could only be achieved for such an arrangement with unstable controllers. Therefore this chapter considers the implementation of unstable controllers. The work in this chapter is presented as follows. First, the experimental headrest system is described. Then the performance of an active headrest system is analysed. Finally, the H_2 controllers are implemented in real-time to attenuate a broadband random disturbance by using DSP TMS320C54x.

8.2 The experimental headrest system

In this section the experimental headrest system is described. The complete active headrest system includes a loudspeaker and a microphone, connected via a feedback controller as shown in Figure 8.1. The acoustic signal is detected by the microphone, filtered by the feedback controller and transmitted to the loudspeaker, then generating the secondary acoustic field to cancel the primary field at the virtual microphone location.

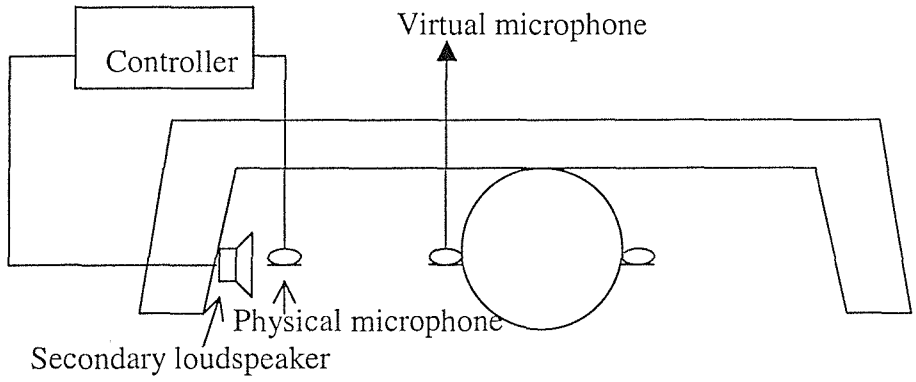

FIGURE 8.1 The headrest system.

A digital control system was connected to the headrest system for the real-time control experiment. The digital control system includes a power amplifier to drive the loudspeaker, a microphone amplifier to enhance the error signal, low-pass filters to prevent aliasing, and an Texas Instrument TMS320C54x DSP board as shown in Figure 8.2.

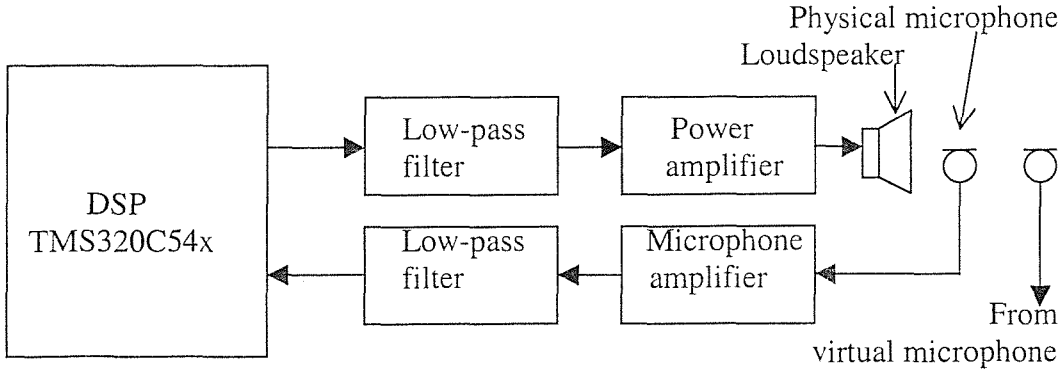

FIGURE 8.2 The headrest control system, which includes a loudspeaker, two microphones, amplifiers, low-pass filters and a digital controller.

The TMS320C54x is a fixed-point digital signal processor. It has a high degree of operational flexibility and speed. It combines an advanced modified Harvard architecture (with one program memory bus, three data memory buses, and four address buses), a central processing unit (CPU) with application-specific hardware logic, on-chip memory, on-chip peripherals, and a highly specialized instruction set. The DSP board has a single-input single-output analogue interface.

8.3 Evaluation of performance of an active headrest system

In this section the performance of an active headrest system using H_2 and H_2/H_∞ feedback controllers to minimise the acoustic pressure at a virtual microphone is evaluated. The formulation used to design the H_2 feedback controllers is as follows (see section 6.3 in chapter 6).

a. Design W using $w_{opt} = -(\boldsymbol{A}+\beta I)^{-1}\boldsymbol{b}$.

b. Repeat (a) until the robust stability condition, $\|WP_{mic0}B\|_\infty < 1$, is satisfied with the smallest β. (8.1)

where $\boldsymbol{A}$ is the auto-correlation matrix of the reference signal x created by filtering the signal d_{mic} with the P_{vir} as shown in Figure 6.6, $\boldsymbol{b}$ is the cross correlation vector of the reference signal x and disturbance signal d_{vir}, P_{mic0} is the nominal physical plant and B is the plant uncertainty bound calculated from measured data as described below.

The formulation for H_2/H_∞ feedback controller design is as follows (see section 6.3 in chapter 6).

$$\begin{aligned} &\textit{min} \left\|(1+WP_{vir0}/F)\sqrt{S_{ddvir}}\right\|_2^2 \\ &\textit{subject to} \left\|WP_{mic0}B\right\|_\infty < 1, \\ &\left\|(1+WP_{vir0}/F)D\right\|_\infty < 1. \end{aligned} \tag{8.2}$$

Where P_{vir0} the nominal virtual plant, F is the response between the physical and virtual microphones, $\sqrt{S_{ddvir}}$ is the square root of the power spectral density of the disturbance pressure at the virtual microphone and $1/D$ is the disturbance enhancement bounds.

We notice that no controller stability constraint is used in the formulation, since the performance was poor with the controller stability constraint in the design process as discussed in chapter 7. The plant responses used here include the elements of a digital controller, such as low-pass filters and the one sample filtering delay. In this work the

frequency responses P_{mic0}, P_{vir0}, F and B were first measured, and then these responses were modelled using IIR filters. The frequency response functions of the models were then evaluated on the unit circle. The nominal physical and virtual plants were modelled by an IIR filter with 18 moving-average (MA) coefficients, and 20 auto-regressive (AR) coefficients by using the function *invfreqz*( ) in MATLAB. The modelling process gave a better representation of the plant at very low frequencies, where the measured data is noisy due to poor signal to noise ratio in the measurements (Rafaely, 1997). Figures 8.3 and 8.4 show the frequency responses of the nominal physical and virtual measured plants and plant models. The disturbance is the same as that used in chapter 7, and was created by filtering the white noise via a shaping filter which is modelled as an 8-pole Butterworth low-pass filter with a cut-off frequency of 400Hz, combined with an 8-pole Butterworth high-pass filter with a cut-off frequency of 200Hz, as shown in Figure 8.5.

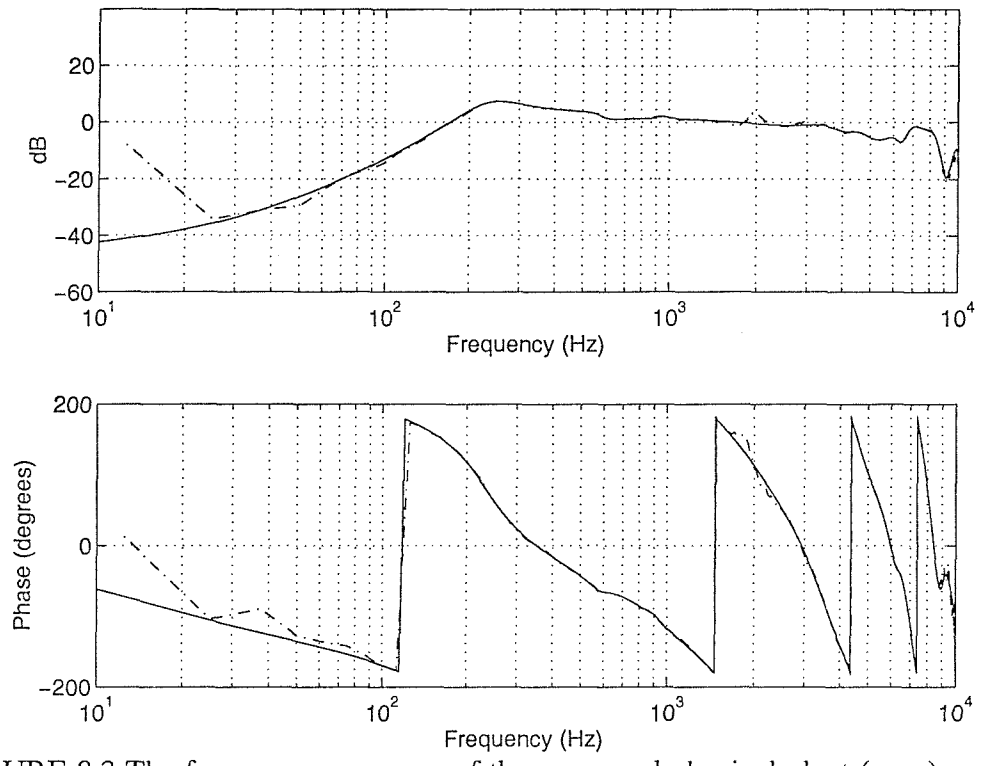

FIGURE 8.3 The frequency responses of the measured physical plant (-.-.-.) and plant model (——).

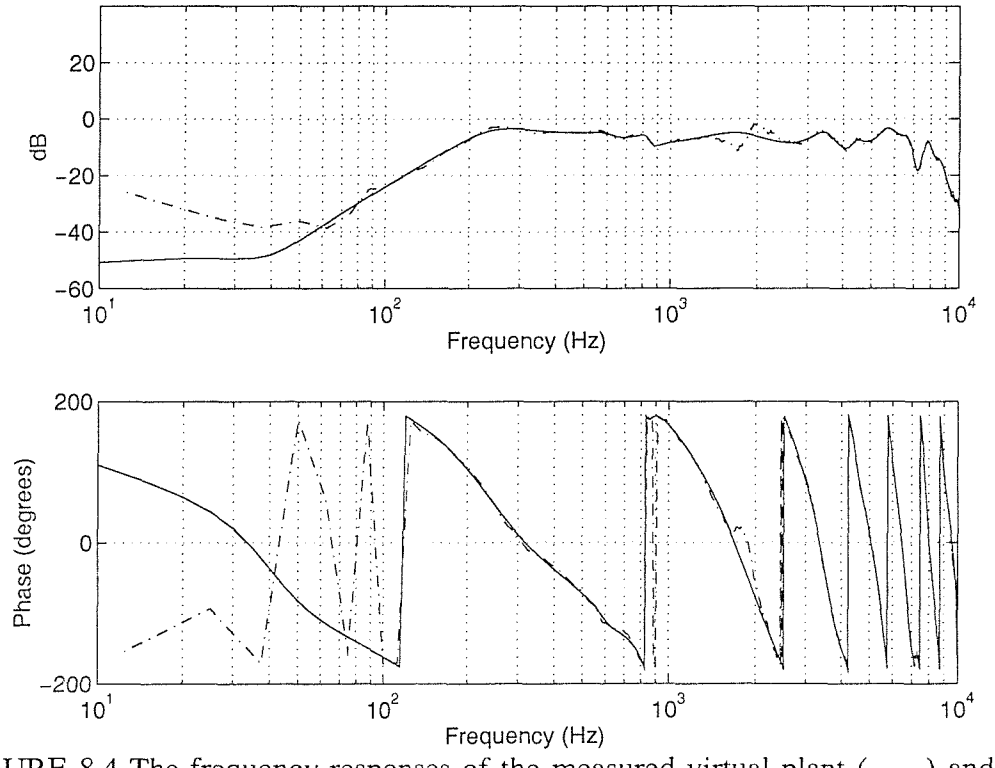

FIGURE 8.4 The frequency responses of the measured virtual plant (-.-.-.) and plant model (——).

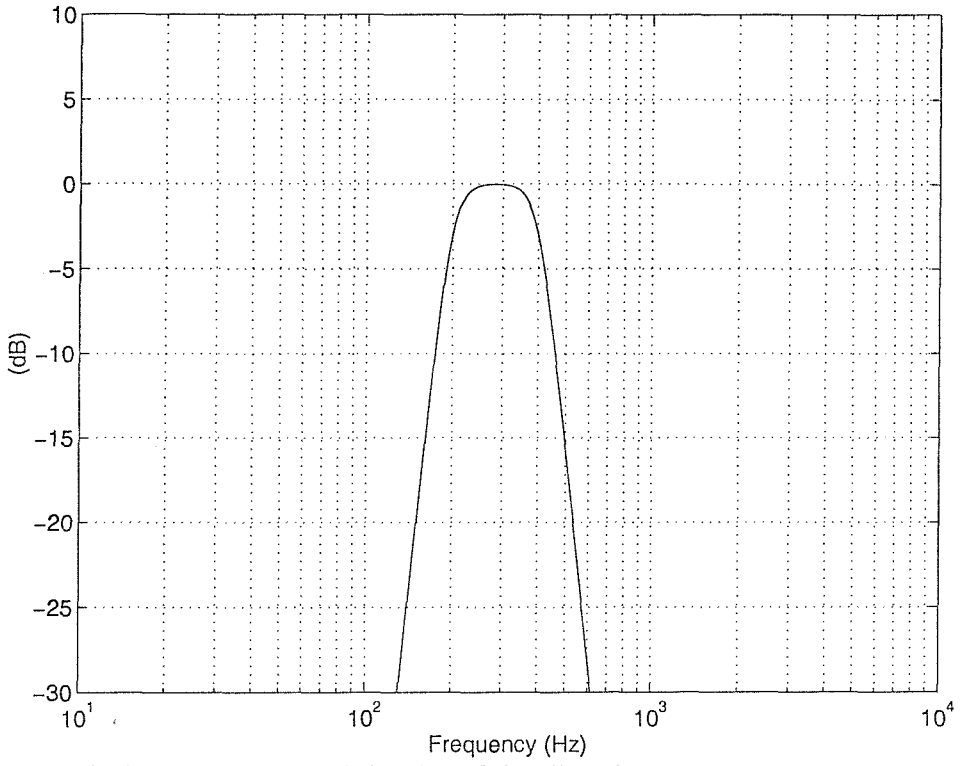

FIGURE 8.5 The power spectral density of the disturbance.

An enhancement constraint of no more than 6dB was used, which corresponded to D=0.5. Plant uncertainty bound B is calculated from:

$$B = \max_{P_{mic} \in \tilde{P}_{mic}} \left| \frac{P_{mic}}{P_{mic0}} - 1 \right| \tag{8.3}$$

where P_{mic} is the frequency response of the true physical plant, P_{mic0} is the nominal physical plant response with the central manikin position, $\tilde{P}_{mic}$ is the set of physical plants with the various manikin positions, which simulates the head movements indicated in Figure 8.6. The frequency response of B was determined from the data measured in a laboratory and is shown in Figure 8.7. A sampling frequency of 20000Hz was used, and the frequency response functions were sampled at 2000 linearly spaced points. An FIR control filter W of 128 coefficients was used.

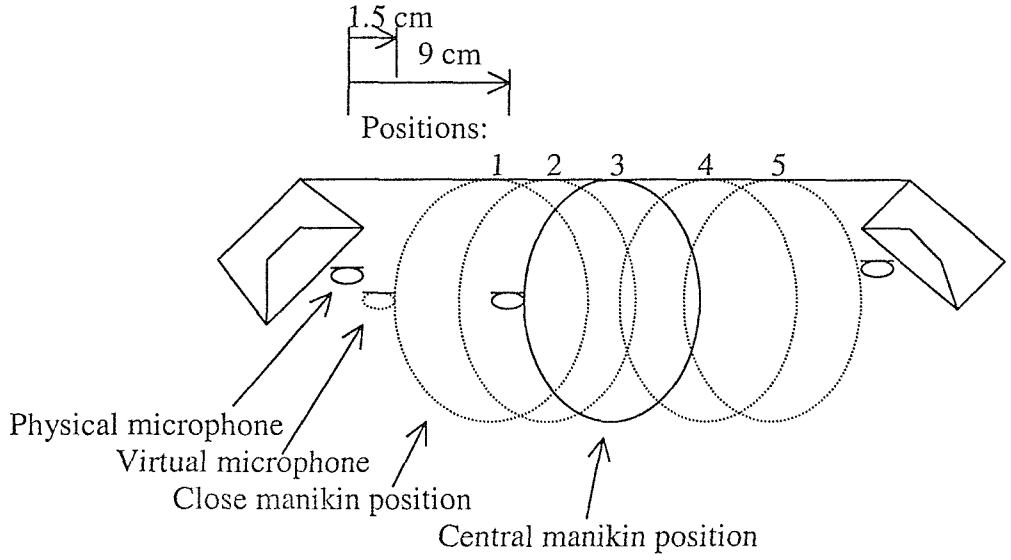

FIGURE 8.6 The experimental headrest arrangement. The manikin was moved to various positions.

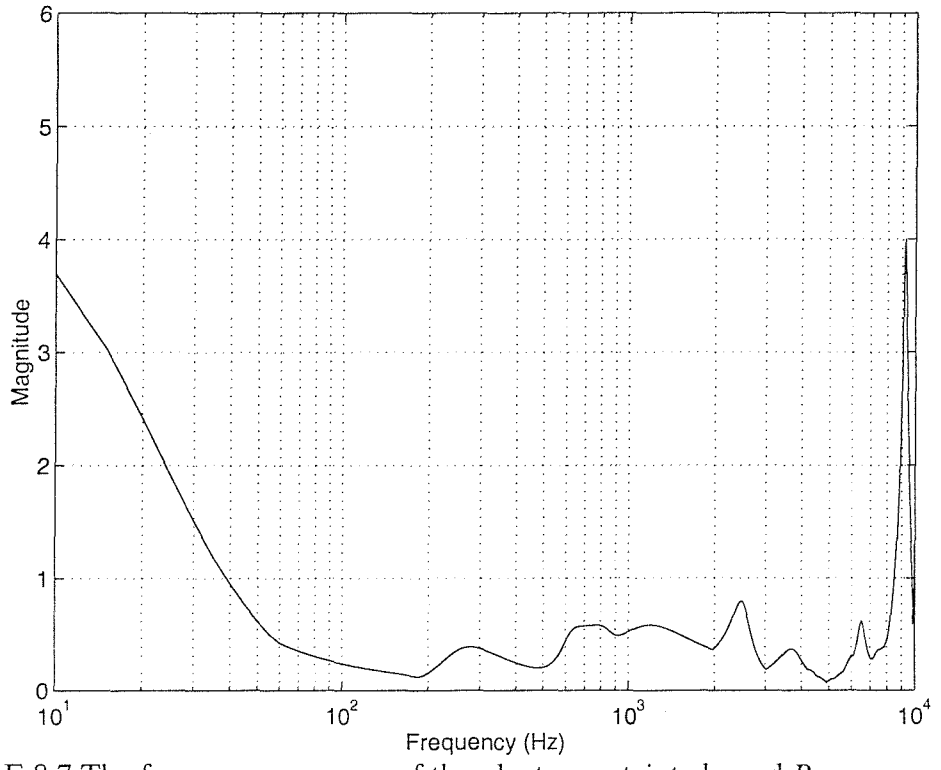

FIGURE 8.7 The frequency response of the plant uncertainty bound B.

Figure 8.8 shows the simulated power spectral density of the disturbance at the virtual microphone, calculated with and without control by using H_2 design method. It shows that an attenuation of 7dB is achieved around the frequency range of 200-400Hz. Figure 8.9 shows the same result as in Figure 8.8 obtained using H_2/H_∞ design approach. As can be seen, an attenuation of 11dB is now achieved around the frequency range of 200-400Hz. Figure 8.10 shows the robust stability constraint, which indicates that the robust stability constraint was accurately met above 600Hz for H_2/H_∞ controller and only met at around 620Hz for H_2 controllers. The impulse response of the two control filters is shown in Figure 8.11. It can be seen that the magnitude of the coefficients of the control filter is very small after 120 coefficients for H_2/H_∞ control filter, and very small after 300 coefficients for the H_2 control filter. Therefore any further increase in the filter length will not significantly improve the performance. In the next section single channel real-time control in a headrest system by using TMS320C54x DSP will be presented.

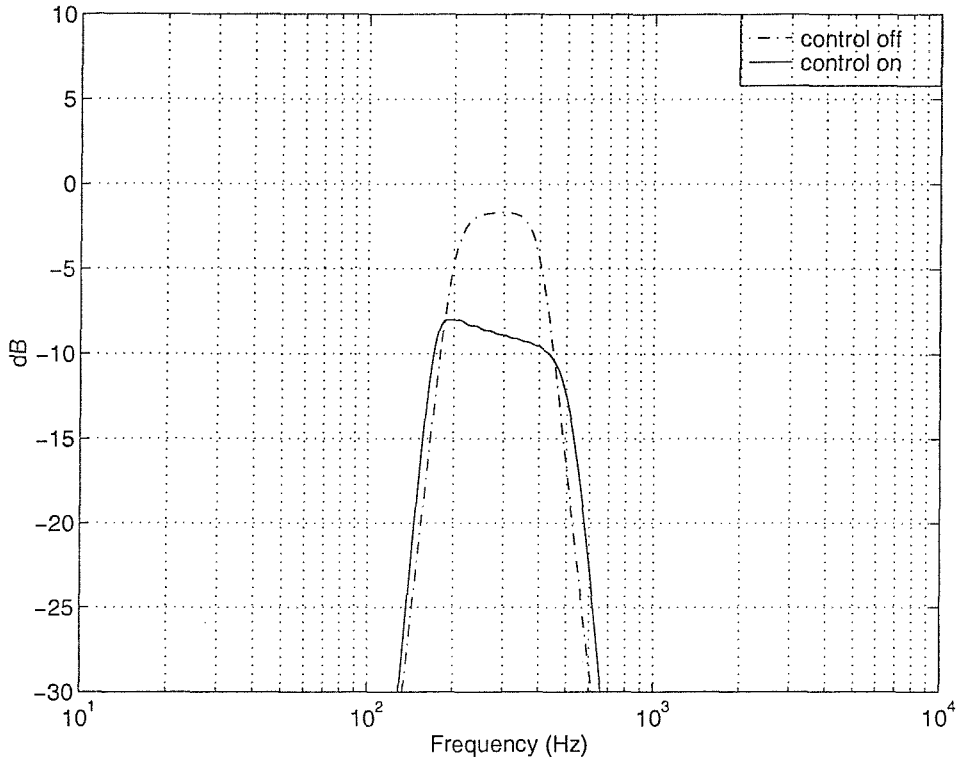

FIGURE 8.8 The simulated power spectral density of the disturbance at the virtual microphone with and without control by using H_2 feedback controller.

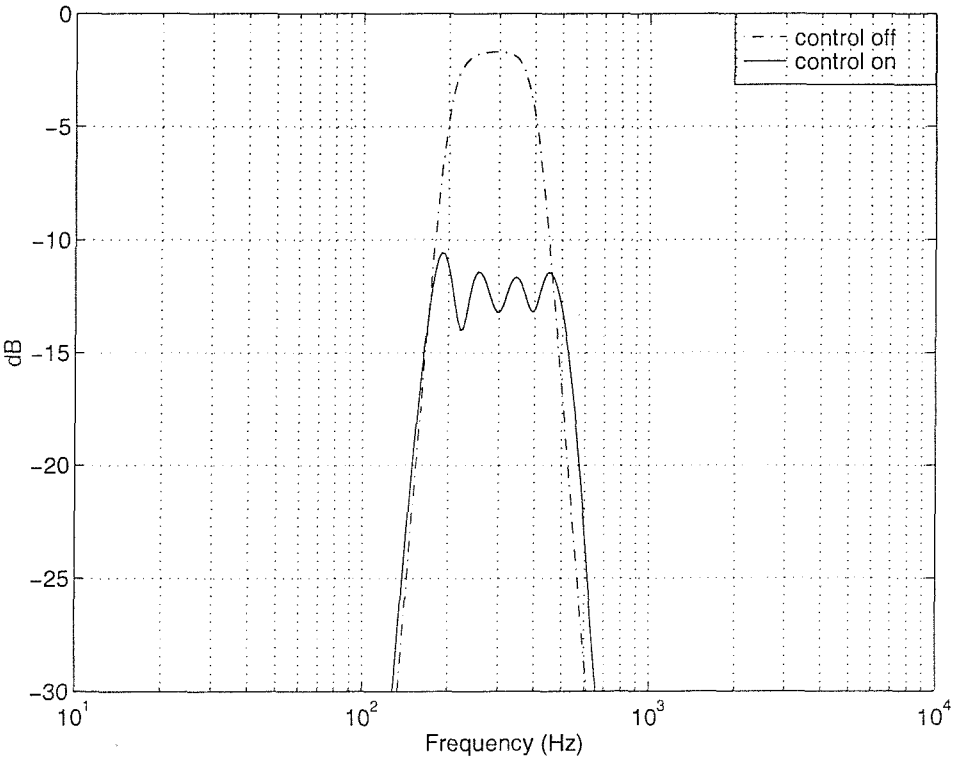

FIGURE 8.9 The simulated power spectral density of the disturbance at the virtual microphone with and without control by using H_2/H_∞ feedback controller.

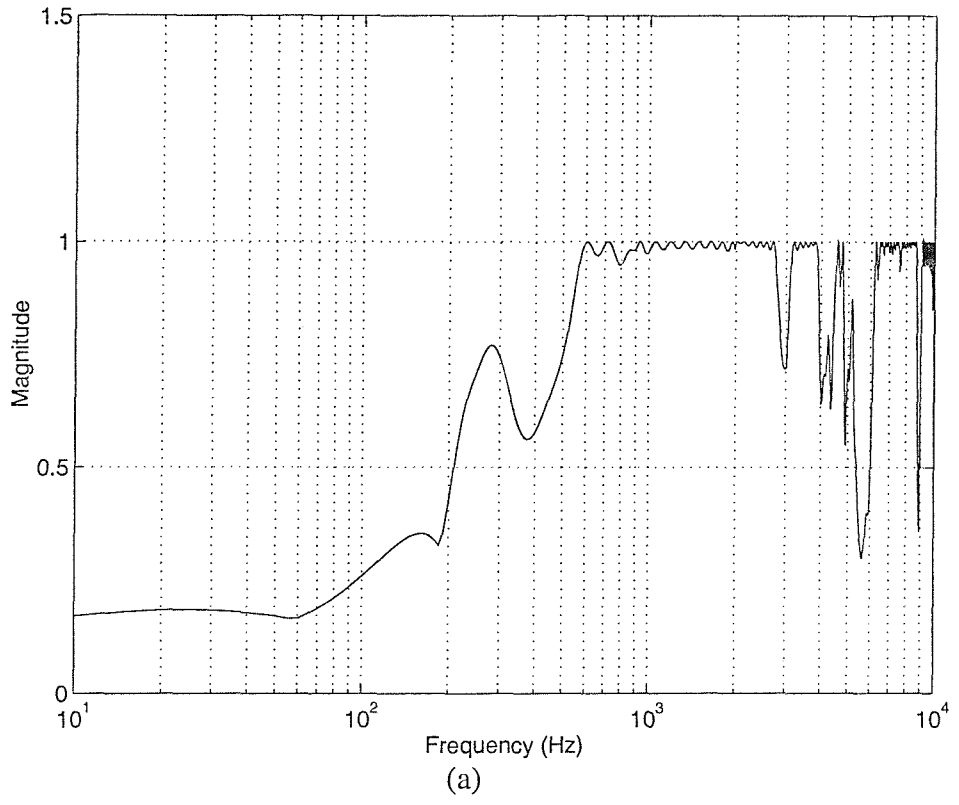

(a)

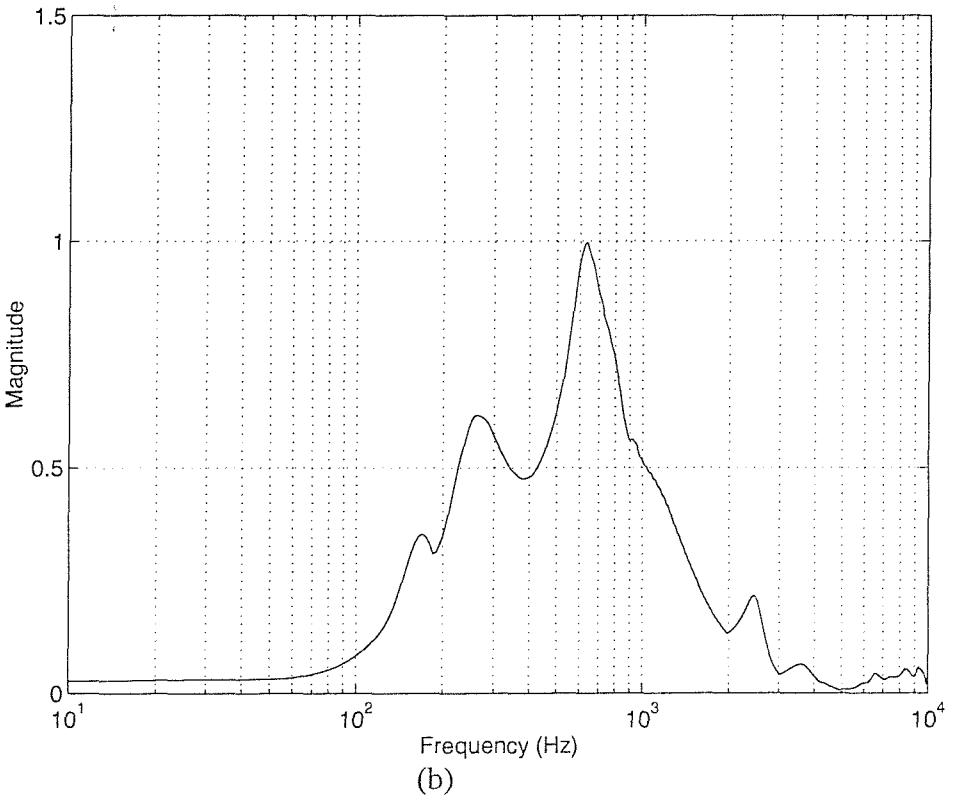

(b)

FIGURE 8.10 The robust stability condition $|WP_{mic0}B|$. (a)H_2/H_∞ feedback controller. (b) H_2 feedback controller.

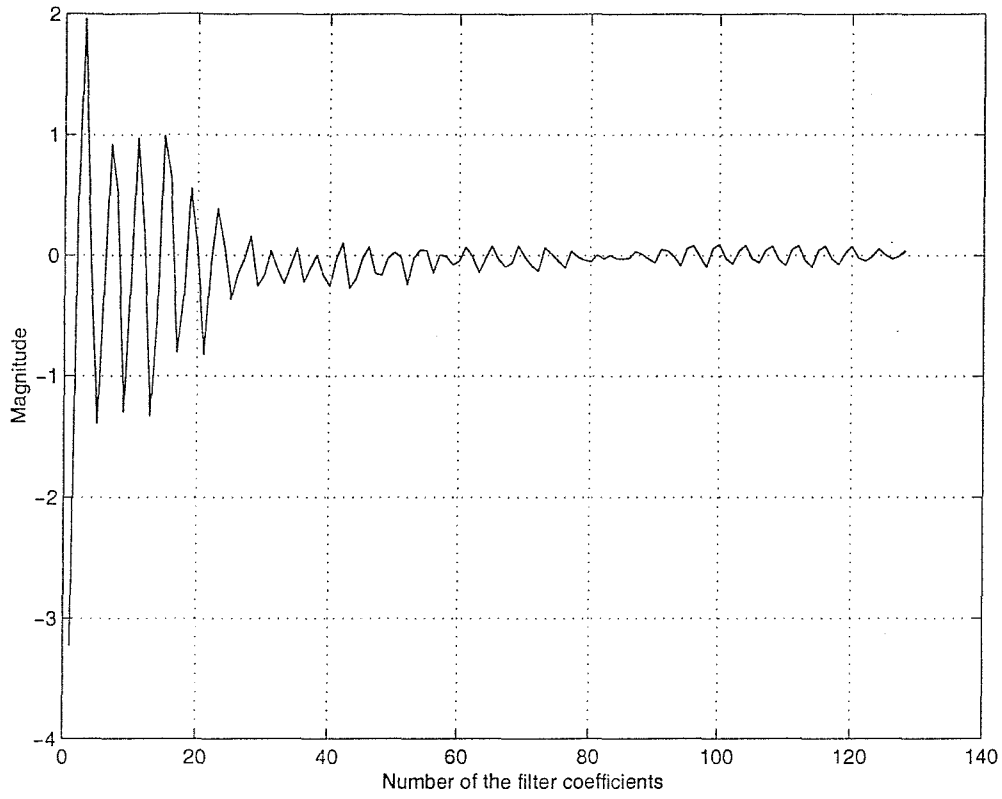

(a)

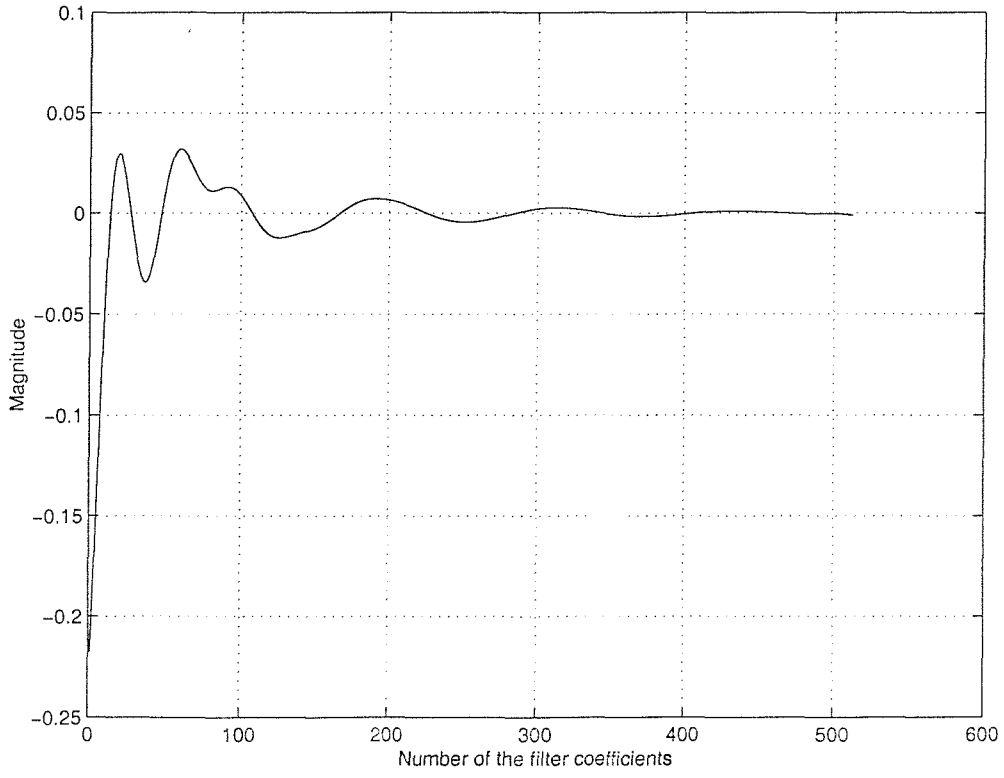

(b)

FIGURE 8.11 The impulse response of the control filters. (a)H_2/H_∞ control filter. (b) H_2 control filter.

8.4 Controller implementation

In this section single channel real-time implementation in the active headrest system as shown in Figures 8.1 and 8.2 are presented. This section investigates the feasibility of implementing H_2 and H_2/H_∞ feedback controllers to minimise the acoustic pressure at a virtual microphone. TMS320C54x DSP was used as the controller. H_2 and H_2/H_∞ feedback controllers described in section 8.3 were implemented.

A sampling frequency of 20kHz was used in the implementation. An FIR control filter, W, with 200 coefficients was used. After the controller design, a real-time controller was implemented on a DSP system, to control the experimental headrest system. The frequency response of the feedback controller is calculated from:

$$C = \frac{W}{1 + WP_{mic0}} \tag{8.4}$$

The implementation of the real-time controller was performed as follows.

(a) The coefficients of the impulse response of the nominal physical plant were implemented in the DSP system using an FIR filter of 200 coefficients as the nominal physical plant model.

(b) The coefficients of the control filter were also implemented directly in the DSP system.

(c) The response of the controller was measured by using FFT analyser to ensure that the frequency response of the controller is accurate. The controller can not be measured directly, since it is unstable. However this is overcome by using two stages. First the responses of the control filter W and the nominal physical plant P_{mic0} were measured separately. Second the response of the feedback controller C with W of smaller gain was measured. The controller can be measured now, since it is stable.

(d) The DSP system was run and the error signal from the virtual and physical microphones before and after control was measured.

(e) Monitoring the attenuation at the virtual microphone by increasing the gain of the power amplifier until the closed-loop system becomes unstable.

The procedure described above could be used to implement the unstable controllers. However this is not recommended for practical or commercial use.

In this work H_2 and H_2/H_∞ controllers were designed to minimise the acoustic pressure at a virtual microphone at central or close manikin positions as shown in Figure 8.6. The virtual microphone is attached to the manikin's ear. The H_2 controller was implemented first and the power spectral density of the disturbance at the virtual and physical microphones before and after control was measured at 5 positions as shown in Figure 8.6. Figure 8.12 shows the power spectral density of the disturbance at the virtual microphone at 5 positions by using H_2 controller designed to minimise the acoustic pressure at the central manikin position. The overall attenuation at the virtual and physical microphones for 5 manikin positions using the H_2 controller, designed to minimise the acoustic pressure at the virtual microphone at the central position, is shown in Figure 8.13. It can be seen that good attenuation at the virtual microphone was achieved for the movement of manikin around the central position. Attenuation at the physical microphone was poor for all manikin positions. The reason for this is that the controller was designed to minimise the pressure at the virtual microphone at the central position, and the zone of quiet should be around the central position. Therefore the attenuation at positions far from the central position is poor. Figure 8.14 also shows the variations in the overall attenuation at the virtual and physical microphones using the H_2 controller, designed to minimise the acoustic pressure at the virtual microphone with the head at position 1. We notice that the performance was good at the virtual microphone at position 1 and poor at other positions. However attenuation is good at the physical microphone for all the manikin positions. It is interesting to note that the attenuation at the location where the controller is designed to minimise the acoustic pressure is good at the virtual microphone. The attenuation is better when the controller is designed to minimise the acoustic pressure at the position 1 than that when minimising the pressure at the position 3. This is because the plant delay is increased when the minimisation point is further away from the secondary loudspeaker.

The real-time implementation by using H_2/H_∞ design method was also performed. However the attenuation was very poor. The reason for this is since the TMS320C54x DSP system is fixed-point. The representation of the controller response is not accurate enough, and the poles or zeros of the controller may change. In H_2/H_∞ design method the stability margins are smaller, and the system is more sensitive to DSP finite precision effects. The system went unstable very easily and the controller gain had to be reduced, which degraded performance significantly.

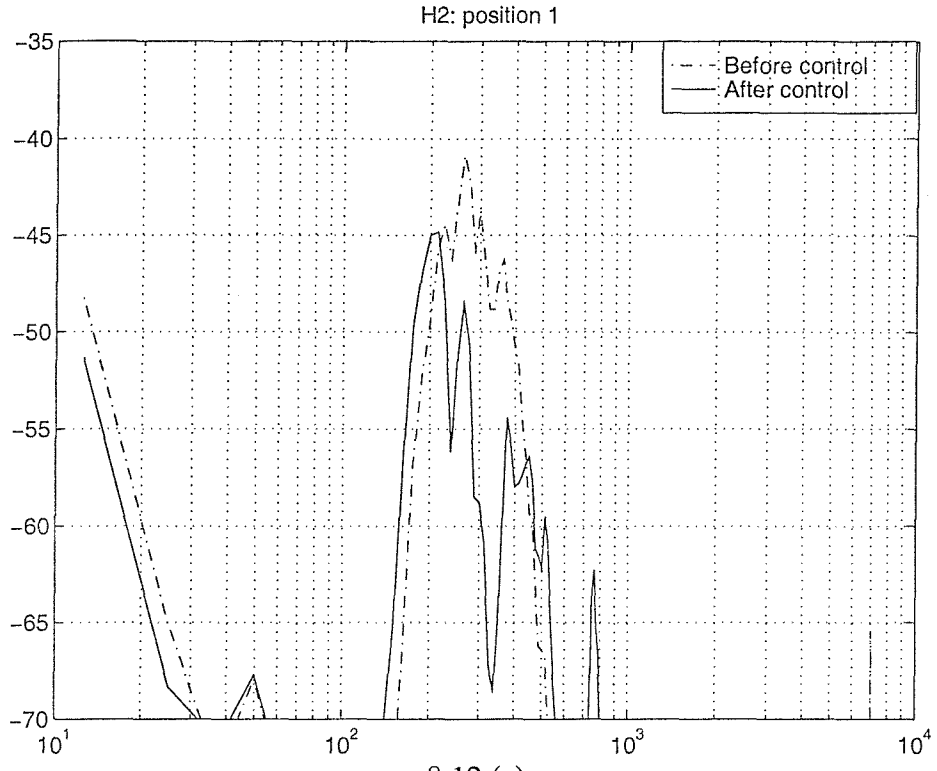
H2: position 1
Before control
After control
-35
-40
-45
-50
-55
-60
-65
-70
10^1
10^2
10^3
10^4

8.12 (a)

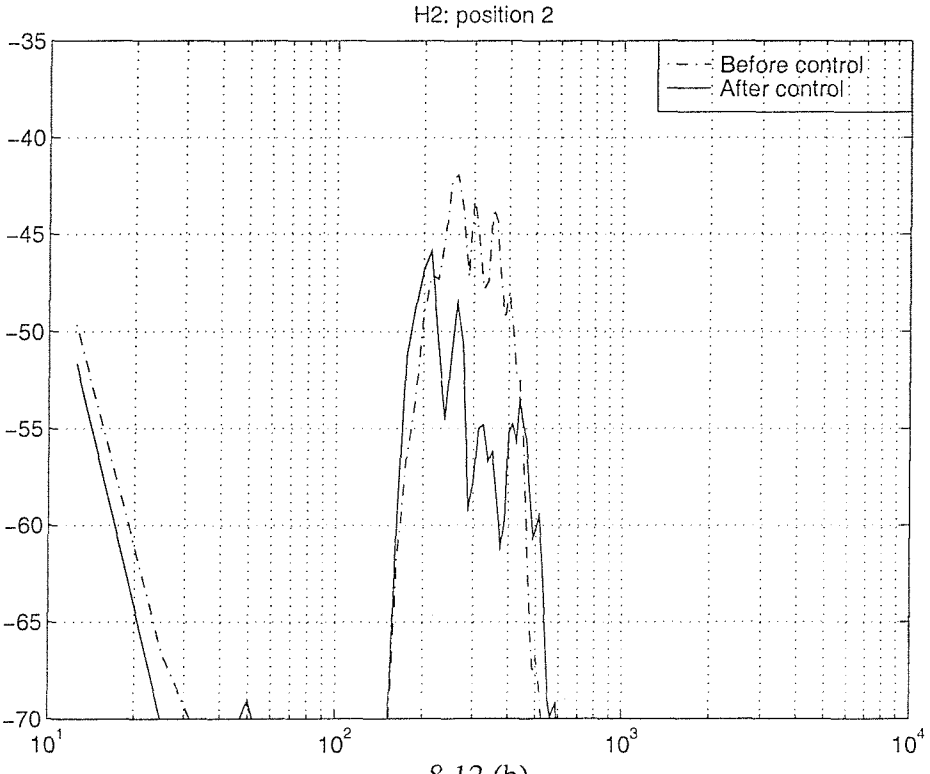
H2: position 2
Before control
After control
-35
-40
-45
-50
-55
-60
-65
-70
10^1
10^2
10^3
10^4

8.12 (b)

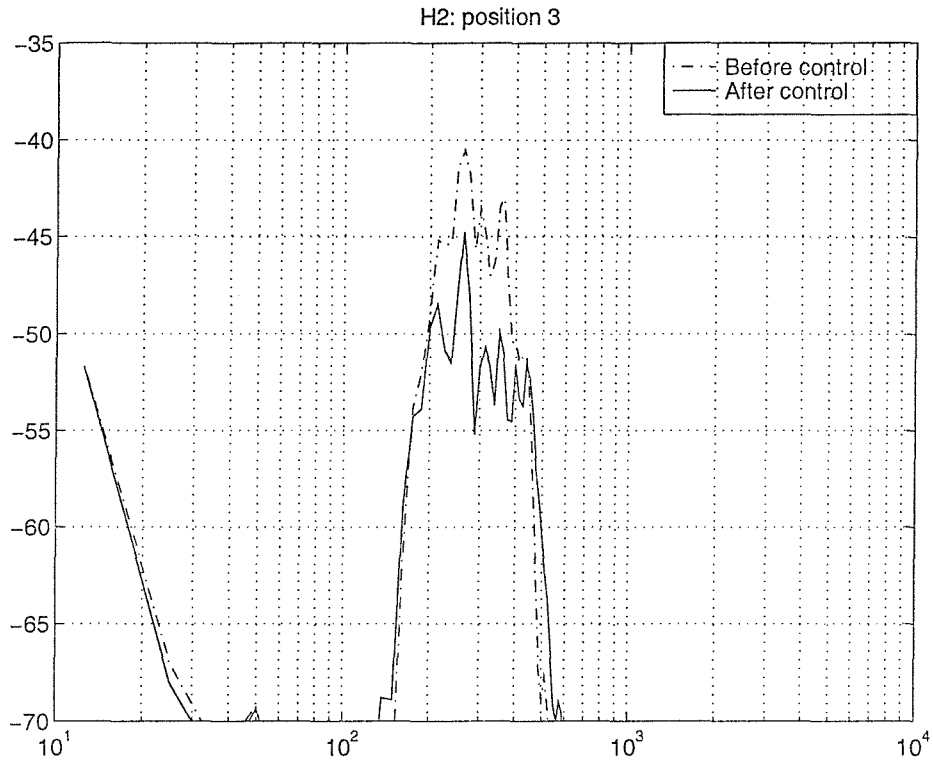
H2: position 3
Before control
After control
-35
-40
-45
-50
-55
-60
-65
-70
10^1
10^2
10^3
10^4

8.12 (c)

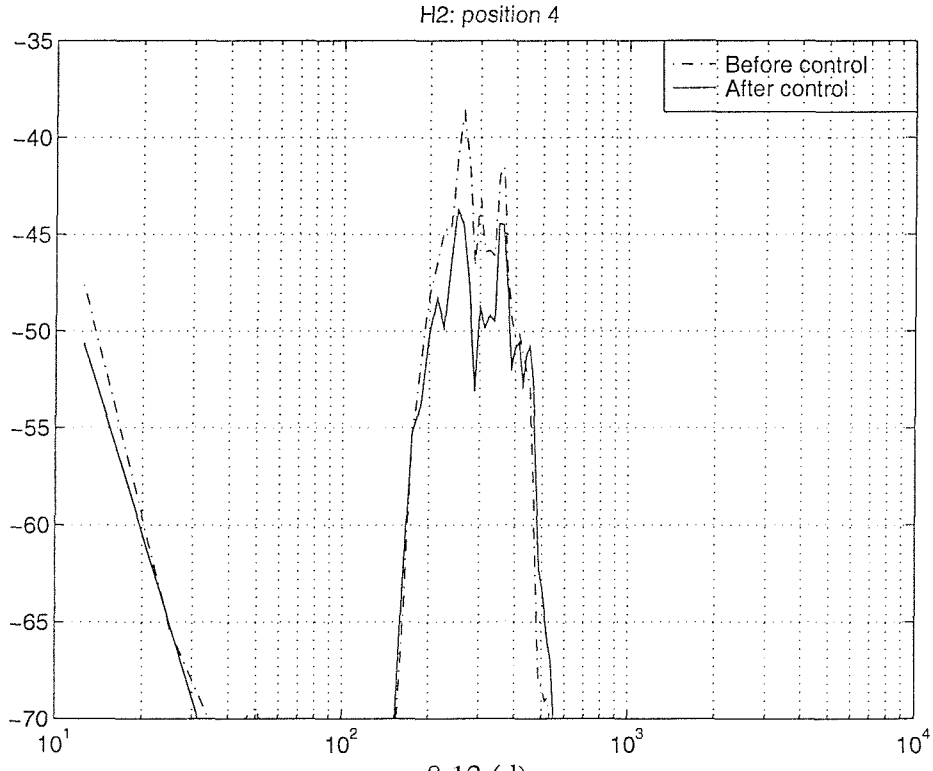
H2: position 4
Before control
After control
-35
-40
-45
-50
-55
-60
-65
-70
10^1
10^2
10^3
10^4

8.12 (d)

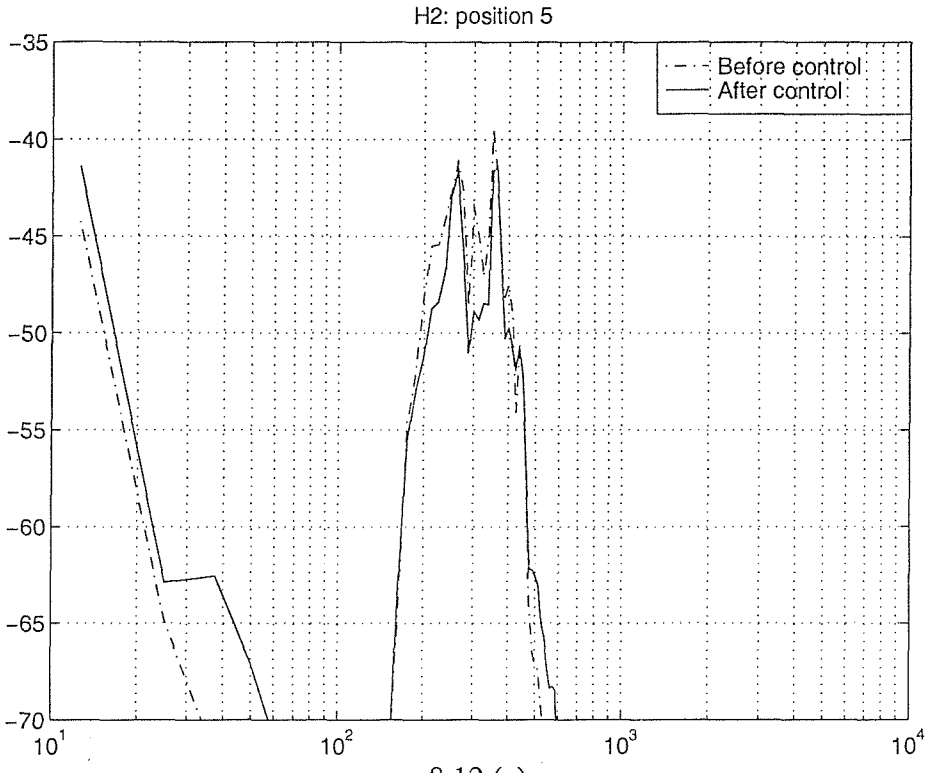

8.12 (e)

FIGURE 8.12 The measured power spectral density of the disturbance at the virtual microphone with and without control using the H_2 controller designed to minimise the pressure at position 3 implemented on TMS320C54x DSP system for 5 manikin positions as shown in Figure 8.6. (a) Position 1. (b) Position 2. (c) Position 3. (d) Position 4. (e) Position 5.

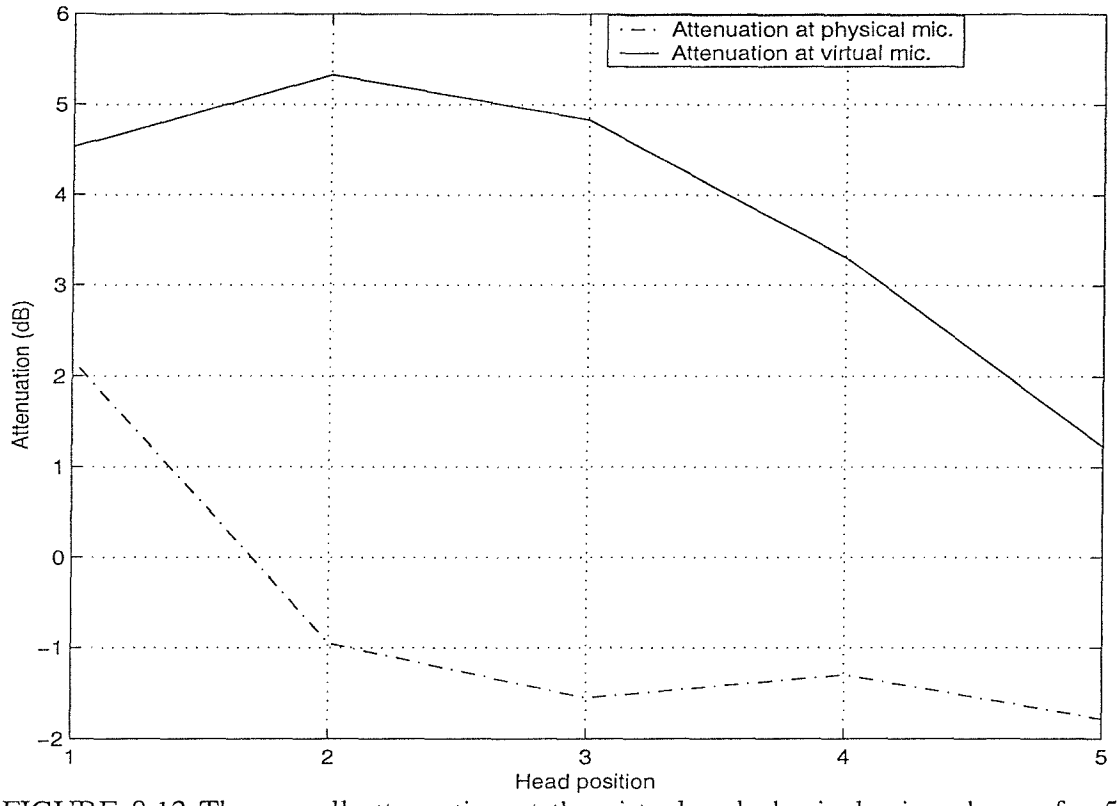

FIGURE 8.13 The overall attenuation at the virtual and physical microphones for 5 different manikin positions using the H_2 controller designed to minimise the acoustic pressure at the virtual microphone at the position 3.

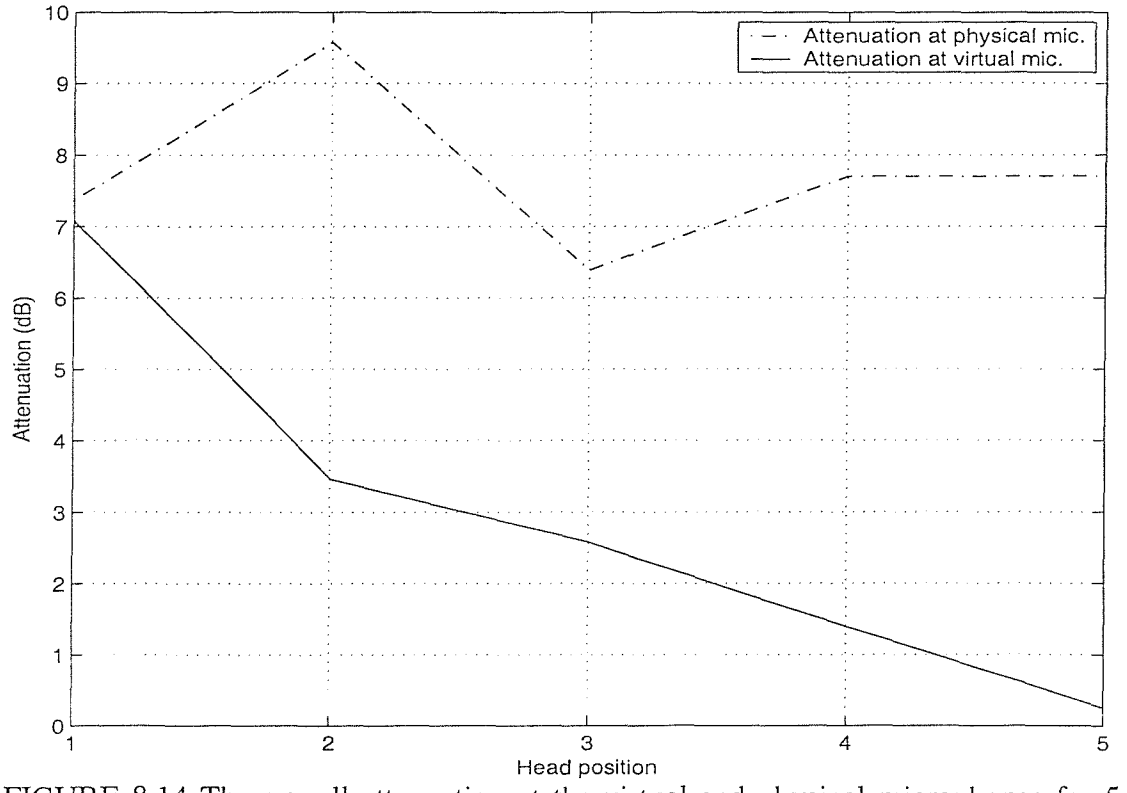

FIGURE 8.14 The overall attenuation at the virtual and physical microphones for 5 different manikin positions using the H_2 controller designed to minimise the acoustic pressure at the virtual microphone at the position 1.

8.5 Conclusions

This chapter presented the real-time implementation for an active headrest system. The performance of the headrest system using H_2 and H_2/H_∞ feedback controllers has been investigated through computer simulations. H_2 feedback controllers have been implemented on a TMS320C54x DSP system to control the experimental headrest system. The results showed that good attenuation was achieved at the location of the virtual microphone. However, the attenuation decreases as the virtual microphone moved further away from the secondary loudspeaker due to head movements. In this work H_2/H_∞ controllers have also been implemented. However the controllers suffered from instability due to the inaccurate representation of the controller response.

Chapter 9 Evaluation of performance of an active headrest system in a realistic environment

9.1 Introduction

The aim of this work is to study potential performance of an active noise control system in the headrest of an aircraft passenger seat. The noise recorded on Boeing 747 is reproduced through a loudspeaker in a laboratory room, and noise reduction at a laboratory headrest system is evaluated using simulation on measured data. Attenuation as a function of source position in the room and head position was also investigated. The results showed that poor overall attenuation of the broadband aircraft noise was achieved at the ear position using a virtual microphone, H_2 controller design. This is because of the long delay to the virtual plant and by the factors discussed in previous chapters. The chapter is presented as follows. First the arrangement of the active headrest system is described in section 9.2. Then the performance of the active headrest system in a realistic environment is shown in section 9.3. Finally the chapter is concluded in section 9.4.

9.2 Arrangement of the active headrest system

In this section we present the arrangement of the active headrest system, different positions of the primary source and different minimisation positions. The laboratory headrest system was slightly different from that used in chapter 8 and is shown in Figure 9.1, which includes two microphones, two loudspeakers and two microphone amplifiers. The headrest system with manikin was placed in the SPCG laboratory room. The size of the room is around 7m×6m×3m.

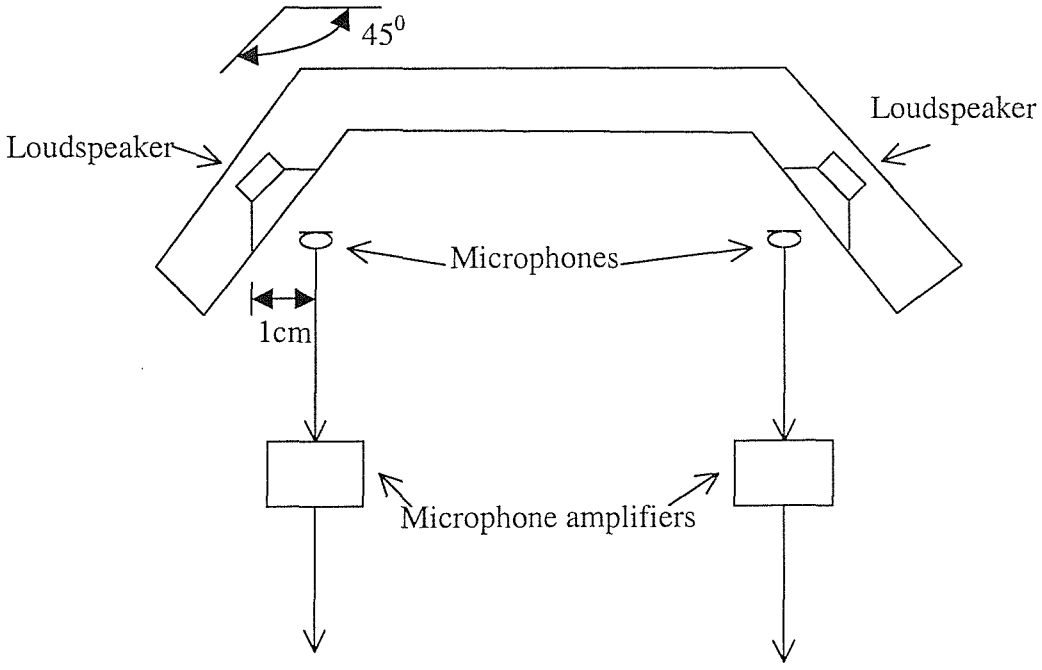

FIGURE 9.1 Arrangement of the active headrest system with 2 microphones, 2 loudspeakers and 2 microphone amplifiers.

The primary source is located at 5 different positions about 1.5m from the active headrest system as shown in Figure 9.2.

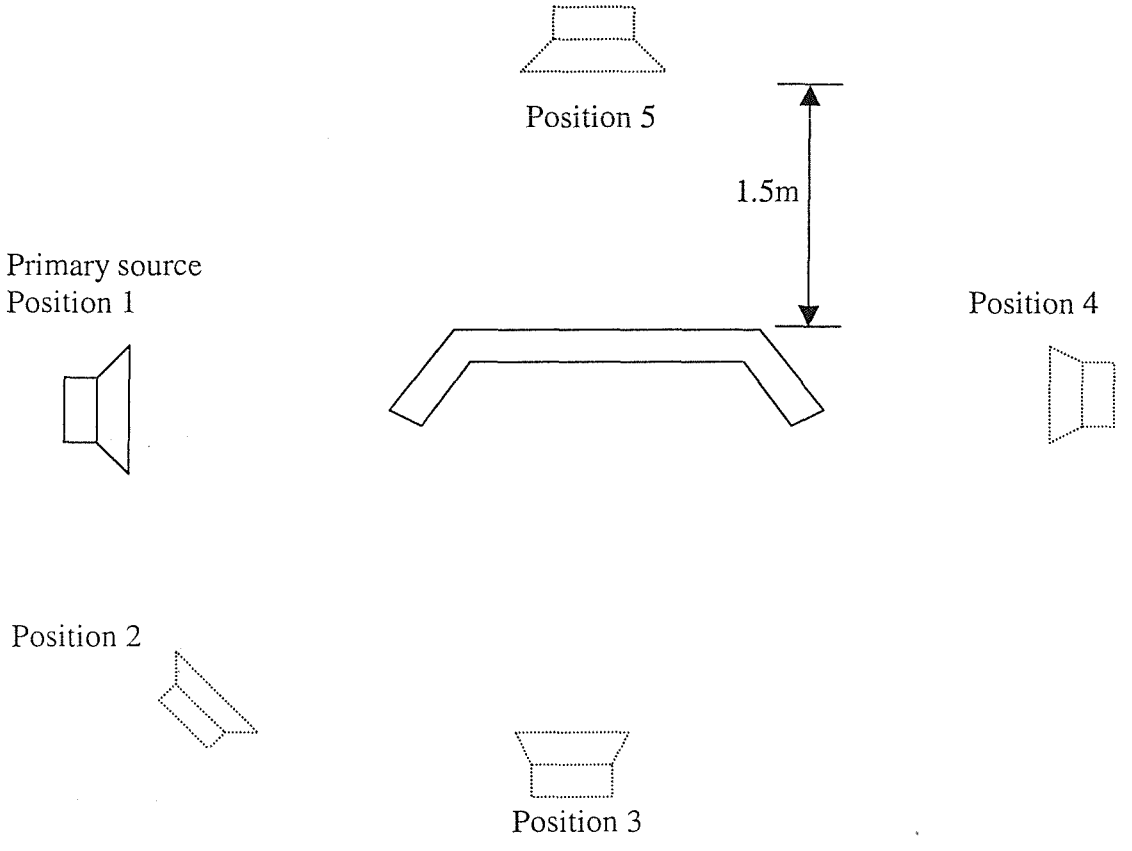

FIGURE 9.2 Configuration of different positions of the primary source.

A microphone is attached to the manikin's ears and the manikin is moved to 4 different positions as shown in Figure 9.3.

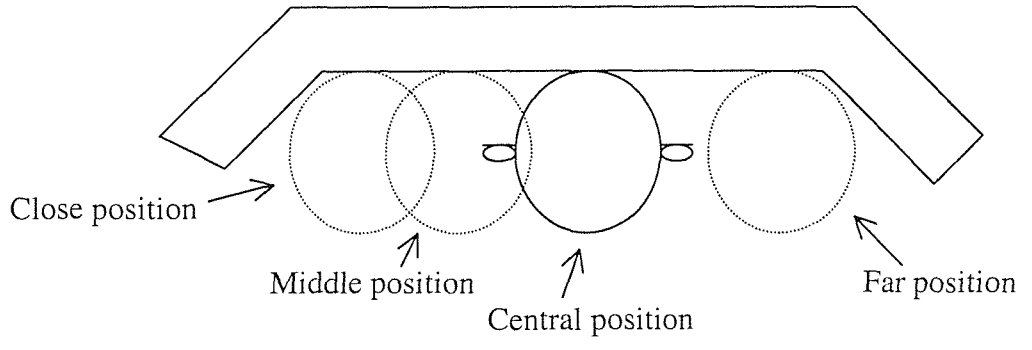

FIGURE 9.3 The configuration of different manikin head positions with a virtual microphone attached to the manikin's ears.

In this work the control simulations are performed to minimise the sound at the manikin's ear, when a primary loudspeaker positioned in the room produces the aircraft noise to simulate the realistic environment. The performance with different source positions and manikin positions is studied as described below.

a. The manikin is located at the central position with the primary source placed at 5 different positions to simulate the noise source coming from different directions. Evaluation of the attenuation at the position of the manikin's ear is performed through computer simulations with measured data in the laboratory room.
b. The primary source is placed in front of the headrest system with the manikin located at 4 different positions to simulate the head movement. Evaluation of the attenuation at the manikin's ear is performed through the simulations with measured data.

In the next section the performance of an active headrest system using H_2 controller design will be shown.

9.3 Performance of the active headrest system

In this section the performance of the active headrest system described above is evaluated. H_2 formulations described in chapter 7 are used as the design methods of feedback controllers. The effect of different positions of the primary source on the performance of the active headrest system and overall attenuation at the ear microphone at four different positions as described above are also investigated in this work.

The disturbance was recorded in BA Boeing 747 aircraft and its power spectral density is shown in Figure 9.4. The disturbance has more power at the frequency range from 100Hz to 400Hz. This means that this disturbance could be attenuated by using the active control method, since the disturbance is at the low frequency range and the size of the quiet zone is more useful. The design method used here is H_2 control strategy. The formulation for H_2 control can be expressed as (see chapter 6):

a. Design W using $w_{opt} = -(A+\beta I)^{-1} b$.
b. Repeat (a) until the robust stability condition, $\|WP_{mic0}B\|_\infty < 1$, is satisfied with the smallest β. (9.1)

where A is the auto-correlation matrix of the reference signal x created by filtering the signal d_{mic} with the P_{vir} (see Figure 6.6 in chapter 6), b is the cross correlation vector of the reference signal x and disturbance signal d_{vir}, P_{mic0} is the nominal physical plant and B is the plant uncertainty bound calculated from measured data as follows.

$$B = \max_{P_{mic} \in \tilde{P}_{mic}} \left| \frac{P_{mic}}{P_{mic0}} - 1 \right| \tag{9.2}$$

Where P_{mic} is the frequency response of the true physical plant, which is the response from the loudspeaker to the physical microphone. P_{mic0} is the nominal physical plant response with the central manikin position and $\tilde{P}_{mic}$ is the set of physical plants with the various manikin positions, which simulates the head movement indicated in Figure 9.3. The plant responses were first measured by using FFT spectrum analyser

and then modelled by using the function *invfreqz()* in MATLAB. The physical and virtual plant models are shown in Figure 9.5. The frequency response of B was then determined from those models and is shown in Figure 9.6. A sampling frequency of 20000Hz was used, and the frequency response functions were sampled at about 7430 linearly spaced points. An FIR control filter W of 1024 coefficients was used.

In order to evaluate the performance of the single virtual microphone controller for different seats in an aircraft the effect of different positions of the primary source on the performance of an active headrest system is first investigated. The primary source is located at 5 different positions around the headrest system as shown in Figure 9.2. Figure 9.7 shows the power spectral density of the disturbance before and after control using H_2 feedback controller designed to minimise the acoustic pressure at the virtual microphone at the central head position for the different positions of the primary source. The overall attenuation over the frequency range of 100-400Hz and the whole frequency range is also shown in Figure 9.8. As can be seen different positions of the primary source do not significantly affect the performance of the active headrest system. The reason for this is that the active headrest is a feedback system. Previous work showed that the performance of the feedback physical microphone controller did not depend significantly on the position of the primary source (Tseng et al, 1998). Although the headrest system in this work used the feedback virtual microphone controller, it is somewhat similar to the feedback physical microphone controller. Therefore the performance of the active headrest system is similar for the different position of the primary source. It can also be seen that the overall attenuation over the frequency range of 100-400Hz is higher than that over the whole frequency range, since the disturbance contains more power at this frequency range and the controller tries to put more effort at this frequency range.

In this work we also investigated the performance at the virtual microphone at four different locations of the manikin head when the feedback controller was designed to minimise the acoustic pressure at the virtual microphone at the central manikin position. The manikin was moved to 4 different positions. Figure 9.9 shows the overall attenuation over the frequency range of 100-400Hz and the whole frequency range at 4 different manikin positions where the controller was designed to minimise the acoustic pressure at the virtual microphone at the central manikin position with the

primary source in front of the headrest system. We notice that the overall attenuation over the whole frequency range at the central position is better than that at other locations. This is because the zone of quiet is centred at the minimisation point (central manikin position). Therefore the attenuation at other locations is poor. However the overall attenuation over the frequency range of 100-400Hz at the close position is better than that at other locations. The reason for this is probably because the controller is designed to minimise the sum of the squared error signal over the whole frequency range at the central manikin position. The magnitude of the response of the virtual plant at the close position is higher than that at the central position. Therefore the attenuation at this frequency range for the close position is better (see the discussion below). However the attenuation at other frequency range might be amplified, since the gain of the control filter may be too high for good performance to be achieved outside the frequency of 100-400Hz. Figures 9.10 (a) and (b) show the sensitivity function, i.e. attenuation, for close and central manikin positions with the primary source at the position 3. It can be seen that the attenuation at the frequency range of 100-400Hz is poor for the central manikin position and better for the close manikin position. However the amplification is higher at other frequencies for the close manikin position as expected.

From Figures 9.7, 9.8 and 9.9 it has been shown that the overall attenuation is poor for all the cases shown in the Figures. This is since the disturbance is broadband and contains many peaks in its power spectral density. It is difficult to control all the peaks. Although some peaks are attenuated other peaks may be amplified. Also the controller was designed to minimise the acoustic pressure at the virtual microphone rather than the physical microphone. The gain of the virtual plant is lower than that of the physical plant and the delay in the virtual plant is large. The performance objective $\left\|(1+WP_{vir0}/F)\sqrt{S_{ddvir}}\right\|_2^2$ is to be minimised, and if we assume F to be unity then best performance is obtained when

$$WP_{vir0} \cong -1. \tag{9.3}$$

However it can be seen from Figure 9.5 that

$$P_{vir0} \cong 0.3\, P_{mic0}. \tag{9.4}$$

Therefore, for best performance, we need

$$0.3\, WP_{mic0} \cong -1, \tag{9.5}$$

and

$$W \cong \frac{1}{0.3P_{mic0}}. \tag{9.6}$$

For robust stability, we require $\|WP_{mic0}B\|_{\infty} < 1$ to be satisfied, and if we assume B to be about 0.3 (see Figure 9.6) then the condition for robust stability becomes

$$|W| < \left|\frac{1}{0.3P_{mic0}}\right|. \tag{9.7}$$

From equations (9.6) and (9.7) it can be seen that there is a trade-off between the performance and stability and the two conditions are on the border of confliction. Therefore good performance might not be achieved. If we minimise the sound at the physical microphone then the control filter which achieves good performance will become

$$W \cong \frac{1}{P_{mic0}}. \tag{9.8}$$

Therefore good performance can be more easily obtained for minimising the sound at the physical microphone. Figure 9.11 shows the actual (designed W) and expected ($W=1/P_{vir0}$) gains of the control filters designed to minimise the sound at the virtual microphone. We notice that the actual gain of the control filter is lower than the expected gain of the control filter designed for best performance. A possible reason for this is that the gain of the virtual plant is lower than that of the physical plant as explained above. Therefore the difference in gains of the physical and virtual plants

degrades the performance. If we reduce the angle of the headrest system shown in Figure 9.1 the distance between the physical and virtual microphones is reduced and the difference in gains of the physical and virtual plants is small. Therefore the performance is expected to improve. It is suggested that a newly designed headrest would therefore have the loudspeakers and microphones placed nearer the ears.

9.4 Conclusion

The performance of an active headrest system in a realistic environment has been evaluated in this chapter. The effect of different positions of the primary source on the performance of the active headrest system has also been investigated. The results showed that different positions of the primary source has a little effect on the performance of the active headrest system, since the active headrest is a feedback system which is less affected by the sound field surrounding and more affected by the plant response. This suggested that a single feedback virtual microphone controller could work for many seats in the aircraft. The overall attenuation over the frequency range of 100-400Hz and the whole frequency range at the virtual microphone for different manikin locations has also been calculated when the controller was designed to minimise the acoustic pressure at the central manikin position. It showed that the overall attenuation over the whole frequency range at the central position was better than that at other locations, since the quiet zone is centred at the central manikin position. The overall attenuation at the virtual microphone for all the cases studied in this work is poor, since the controller was designed to minimise the sound at the virtual microphone. However the gain of the virtual plant is lower and the delay in the virtual plant is longer than those in the physical plant. For good performance to be achieved we could design the headrest system as close to the head as possible to reduce the delay in the virtual plant and the gain difference between the physical and virtual plants.

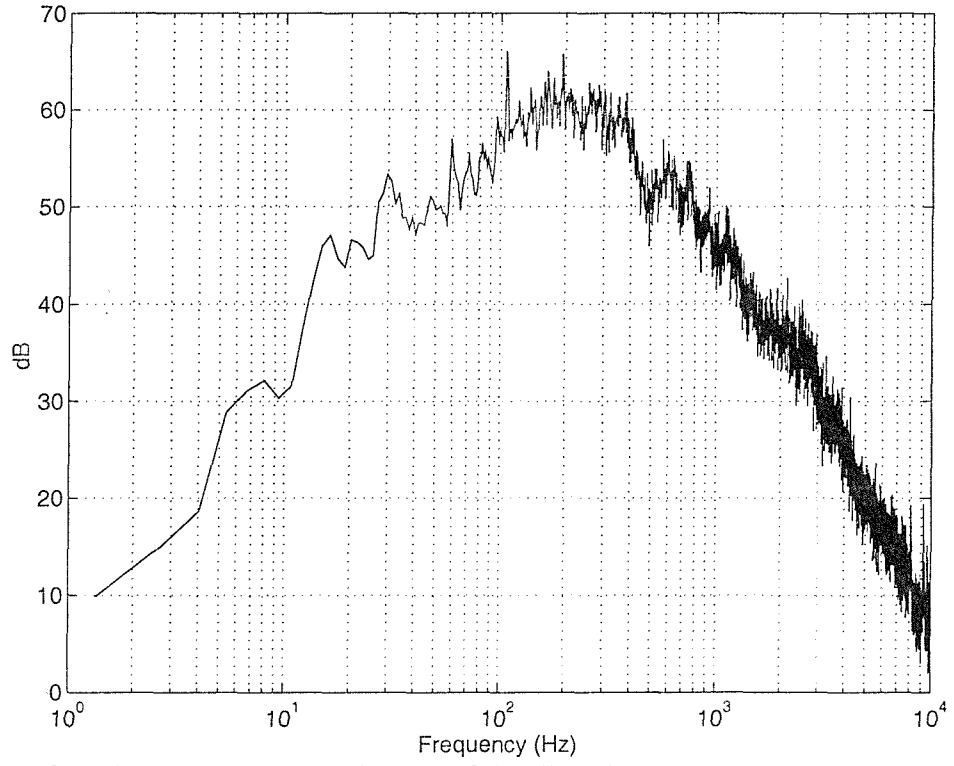

FIGURE 9.4 The power spectral density of the disturbance.

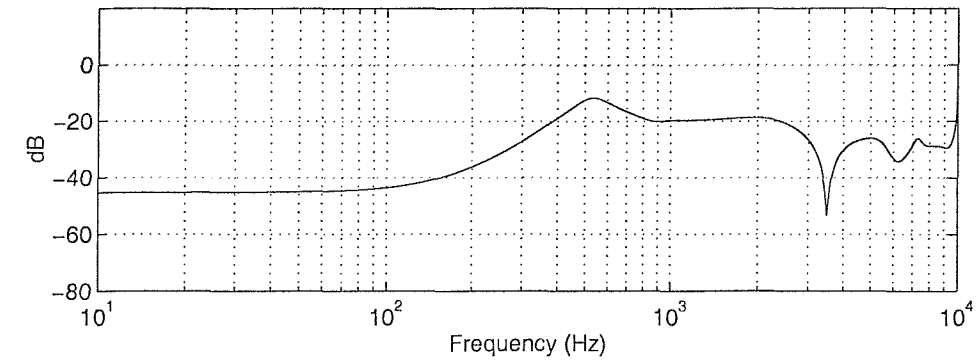

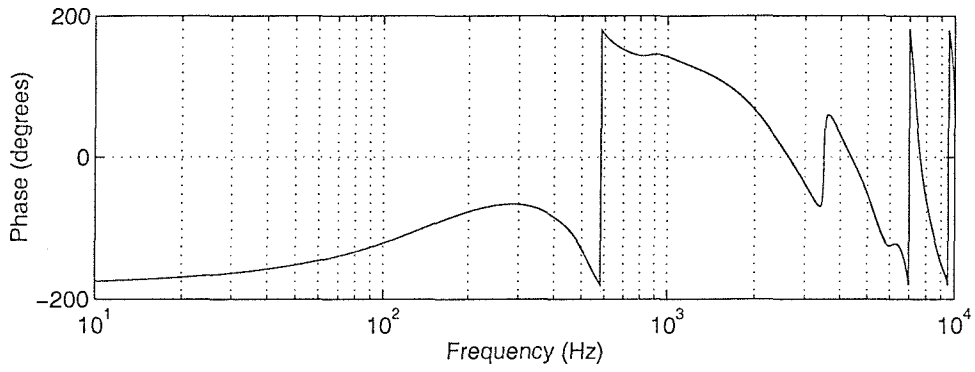

9.5(a)

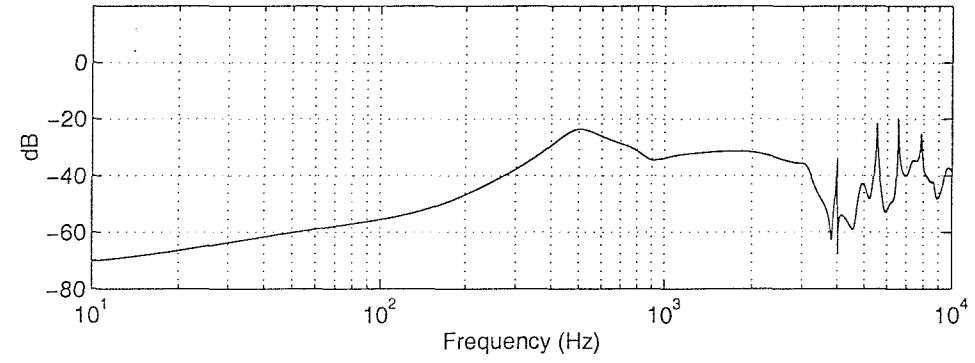

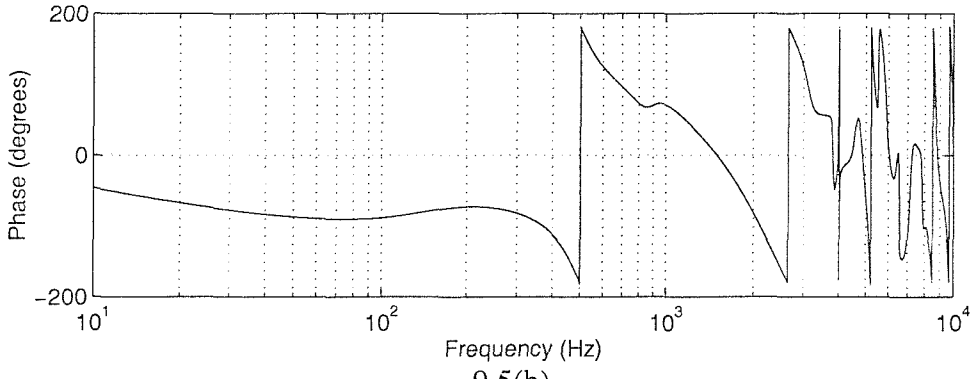

9.5(b)

FIGURE 9.5 The frequency responses of the plant models. (a) Physical plant. (b) Virtual plant.

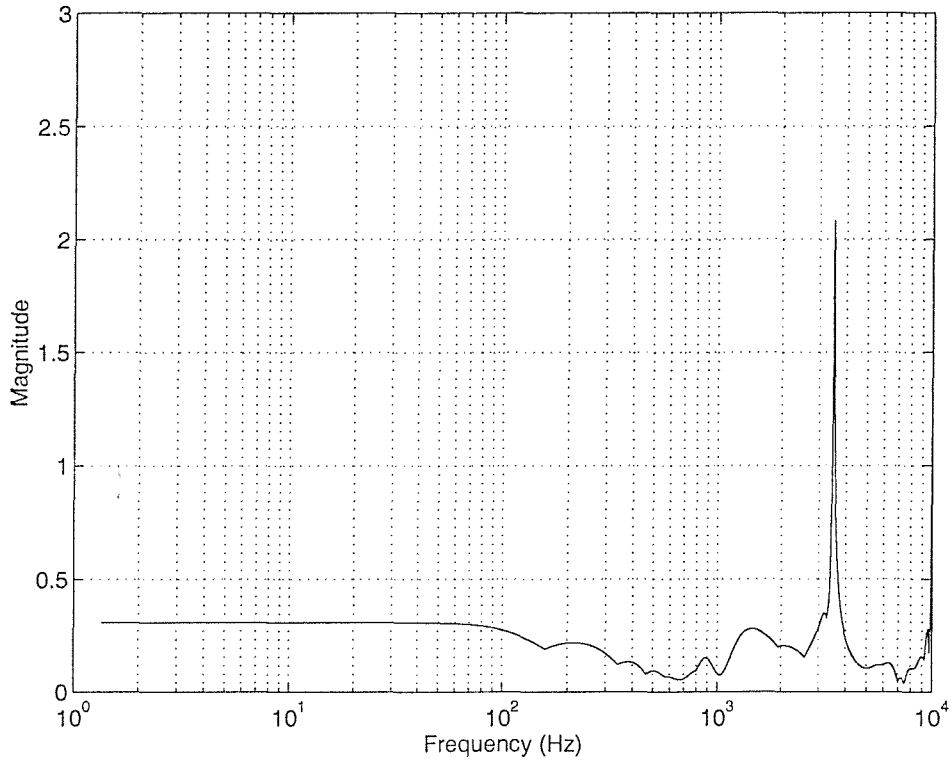

FIGURE 9.6 The frequency response of the physical plant uncertainty bound.

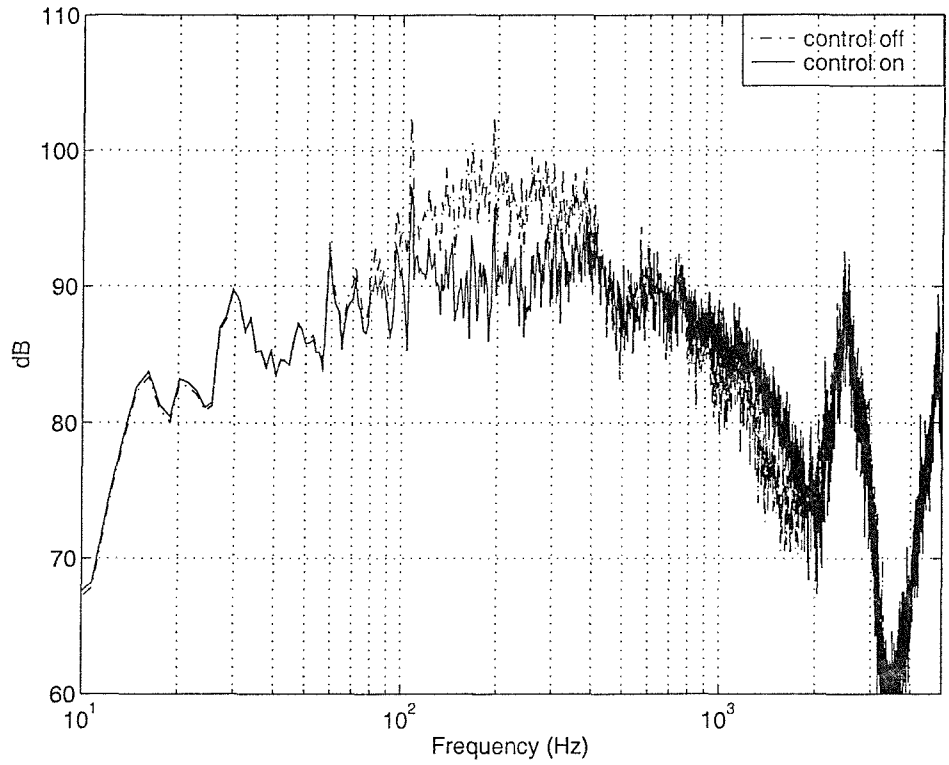

9.7 (a) Primary position 1

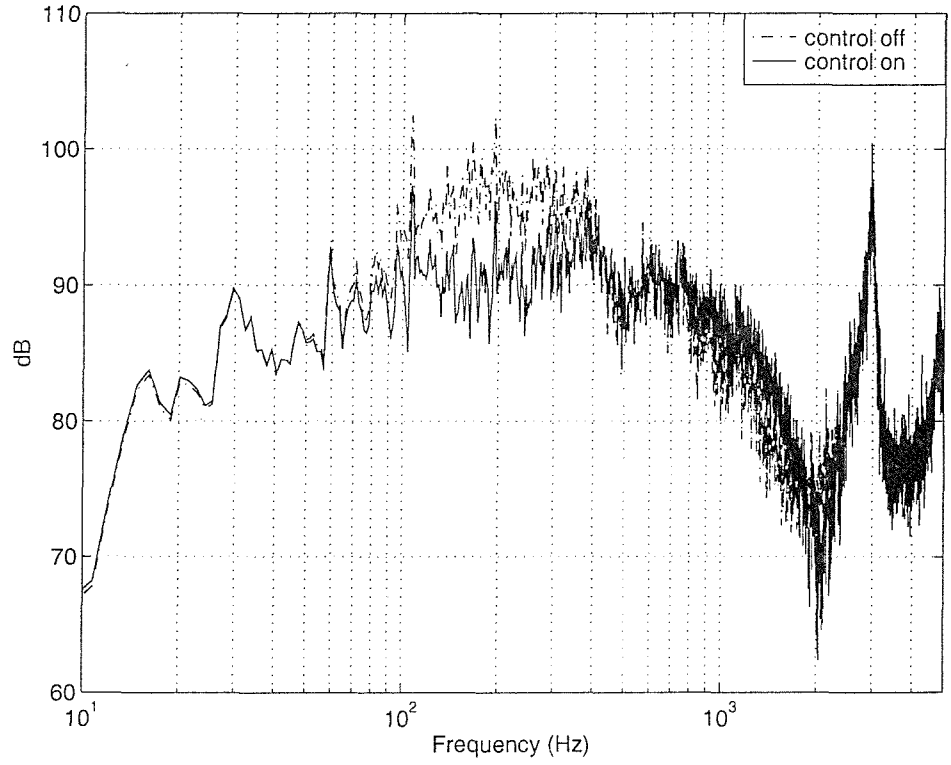

9.7 (b) Primary position 2

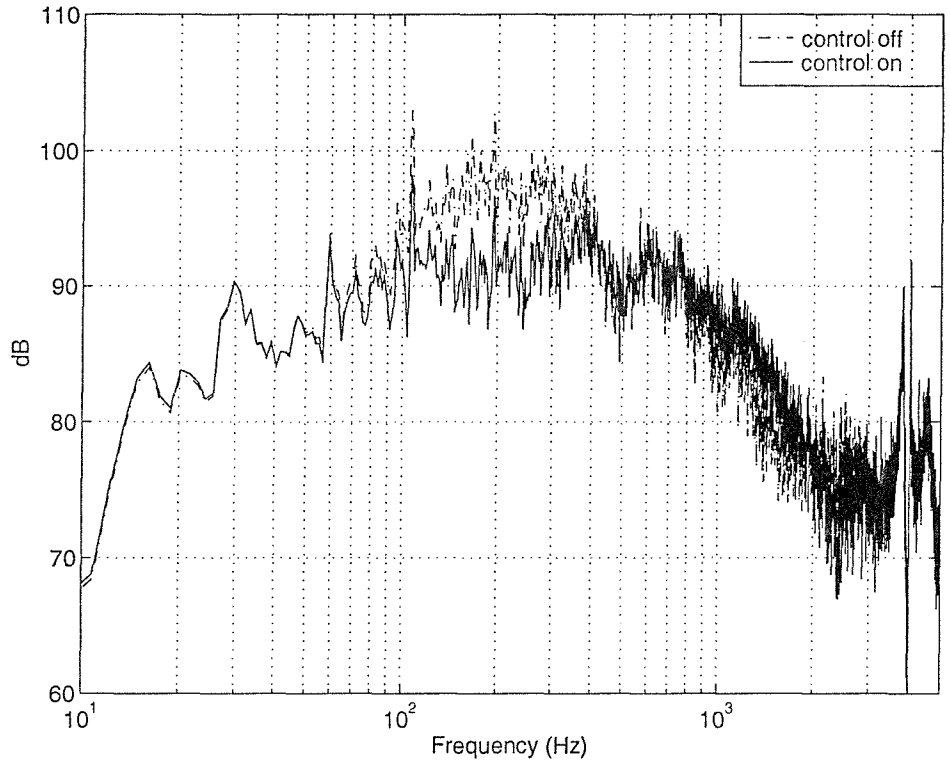

9.7 (c) Primary position 3

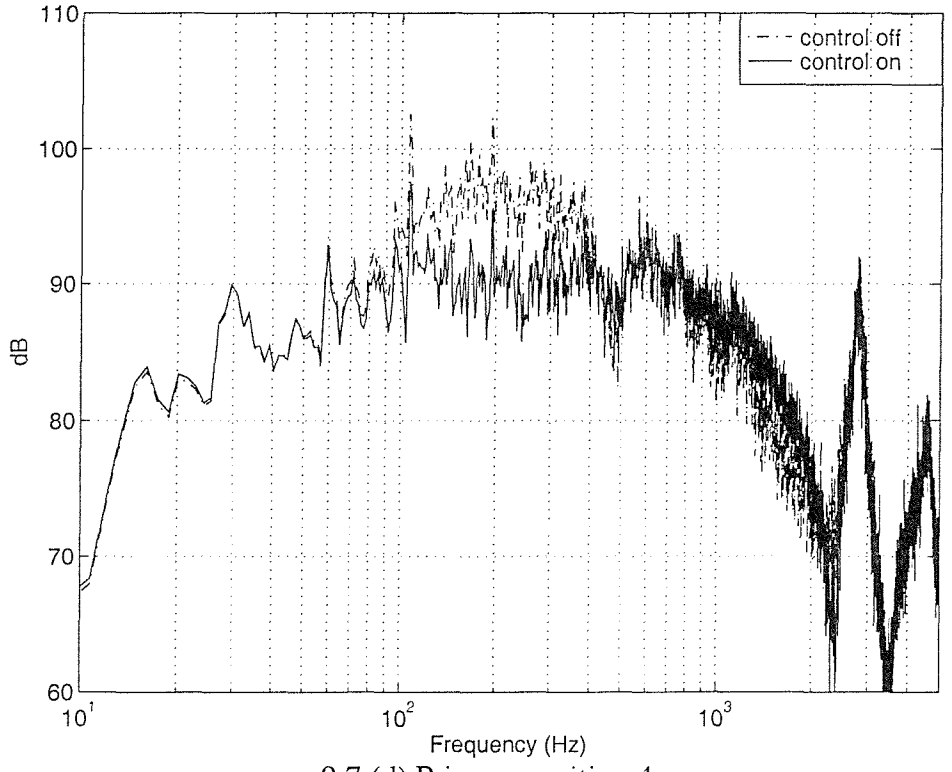

9.7 (d) Primary position 4

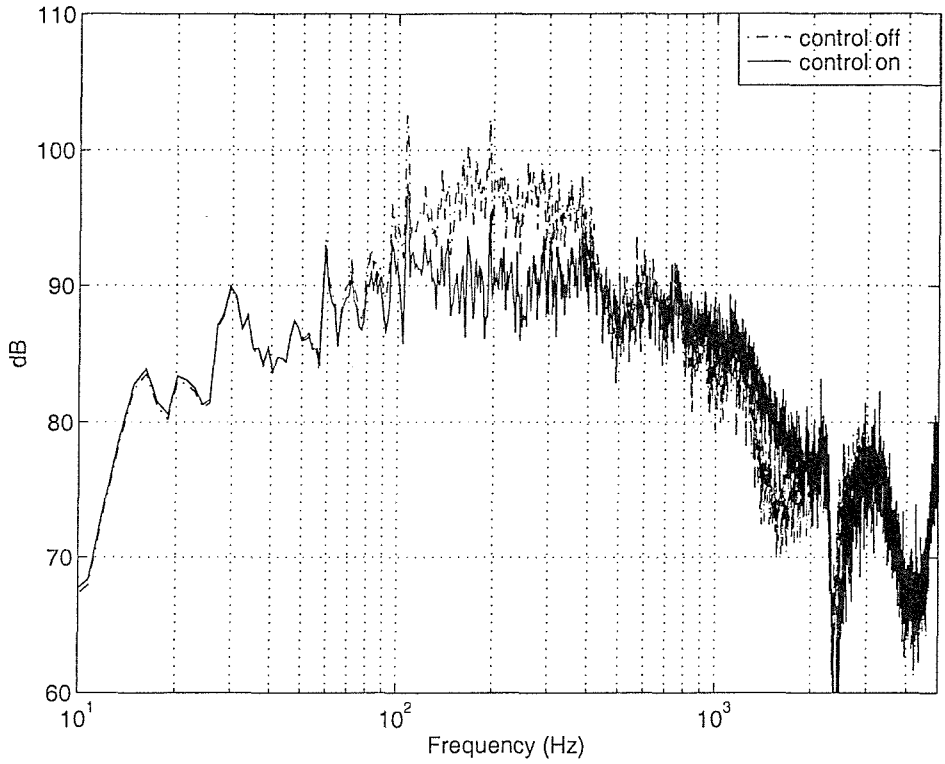

9.7 (e) Primary position 5

FIGURE 9.7 The power spectral density of the disturbance before and after control using H_2 feedback controller designed to minimise the acoustic pressure at the virtual microphone at the central head position for the different position of the primary source. (a) Position 1. (b) Position 2. (c) Position 3. (d) Position 4. (e) Position 5.

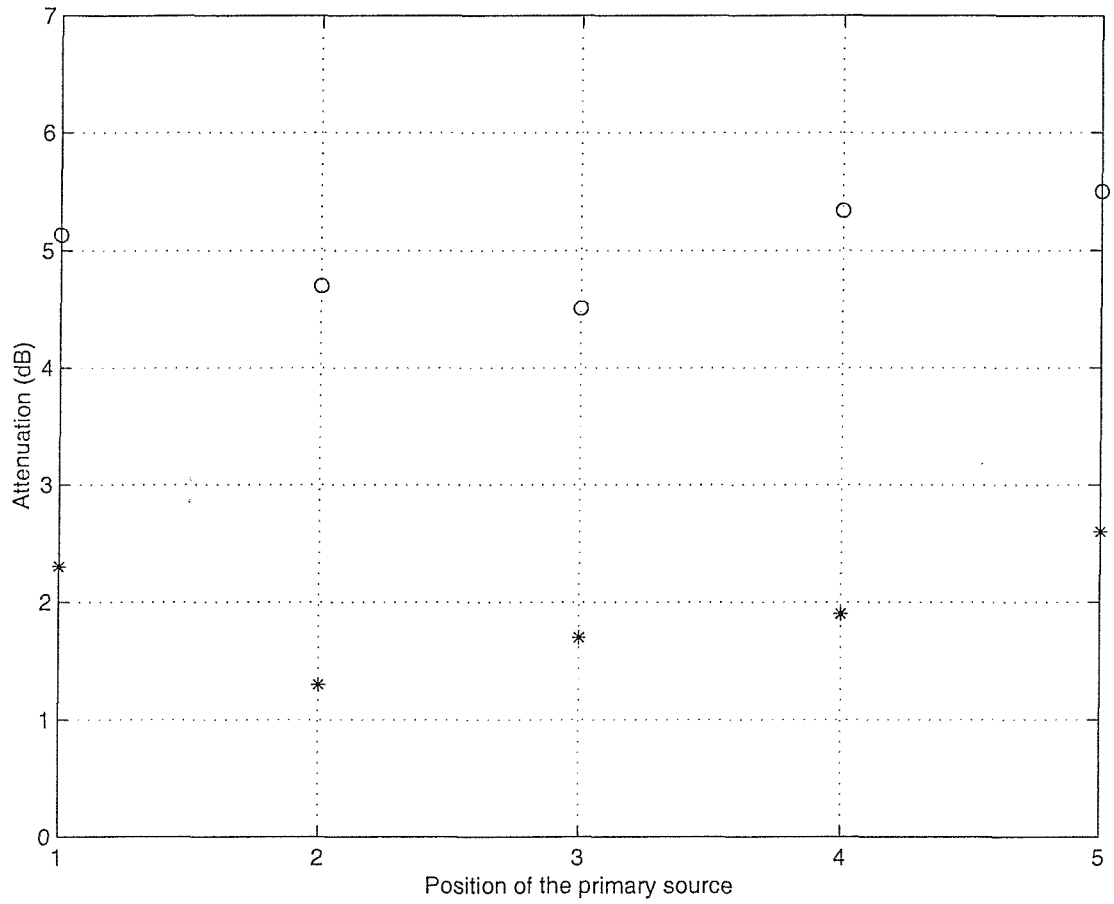

FIGURE 9.8 The overall attenuation at the virtual microphone for different position of the primary source as in Figure 9.7. (ooo) represents the overall attenuation over the frequency range of 100-400Hz and (***) over the whole frequency range.

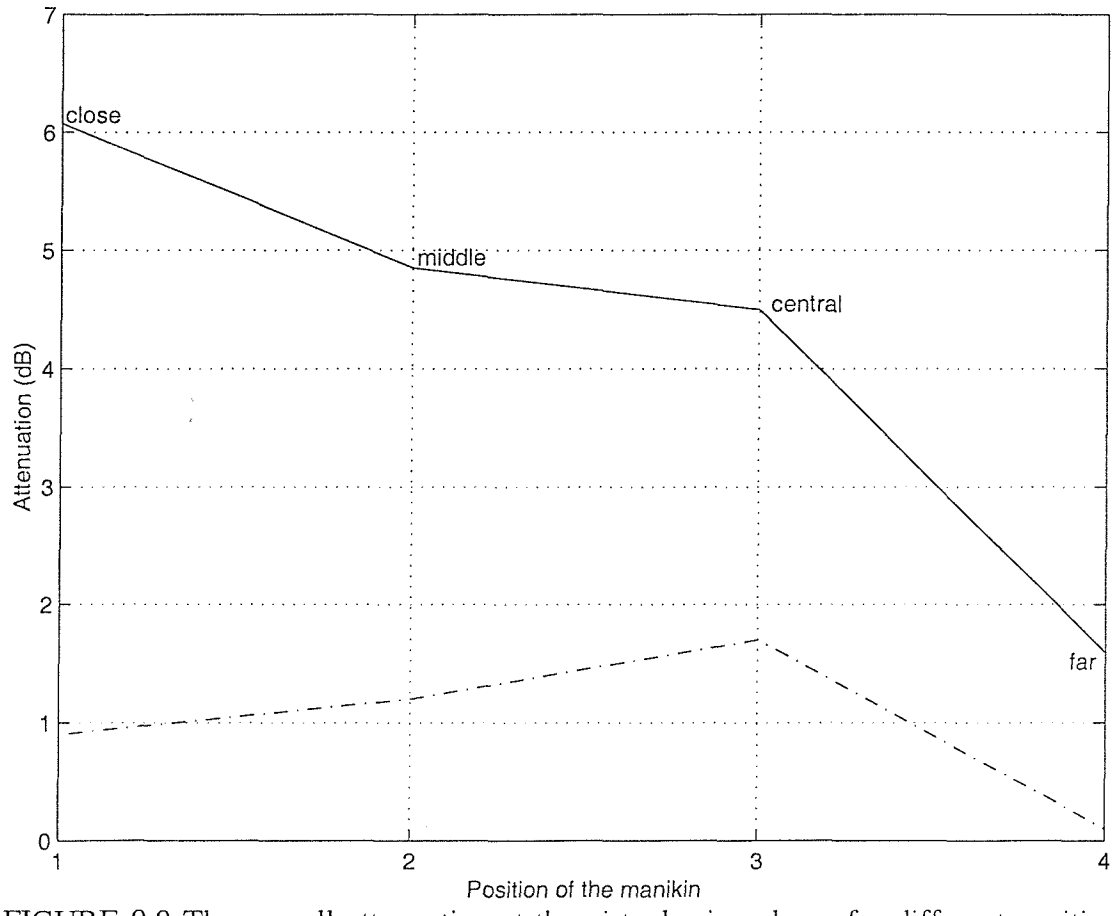

FIGURE 9.9 The overall attenuation at the virtual microphone for different position of the manikin with the primary source in front of the manikin at position 3. (———) represents the overall attenuation over the frequency range of 100-400Hz and (-.-.-.) over the whole frequency range.

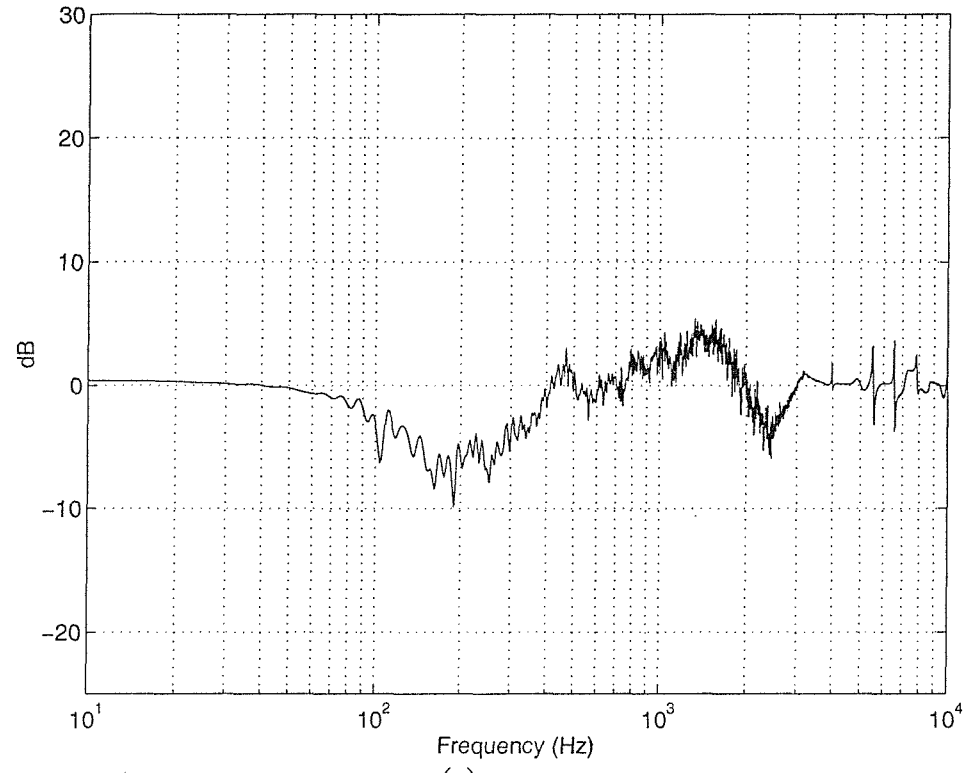

(a)

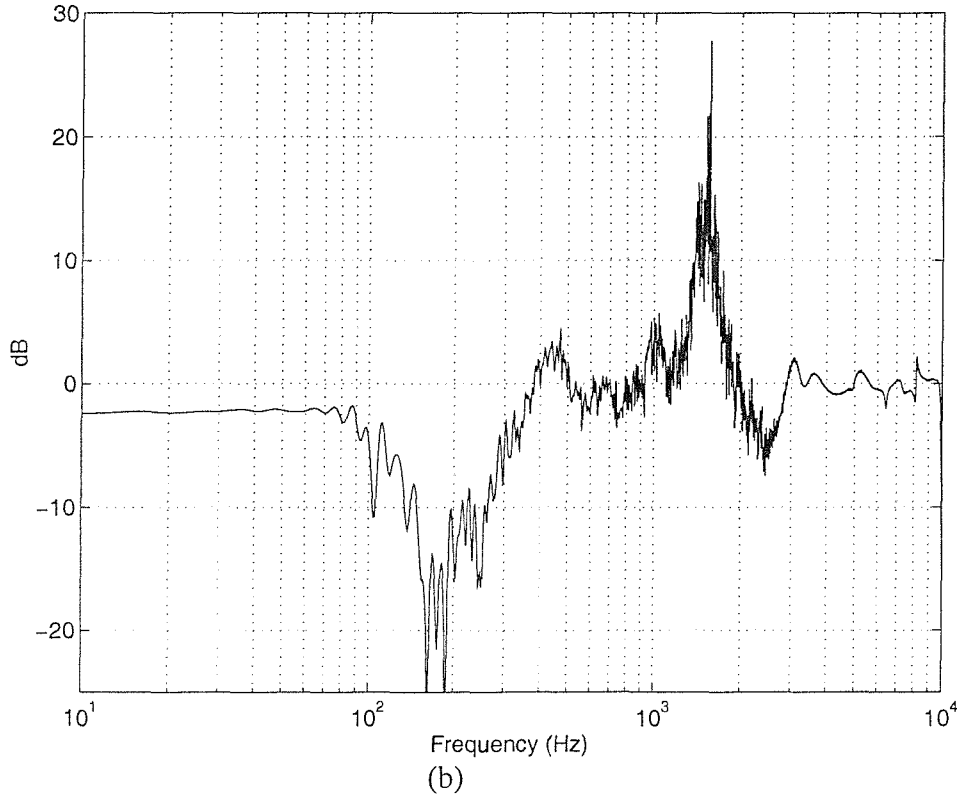

(b)

FIGURE 9.10 The sensitivity function with the primary source at position 3. (a) Central manikin position. (b) Close manikin position.

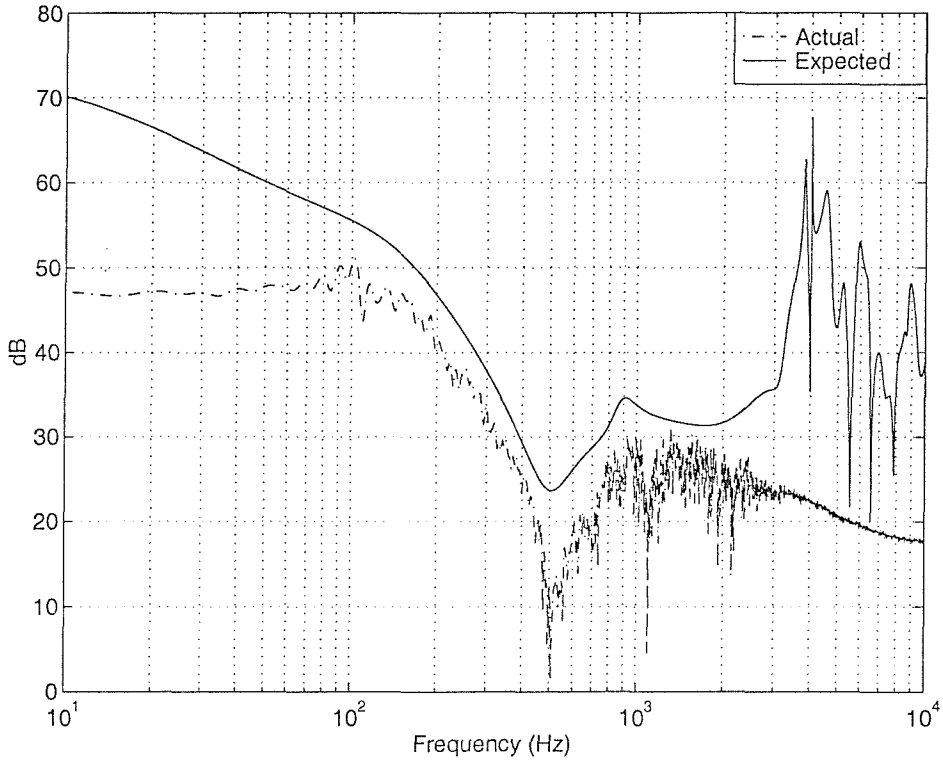

FIGURE 9.11 The gains of the control filters. Actual gain of the control filter (-.-.-.) and expected gain of the control filter for good performance to be achieved (———).

Part V

Chapter 10 Conclusions and suggestions for future research

10.1 Conclusions

This thesis is concerned with sound minimisation for local active control. The theory is based on the principle of pressure minimisation over space or space and frequency, which in practice can be applied to an active headrest system by using virtual microphone approaches. In this chapter the conclusions from this work and suggestions for future research are summarised.

In chapter 3 the general formulation for 2-norm and ∞-norm sound minimisation over space was presented. There are no cancellation points within the minimisation region in this method, nevertheless, the best overall attenuation of sound is achieved due to the optimal design. The method of pressure minimisation over a region in space is novel, although some previous work used pressure minimisation at several points with the optimal spacing between the cancellation points varying with frequency.

The average zones of quiet created by introducing one, two and three secondary sources using 2-norm and ∞-norm minimisation approaches described in chapter 3 to reduce the acoustic pressure at a desired region in a tonal propagating primary field and diffuse primary field have been investigated through computer simulations in chapter 4. It has been shown that larger zones of quiet could be obtained with two or three secondary sources using 2-norm and ∞-norm strategies compared to pressure or pressure and particle velocity cancellation at one point. This is since the secondary field is designed to better match the primary field at the specified region, not only at one point. The effect of different locations and shapes of the minimisation area on the quiet zones has also been explored. It has been shown that the locations and shapes of the quiet zones could be controlled by changing the minimisation region. An experiment has been performed to validate the local active control simulations when using 2-norm and ∞-norm minimisation strategies. The results showed that 2-norm minimisation strategy created slightly better zones of quiet at 270Hz when using two secondary sources. In practice 2-norm and ∞-norm minimisation strategies could be

used to control an active headrest system if the primary and the secondary fields are known. This potentially could be achieved by using virtual microphone approaches.

In chapter 4 only pure tone primary fields were considered. However this could be extended to broadband noise. In chapter 5 the theory and performance of active control for broadband disturbance using single-channel and two-channel systems have been presented. This involved optimisation over both space and frequency. A constraint on the amplification was also included in the design process. It has been shown that good attenuation could be achieved at the microphone or other desired region and over a selected frequency range using a single-channel system. However better performance could be achieved using a two-channel system. When constraints on amplification were introduced the performance began to degrade. Pressure minimisation over space and frequency could potentially be used in the control of broadband noise in an active headrest system. The pressure fields over space could potentially be predicted by using virtual microphones.

In chapter 6 we presented the theory behind design methods of a single channel feedback controller used in an active headrest system with robust H_2 and H_2/H_∞ formulations. The feedback controller is configured using Internal Model Control. Performance can be estimated by using an H_2 method since it has a simple and efficient solution. However when good performance can not be achieved an H_2/H_∞ method can be used but with the expense of a greater computational complexity. The methods described in this chapter were used to control an active headrest system presented in chapter 8.

In chapter 7 the performance and stability issues of the single-input single-output feedback controller designed to minimise the acoustic pressure at a virtual microphone were analysed. A novel method of designing stable feedback controllers has also been developed to guarantee the controller stability. It showed that good performance could only be achieved with unstable controllers. A novel analysis showed that the reason for poor performance was the relatively lower magnitude of the virtual plant response.

The real-time implementation of an active headrest system has been presented in chapter 8. The methods described in chapter 6 were used in this work. A TMS320C54x DSP system was used to control the experimental headrest system. The results showed that good attenuation was achieved at the virtual microphone location. However, the attenuation decreased as the virtual microphone, or ear, moved further away from the secondary loudspeaker. From chapters 7 and 8 we can conclude that the performance of an active headrest system could be improved if the physical configuration of the active headrest system is modified in order to reduce the gain difference between the physical and virtual plant which can be achieved by reducing the distance between the loudspeaker and the ear.

Chapter 9 investigated the potential performance of an active headrest system in an aircraft passenger seat. The noise recorded on Boeing 747 was used as the noise source. The effect of different positions of the primary source on the performance of the active headrest system has also been evaluated. It has been shown that different positions of the primary source has a little effect on the performance of the active headrest system. Therefore it can be concluded that a single feedback virtual microphone controller could work for many seats in the aircraft. In this chapter we also investigated the performance at the virtual microphone at four different locations of the manikin head when the feedback controller was designed to minimise the acoustic pressure at the virtual microphone at the central manikin position. It has been shown that the overall attenuation over the whole frequency range at the central position is better than that at other locations. The results in this chapter could be used to estimate the performance of an active headrest system in aircraft and help to better understand the applicability of an active headrest system.

10.2 Suggestions for future research

In this work we concentrated on the 2-norm and ∞-norm minimisation strategies to design quiet zones for local active control. Future research could concentrate on other minimisation strategies, such as the maximisation of 10 dB quiet zone area, in order to increase the size of the 10 dB quiet zone. Minimisation of the acoustic pressure over both space and frequency for broadband noise reduction was also investigated in this work, however, it was only concerned with a plane wave primary field. Future work

could also concentrate on active control of broadband noise in diffuse fields. In practice the pressure fields, primary and secondary fields, could be predicted by using virtual microphones at a given region over space. Once the pressure fields over space are known the strategy of pressure minimisation over space and frequency could be realised to control broadband noise. The applicability study of such scheme is proposed for future work.

The performance and stability issues of the feedback controller for an active headrest system have been investigated in this work. It was shown that good performance could only be obtained with an unstable controller. Therefore future research could concentrate on improving the performance of the active headrest system with a stable controller designed to attenuate the noise at the virtual microphone, or on studying the practical application of an open-loop unstable controller. A possible solution to this could be an improved configuration for the headrest system with the ears closer to the loudspeaker, therefore increasing the magnitude of the virtual microphone plant and potentially improving performance.

The real-time implementation of a SISO virtual microphone feedback controller for an active headrest system has also been performed in this work. Future work could concentrate on the implementation of multi-channel feedback controllers to improve the performance of the active headrest system, i.e. applying the sound minimisation methods developed in this work to a real headrest system, which has two loudspeakers as secondary sources.

REFERENCES

Boyd, S.B., Balakrishnan, V., Barrat, C.H., Khraishi, N.M., Li, X., Meyer, D.G. and Norman, S.A. (1988). "A new CAD Method and Associated Architectures for Linear Controllers". *IEEE Trans. Automat. Cont.*, 33(3), 268-283.

Broyden, C.G. (1970). "The convergence of a class of double-rank minimisation algorithms". *J. Inst. Maths. Applics.*, Vol. 6, pp. 76-90.

David, A. and Elliott, S. J. (1994). "Numerical studies of actively generated quiet zones". *Appl. Acoust.* 41, 63-79.

Doyle, J. C., Francis, B. A. and Tannenbaum, A. R. (1992). *Feedback control theory.* Maxwell MacMillan International.

Elliott, S. J., Joseph, P, Nelson, P. A., and Johnson, M. E. (1991). "Power output minimisation and power absorption in the active control of sound". *J. Acoust. Soc. Am.* 90, 2501-2512.

Elliott, S.J. and David, A. (1992). "A virtual microphone arrangement for local active sound control". *1st International conference on motion and vibration control*, Yokahama, Japan.

Elliott, S.J. (1994). "Active control using feedback". *Technical memorandum No. 732, ISVR*, University of Southampton.

Elliott, S. J. and Garcia-Bonito J. (1995). "Active cancellation of pressure and pressure gradient in a diffuse sound field". *J. Sound Vib.* 186 (4), 696-704.

Elliott, S.J. and Sutton, T.J. (1996). "Performance of feedforward and feedback systems for active control". *IEEE Transactions on Speech and Audio Processing*, 4(3), 214-223.

Elliott, S.J., Joseph, P., Bullmore, A.J. and Nelson, P.A. (1998). "Active cancellation at a point in a pure tone diffuse sound field". *J. Sound Vib.* 117, 35-38.

Fletcher, R. (1970). "A new approach to variable metric algorithms". *Computer Journal*, Vol. 13, pp. 317-322.

Fletcher, R. (1987). *Practical methods of optimisation*, 2nd ed. John Wiley & Sons.

Franklin, G. F., Powell, J. D. and Emamni-Naeini, A. (1994). *Feedback control of dynamic systems*, 3rd ed. Addison-Wesley, MA.

Garcia-Bonito J. and Elliott, S. J. (1994). "Alternative strategies for actively generating quiet zones". *ISVR Techincal Memorandum* 745.

Garcia-Bonito, J. (1996). "Local active control in pure tone diffracted diffuse sound fields". *Ph.D. thesis*, University of Southampton, England.

Garcia-Bonito, J, Elliott, S.J. and Boucher, C.C. (1997). ''A novel secondary source for a local active noise control system''. *ACTIVE 97*, 405-418.

Golfarb, D. (1970). ''A family of variable metric updates derived by variational means''. *Mathematics of Computing*, Vol. 24, pp. 23-26.

Gonzalez, A., Albiol, A. and Elliott, S.J. (1998). ''Minimisation of the maximum error signal in active control''. *IEEE Trans. on Speech and Audio Processing* **6** (3), 268-281.

Grace, A. (1995). *Matlab Optimization Toolbox*. The Math Works, Inc.

Greig, D.M. (1980). *Optimisation*. Longman Group.

Guo, J. and Pan, J. (1995). ''Analysis of active noise control in a free field''. *Proceedings of Active 95*, Newport Beach, California, 649-660.

Guo, J., Pan, J., and Bao, Chaoying (1997). ''Avtively created quiet zones by multiple control sources in free space''. *J. Acoust. Soc. Am.* 101, 1492-1501.

Ise, S. (1994). ''Theory of acoustic impedance control for active noise control''. *Inter-noise* 94, 1339-1342.

Jacobsen, F. (1979). ''The diffuse sound field''. *Report no. 27*, The Acoustics Laboratory, Technical University of Denmark.

Joseph, P. (1990). ''Active control of high frequency enclosed sound fields''. *Ph.D. thesis*, University of Southampton.

Joseph, P., Elliott, S. J., and Nelson, P. A. (1994). ''Nearfield zones of quiet''. *J. Sound Vib.* 172, 605-627.

Miyoshi, M., Shimizu, J., and Koizumi, N. (1994). ''On arrangements of noise controlled points for producing larger quiet zones with multi-point active noise control''. *Inter-noise* 94, 1229-1304.

Morari, M. and Zafiriou, E. (1989). *Robust process control*. Prentice-Hall, NJ.

Nelson, P.A., Elliott, S.J. (1986). ''The minimum power output of a pair of free field monopole sources''. *J. Sound Vib.* 105, 173-178.

Nelson, P. A. and Elliott, S. J. (1992). *Active control of sound*. Academic, London.

Rafaely, B. and Elliott, S.J. (1996). ''H_2/H_∞ output feedback design for active control''. *Tech. Memo 800*, ISVR, University of Southampton, UK.

Rafaely, B. (1997). ''Feedback control of sound''. *Ph.D. thesis*, ISVR University of Southampton, UK.

Rafaely, B. (1999). ''Active control with optimisation over frequency and space''. *ACTIVE 99*.

Rafaely, B. and Elliott, S.J. (1999). ''H_2/H_∞ active control of sound in a headrest: design and implementation''. *IEEE Trans. Cont. Sys.*, vol. 7, No. 1, 79-84.

Rafaely, B., Elliott, S.J. and Garcia-Bonito, J. (1999). ''Broadband performance of an active headrest''. *J. Acoust. Soc. Am.* 106 (2), 787-793.

Roberts, A.W. and Varberg, D.E. (1973). *Convex Functions*. Academic Press.

Ross, C. F. (1980). ''Active control of sound''. *Ph.D. thesis*, University of Cambridge.

Shanno, D.F. (1970). ''Conditioning of Quasi-Newton methods for function miimisation''. *Mathematics of Computing*, Vol. 24, pp. 647-656.

Skogestad, S. and Postlethwaite, I. (1996). *Multivariable feedback control*. John Wiley and Sons, Chichester, UK.

Tseng, Wen-Kung, Rafaely, B. and Elliott, S.J. (1998). ''Combined feedback-feedforward active control of sound in a room''. *J. Acoust. Soc. Am.* 104 (6), 3417-3425.

Tseng, Wen-Kung, Rafaely, B. and Elliott, S.J. (1999). ''2-norm and ∞-norm pressure minimisation for local active control of sound''. *ACTIVE'99*, 661-672.

Tseng, Wen-Kung, Rafaely, B. and Elliott, S.J. (2000). ''Local active sound control using 2-norm and ∞-norm pressure minimisation''. *Journal of Sound and Vibration*, 234(3), 427-439.

Vandenberghe, L. and Boyd, S. (1996). ''Semidefinite programming''. *SIAM review* **38**(1), 49-95.